Beyond Blue Stragglers: Binary Stellar Evolution Across the M67 Color-Magnitude Diagram

by

Emily M. Leiner

A dissertation submitted in partial fulfillment of

the requirements for the degree of

Doctor of Philosophy

(Astronomy)

at the

University of Wisconsin–Madison

2018

Date of final oral examination: 14 May 2018

The dissertation is approved by the following members of the Final Oral Committee:
Robert Mathieu, Professor, Astronomy
Richard Townsend, Associate Professor, Astronomy
Ellen Zweibel, Professor, Physics & Astronomy
Aaron Geller, Research Assistant Professor, Center for Interdisciplinary Exploration and Research in Astrophysics (CIERA), Northwestern University

Abstract

Optical color-magnitude diagrams (CMDs) of open clusters reveal large populations of stars that do not fall along standard isochrones, and thus are not evolving according to standard theory. The most numerous of these stars are the blue stragglers, stars brighter and bluer than the cluster turnoff that are likely formed from mass transfer in a binary, stellar mergers, or collisions during dynamical encounters. Many other non-standard stars are also found in clusters, but their origins are not well understood. These include the 'yellow stragglers' found between the blue straggler region and the red giant branch, and 'sub-subgiants' found fainter and redder than the giant branch. Using the 4 Gyr open cluster M67 as an exemplar, I present results of the first comprehensive study to move beyond the blue straggler population and begin to understand these other types of alternative stellar evolution products. First, I present an asteroseismic analysis of a yellow straggler in M67, demonstrating that it is a helium burning giant star with a mass of approximately twice the cluster turnoff. This large mass indicates this yellow straggler is an evolved blue straggler star, likely formed via a stellar merger or collision. Next, I present theoretical formation models for the sub-subgiant stars, focusing on reproducing the observed stellar and orbital properties of the two sub-subgiants in M67 and four sub-subgiants in open cluster NGC 6791 (8 Gyr). I focus on three hypotheses of sub-subgiant formation: 1) Roche lobe overflow in binary systems, 2) rapid envelope mass loss from subgiant stars, e.g. during a grazing dynamical encounter, and 3) under-luminosity due to inhibition of convection in subgiant

and giant stars in tidally synchronized close binaries due to their strong magnetic fields. Finally, I use Kepler K2 light curves of the M67 main-sequence to identify stars with unusually fast rotation rates given the old age of the cluster. I hypothesize that these stars have been spun up due to recent mergers, collisions, or episodes of mass-transfer, and thus represent lower-luminosity analogs to the blue stragglers that blend photometrically with the main-sequence. Together, these studies present a much more complete view of the post- merger, collision, and mass-transfer population of the cluster M67, and demonstrate that blue stragglers account for only about half of the post-interaction population. M67 is one example, but it is certainly not unique. These post-interaction stars exist in many clusters as well as the field. They represent the early stages of binary evolution pathways that may lead to many astrophysically important objects including X-ray binaries, double degenerates, and Type 1a supernovae. Studying these products of binary evolution across cluster color-magnitude diagrams is a critical step to developing better models of binary evolutionary pathways and understanding the impact of binaries on stellar populations in clusters, in the Milky Way, and in other galaxies.

Acknowledgments

The past 6 years in Madison have been exciting, rewarding, and great fun; at times they have also been difficult and frustrating. I've been fortunate to have great mentors, collaborators, friends, and family there for me every step of the way. This thesis is dedicated to them.

First, thank you to my advisor Bob Mathieu. You've given me so many opportunities– access to a trove of data built over your long career, introductions to wonderful collaborators, chances to travel and present my work. Thank you for always having faith in my ability to do good science, providing encouragement when I needed it most, and allowing me the freedom to follow my research interests and instincts. I've learned so much from you about being a good scientist and teacher, and I look forward to making more discoveries together.

To Dennis Stello, my EAPSI mentor, many thanks for hosting me for an amazing summer in Sydney and patiently teaching me the ways of asteroseismology. To Aaron Geller, working with you has been a real pleasure, and the creativity you bring to your science is an inspiration. I'm so excited for the work we will do together in the years to come. To Natalie Gosnell, a most excellent collaborator and friend, thank you for always being there with a sympathetic ear, good advice, and exceptional pep talks. Your students are lucky to have such a strong, wise, and devoted mentor. To the rest of my committee and the many other wonderful teachers and collaborators I've had a chance to work with

and learn from in my time here, thank you for your guidance and support.

This thesis also rests on the shoulders of many other students in Bob's group, past and present. Thank you to anyone who has ever spent their nights at Kitt Peak observing WOCS clusters. Special thanks to Katelyn, Ben, Erika, and Max. Its been a pleasure working with all of you. Ben– I really lucked out getting you as my research sibling and friend for my entire time here, from classes, to observing runs, conferences, and job market commiseration, with more than a few Hamm's in between. You are a rock star, and I can't wait to hear about all your future successes.

Thanks to all the other grad students in the UW Madison Astronomy Department. I can't imagine a better group of fun, smart, supportive, cool people to have spent 6 years with. I've made some incredible friends here. Thanks especially to the other members of my class, Erin, David, and Alisha, who made the many hours working on problem sets a lot more fun. David, bonus points for being a super laid-back office mate who is always good for a laugh. I'll really miss seeing you every day. Alisha, thanks for biking all over south central Wisconsin with me. You've been a great friend throughout all the grad school ups and downs, cat-related tragedies, and wisdom tooth surgeries. Thanks also to Claire "You're Doing Great!" Murray, for making everything better with your enthusiasm. You made me feel welcome in Madison from the moment I arrived, and it's always more fun to have you around. Here is to many more games and grogs in the years to come! Most of all, thanks to Corey, for adventuring through life with me. You are always there for me, whether to save me from a deranged moose or make me a morning coffee. I couldn't ask for a more confident, caring partner in all things, and I am so happy to have you in my life.

To my non-astronomy BFFs Danielle and Brendan, thank you for the last ten years. You have seen me through it all. I love you both.

Finally, I want to thank my parents. To my hardworking and dependable Dad, you've

taught me to be determined, focused, and to always challenge myself. You are are a rock, and I'm grateful to always have you behind me. To my brilliant, funny, and generous Mom, you've taught me to be curious, creative, compassionate, and to find joy in the simple things. I wish so much you could be here to share in this accomplishment. I could never have done it without you.

Contents

List of Tables

List of Figures

Chapter 1

Introduction

The theory of stellar evolution is one of the great accomplishments of 20th century astrophysics. Certainly many questions still remain at the heart of stellar evolution – the evolution of angular momentum, details of short-lived phases like the thermally pulsating AGB, wind mass loss rates, the effects of magnetic fields, etc. – but the broad strokes of a single star's evolution are clear. Given a star's initial mass, the course of the star's life can be well predicted, from pre-main-sequence, to main sequence, to giant, and eventually to a black hole, neutron star, or white dwarf remnant. This understanding undergirds so much of astrophysics. It enables us to model synthetic stellar populations of entire galaxies, age-date stellar systems from isochrone fitting, measure distances from red-clump and RGB-tip standard candles, understand the chemical evolution of our galaxy through stellar processing, etc.

Yet the reality of stellar evolution is more complex than these models suggest. While the entire course of a single star's life can be predicted to first order from just its mass, many stars are not single. About 50% of solar-type stellar systems are binary or higher order systems, and ∼40% of these are in close enough orbits to interact and exchange material over the course of their lifetimes (Raghavan et al. 2010), dramatically altering the course of their evolution. For the more massive O and B stars, the fraction of stars with companions rises to 3 out of 4 (Sana et al. 2008).

The evolution of stars in binary systems can no longer be predicted from just a mass. Here the mass of the primary star, the mass of the secondary star, and the orbital separation and eccentricity all play a key role in the evolution and ultimate fate of the system. Furthermore, many of the remaining uncertainties in stellar evolution become more problematic when considering binary systems. Angular momentum evolution impacts not only the rotation rate of the stars, but also their orbital evolution. In close binaries, tidal forces synchronize stellar rotation periods with their orbital periods, exchanging angular

momentum between the stars rotation rates and their orbits. Rapid rotation can give rise to unusually strong magnetic fields, amplifying the importance of magnetic effects. Mass loss rates may be impacted by the presence of a companion, and material from the primary may be accreted by the companion thereby changing the mass ratio of the binary. In short, remaining uncertainties in stellar astrophysics compound to such an extent that we cannot accurately predict the end state of a binary– whether the two components will remain in a wide orbit, shrink to be a very close system like an X-ray binary or cataclysmic variable, or merge to form a single system.

While this presents a problem when it comes to modeling detailed binary evolutionary pathways, it also represents an opportunity. The complex physics at work in binary systems makes them excellent tests of forefront developments in stellar astrophysics– from magnetic stellar evolution to AGB nucleosynthetic yields. Additionally, many astrophysically significant objects are produced predominantly or exclusively through binary evolution channels– among them the binary black holes and neutron stars that are the source of recently detected gravitational waves, and Type Ia supernovae used to measure the accelerating rate of expansion of the universe. Understanding binary evolution is thus a goal at the forefront of stellar research, and has broad implications across many different areas of astrophysics.

Just as developing single-star stellar evolution theory relied on cluster color magnitude diagrams (CMDs), star clusters are excellent observational laboratories to study binary stellar evolution due to their uniform age and homogenous composition. Star cluster populations reveal the significant impact binary populations have on stellar evolution. Cluster CMDs reveal large populations of stars that are not following standard single-star evolutionary tracks. In older open clusters, $\sim 25\%$ of the brightest stars in the cluster do not fall on a standard isochrone. The most famous of these stars are the blue straggler

stars (BSSs), thought to result from binary mass-transfer (McCrea 1964; Gosnell et al. 2015), binary mergers (Perets & Fabrycky 2009; Andronov et al. 2006), or stellar collisions during dynamical encounters involving binaries (Leonard 1989; Sills et al. 2001). As such, blue stragglers are in the early stages of binary stellar evolution channels– after the first merger, collision, or mass-transfer onto a main-sequence star. As blue stragglers continue to evolve, they may create other interesting binaries such as cataclysmic variables, symbiotics, and other types of low-mass X-ray binaries.

Blue stragglers are only one facet of a larger population of stars in the early stages of stellar evolution, including evolved blue stragglers on the giant branch or in the yellow-straggler region, low-luminosity blue stragglers on the main sequence, and sub-subgiants that are fainter and redder than the giant branch (Figure 1.1). In this dissertation, I present the first integrated study of this broader early-stage binary evolution population in the open cluster M67 and discuss the insights we may gain from studies of these non-standard stellar populations.

Below I outline the key processes that create blue stragglers and other early-stage binary evolution products– stable Roche lobe overflow, common-envelope evolution, stellar mergers, and dynamical collisions. I then summarize what is known about blue straggler populations in clusters and in the field. I also discuss some of the other non-standard stars found in both clusters and the field, and how they may be related to blue straggler stars. Finally, I discuss current and past observations of the open cluster M67, the primary cluster whose post-interaction binary population this work explores in detail. At 4 Gyr, it is one of the few old, nearby open clusters in the Milky Way, and serves as an important benchmark for studying stellar astrophysics. In particular, I focus on observations of the cluster provided by the WIYN Open Cluster Study and an ongoing *Kepler* K2 study.

1.1 Binary Interactions

Several types of binary-star interactions have been proposed, each with the power to dramatically alter the configuration of a binary system and the evolution of the stars within it. These include binary mass transfer that results from one star filling its Roche lobe as it evolves, binary mergers in hierarchical triple systems induced by Kozai oscillations, and stellar collisions during dynamical encounters in dense cluster environments.

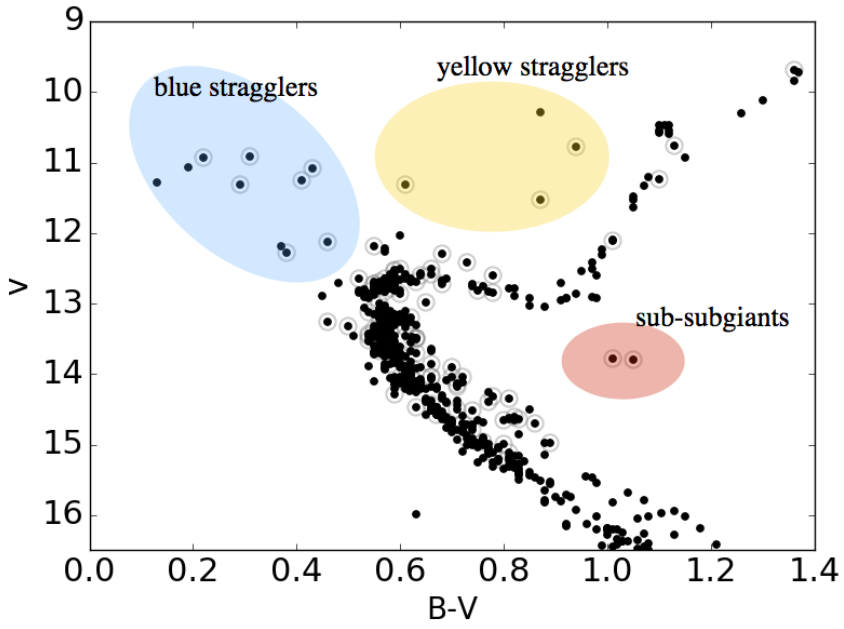

Figure 1.1 : A color-magnitude diagram of M67 showing all the 3-dimensional kinematic members (Geller et al. 2015). Single stars are shown with points, and binaries are circled. Populations of blue stragglers, yellow stragglers, and sub-subgiants are as labeled.

1.1.1 Roche lobe overflow

McCrea (1964) first suggested that blue straggler stars may form through mass transfer in binary systems when one star overfills its Roche lobe. This often occurs because the radius of one star in the binary begins to grow as it evolves off the main sequence, but can also occur if the orbital separation of the binary shrinks due to angular momentum loss. The Roche lobe of a binary is commonly expressed using the approximation of Eggleton (1983):

$$\frac{r_L}{a} = \frac{0.49q^{\frac{2}{3}}}{0.6^{\frac{2}{3}} + ln(1+q^{\frac{1}{3}})} \tag{1.1}$$

where r_L is the Roche lobe radius of the binary, a is the orbital separation of the binary, and q is the mass ratio of the binary system. The radius at which a star will begin to overfill its Roche lobe, then, depends only on the mass ratio of the binary system and the orbital separation of this binary.

Mass transfer can be divided into several categories based on when a star begins to overfill its Roche lobe.

- **Case A mass transfer** refers to mass transfer that occurs while the Roche-lobe filling star is on the main sequence. This is expected to lead to a contact binary (Webbink 1976). As the binary system loses angular momentum through magnetic braking, the two stars should eventually merge and likely form a rapidly rotating single star. The binaries expected to go through Case A mass transfer leading to coalescence have initially short periods of just a few days (Paczyński 1971; Chen & Han 2008a; Andronov et al. 2006).

- **Case B mass transfer** refers to mass transfer that occurs while the Roche-lobe filling star is on the red giant branch (RGB). For the solar-type stars that are the focus of this thesis, these are binaries in orbits of tens or hundreds of days (Paczyński 1971;

Chen & Han 2008). The post-mass-transfer binary will be a a main sequence star or blue straggler with a helium white dwarf companion. Since the surface material of the blue straggler was once material deep within the envelope of a giant star, these stars are predicted to have a deficiency of lithium and CNO elements (Carney et al. 2001; Shetrone & Sandquist 2000; Ferraro et al. 2006)

- **Case C mass transfer** refers to mass transfer that occurs while the Roche-lobe filling star is on the asymptotic giant branch (AGB), and occurs for solar type stars in orbits of up to a few thousand days (Paczyński 1971; Chen & Han 2008). The post-mass-transfer binary will have a main-sequence star or blue-straggler primary with a carbon-oxygen white dwarf companion. Since the surface material of the primary came from an AGB star, enhancements in s-process elements like barium are sometimes observed in these systems (Milliman et al. 2015; Jorissen et al. 1998).

In recent years, a fourth class of Roche lobe overflow has been introduced called "Wind Roche Lobe Overflow" or **Case D mass transfer**. In this type of interaction, the AGB donor remains technically within its Roche lobe, but drives a slow wind across its Roche radius that can be efficiently accreted by a companion through the first Lagrangian point (Mohamed & Podsiadlowski 2012). Wind Roche lobe overflow is expected to occur in solar-type stars with periods out to $\sim 10,000$ days (Mohamed & Podsiadlowski 2012; Abate et al. 2013). Case D blue stragglers are expected to be in wider binaries than Case C systems, but also have carbon-oxygen white dwarf companions. They may have observed s-process enrichment due to contamination from the AGB companion.

Given the orbital-period distribution of solar-type binaries, it is clear that a large fraction of these binaries will evolve through Roche lobe overflow, most of them during AGB evolution. Figure 1.2 shows the period distribution of field solar-type binaries from

Raghavan et al. (2010) with the expected type of Roche lobe overflow labeled. Given this period distribution, around 40% of solar-type binaries may evolve through mass-transfer at some point in their evolution.

1.1.2 Mass Transfer Stability and Common-Envelope Evolution

Roche lobe overflow as discussed above can be classified as "stable" or "unstable". In stable mass transfer, mass loss from the Roche-lobe-overflowing primary occurs slowly enough for the material to be largely accreted by the secondary. If mass transfer is dynamically unstable, the donor may shed most of its envelope far more quickly than the secondary can accrete the material, and the accreting companion begins to orbit inside the

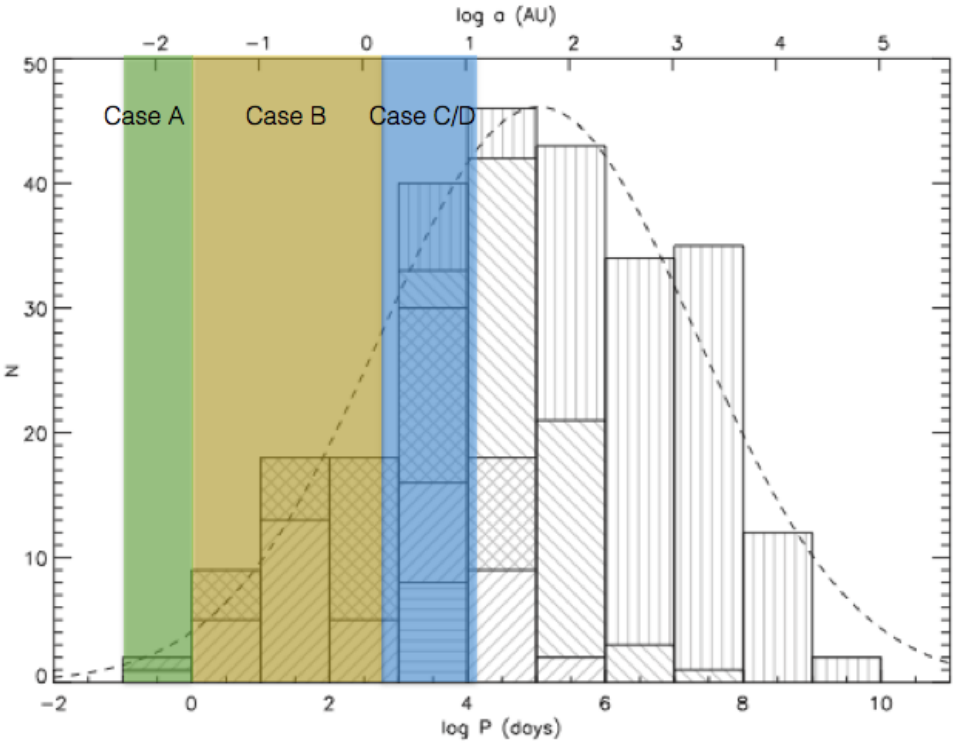

Figure 1.2 : The period distribution of a sample of solar-type field binaries from Raghavan et al. (2010). Overlaid with colors are the approximate domains in which a binary would be expected to undergo Case A, Case B, or Case C/D mass transfer, respectively.

envelope of material (Paczynski 1976). This phase is known as common envelope evolution. For many possible binary orbital configurations, mass transfer is predicted to be unstable and common envelope evolution is predicted to occur. Despite the prediction that this is a common evolutionary path, the criteria for stable mass transfer and the physics of the common envelope phase are two outstanding problems in binary evolution physics.

Stability is determined based on whether the radius of the mass losing star shrinks or expands in response to mass loss, and whether the Roche lobe radius shrinks or expands due to mass transfer. In the case that the donor shrinks and/or the Roche lobe expands as a response to mass loss, mass transfer can often proceed stably. In this case, mass loss proceeds on a thermal or evolutionary time scale and is relatively straightforward to model with a stellar evolution code. However, if the donor expands due to mass loss faster than the Roche lobe expands, mass transfer becomes unstable. In this case, mass loss rates become quite large and the mass loss occurs on a dynamical time scale, usually thought to lead to a common envelope event.

Ivanova et al. (2013) provide an excellent review of what is known about common envelope evolution. In brief, the phase is so short lived that it is extremely unlikely to be observed[1]. The overall process starts with nuclear- or thermal- timescale evolution as Roche lobe overflow begins, but then evolves into rapid dynamical-timescale evolution as the systems in-spirals and merges. As a result, the full process cannot be modeled by a simple 1D stellar evolution code on its own, and computationally expensive 3D hydrodynamic simulations are required to model the common envelope phase in detail.

As a result of these modeling difficulties, parameterizations are often used in population synthesis codes that try to predict the onset of common envelope based on the

[1]A few rare events known as "red novae" have been observed and hypothesized to be stellar mergers (e.g. Tylenda et al. 2011; Kulkarni et al. 2007), which could include common envelope events

evolutionary state of the donor and the mass ratio of the binary. A standard assumption is that the donor can be described by a simple polytropic model, and stability then depends primarily on the mass of the donor's core, whether the donor has a convective or radiative envelope, and the mass ratio of the binary (Hjellming & Webbink 1987). These parameterizations are known to be inaccurate. They underestimate mass transfer stability (Pavlovskii & Ivanova 2015; Passy et al. 2012), and cannot reproduce many of the observed properties of post-mass-transfer binaries (Geller et al. 2013; Chen et al. 2014). Many uncertainties contribute to these inaccuracies including: how much mass may be lost by the donor through winds prior to Roche lobe overflow (Tout & Eggleton 1988), how conservative mass transfer is (i.e. the fraction of material lost by the primary that is accreted by the companion), how the superadiabatic surface layer of the donor may impact its response to mass loss (Woods & Ivanova 2011), what fraction of the envelope may be retained after in-spiral, etc. Improving these parameterizations requires more detailed simulations of the common envelope phase, as well as well-characterized samples of post-mass-transfer binaries to compare to model predictions.

Blue stragglers, yellow stragglers, and sub-subgiants are all possible examples of mass-transfer binaries that may be useful tests of common envelope theory and the criteria for stable mass transfer. The very existence of large populations of mass-transfer blue stragglers indicates stable mass transfer is more common than common envelope parameterizations predict (Geller et al. 2013), and blue/yellow straggler binaries with well-characterized stellar and orbital parameters offer interesting tests of detailed mass-transfer models (Gosnell et al. 2015; Landsman et al. 1997).

1.1.3 Stellar Mergers in Triple Systems

The fraction of triple systems among solar-type stars is ~ 10 % (Raghavan et al. 2010). Most of these are hierarchical triple systems in which a distant tertiary companion orbits a close inner binary. In these cases, a type of gravitational interaction called Kozai-Lidov oscillations can take place (Lidov 1962). In this situation the orbit of the inner binary can be perturbed by the distant tertiary, which can lead to a periodic exchange between orbital eccentricity and inclination. This mechanism can drive the orbit of the inner binary to very high eccentricities, and with the aid of tidal friction this can potentially induce a merger of the inner binary system similar to Case A mass-transfer. Several groups have suggested this mechanism could create significant numbers of blue straggler stars (Perets & Fabrycky 2009; Ivanova et al. 2008; Naoz & Fabrycky 2014). This scenario would leave behind a blue straggler with a wide main-sequence companion. Observationally, it is difficult to distinguish definitively between blue stragglers formed from this mechanism compared to collisions or Case A mass-transfer, but they can be distinguished from Case B/C mass-transfer blue stragglers by their lack of white dwarf companions.

Triple systems are a computational challenge to include in N-body and population synthesis studies, and thus this channel is often excluded from studies seeking to model blue straggler populations and other products of binary evolution (Geller et al. 2013; Hurley et al. 2002; Chen & Han 2008). Due to the difficulties of both the modeling and observational approaches, it is still unclear to what degree this channel may contribute to the observed populations of blue stragglers and related stars.

1.1.4 Stellar Collisions

Hills & Day (1976) demonstrated that in dense star clusters direct collisions between main sequence stars could create blue stragglers. Leonard (1989) later demonstrated that

binaries had a much larger cross section for gravitational interaction, and thus collisions between binary systems can form blue stragglers much more frequently.

Binary-binary or binary-single encounters (or interactions with triple and higher-order systems) can leave behind a variety of different kinds of systems (e.g. Heggie 1975). Some interactions may be "hardening" interactions, in which a binary orbit shrinks when it imparts energy to a passing stars. Others may be "exchange" interactions, in which one component of the binary is ejected and the third interacting star becomes bound. In the most dramatic encounters, called "collisions", two or more stars can merge into a single star (Benz & Hills 1987; McMillan et al. 1990). The outcome of such a collisions could be a single star, or a binary system, depending on whether or not a third star involved in the interaction remains bound. If the combined mass of the colliding star is sufficient, it may form a star with a mass larger than the cluster turnoff, and therefore appear as a blue straggler star. Both analytic and numerical tools have been developed to calculate the rates and outcomes of such encounters (e.g. Leigh et al. 2013; Fregeau et al. 2004; Aarseth 2001).

Angular momentum evolution of collision products remains a topic of debate. Immediately post-collision, the new star is expected to be rotating very rapidly and swell to a large radius due to the large amount of energy deposited in the stellar envelope. These stars must then shed angular momentum and spin down in order to contract back down to the main sequence. The timescale and mechanism for this angular momentum loss is unclear, with models usually invoking a combination of magnetic braking and disk locking (Sills et al. 2001, 2005). Another question is how the stellar material will be mixed after the collision. Early studies predicted that blue stragglers formed via collisions would be thoroughly mixed, resulting in a marked helium overabundance (Benz & Hills 1987; Bailyn 1992). More recent work has concluded that large amounts of mixing does not occur,

making these stars harder to identify from abundances (Lombardi et al. 1995; Sills et al. 2005).

1.2 Blue Straggler Populations

All the mechanisms discussed in the previous section – mass transfer, Kozai mergers, and dynamical collisions– are proposed formation pathways for blue straggler stars. The relative frequency of each production mechanism is still a matter of debate. It is likely that this is dependent on several factors, including the binary fraction and local environment of a stellar population. Here I outline the observations of blue straggler populations in older open clusters, globular clusters, and in the field and the current thinking on the production mechanisms in each environment.

1.2.1 Open Cluster Blue Stragglers and The Blue Stragglers of NGC 188

The blue stragglers of the old (7 Gyr) open cluster NGC 188 have been the subject of extensive study. A binary fraction of 76% (Mathieu & Geller 2009) and a secondary mass function that peaks at the characteristic CO white dwarf mass of 0.5 $M_{\odot}$(Geller & Mathieu 2011) point to mass-transfer formation for the majority of blue straggler stars in the cluster. Gosnell et al. (2014) followed up these studies with UV photometry from the Hubble Space Telescope to directly detect hot white dwarf companions, finding 4 secure 3σ detections of hot white dwarfs implying ages of < 300 Myr. Three additional sources with $2 - 3\sigma$ UV excesses implied slightly cooler white dwarf companions with ages of 300-400 Myr. Gosnell et al. (2015) conclude that the age distribution of these blue stragglers is consistent with at least 2/3 of the cluster's 20 blue stragglers having a mass-transfer origin, with many of the white dwarf companions being old enough to have cooled to temperatures and luminosities below the detection threshold of the UV study. This conclusion implies

that mass transfer is the dominant formation mechanism in this cluster. Given the orbital periods of these post-mass-transfer blue stragglers, one seems to have formed from Case B mass transfer and the rest from Case C/D mass transfer.

NGC 188 also possesses at least 2 double lined spectroscopic binaries, revealing them to have main-sequence companions rather than white dwarfs. In addition, several blue stragglers are not observed to be radial-velocity variable, and thus do not appear to have companions at all (Geller et al. 2008, 2009). In these cases, Case B/C/D mass transfer is not the expected formation process and these stars likely formed through Case A mass transfer, Kozai mergers, or dynamical collisions. Mass transfer may be the dominant mechanism, but it is certainly not the only one at work in these clusters.

Blue straggler populations of older open clusters sometimes resemble NGC 188, and sometimes seem to have key differences. For example, the old open cluster M67 (4 Gyr) has a similar high binary fraction among its blue straggler population of 80% (Latham 2007; Geller et al. 2015), but the somewhat younger open cluster NGC 6819 (2.5 Gyr) has a lower binary fraction closer to 50% (Milliman et al. 2014). The reasons for these differences are still not clear, and comparative studies of more cluster blue straggler populations are necessary.

1.2.2 Globular Cluster Blue Stragglers

Studies with the Hubble Space Telescope enabled the construction of color-magnitude diagrams of dense inner regions of globular clusters, for the first time reaching into the crowded cluster cores and allowing identification of blue straggler populations there. These studies revealed globular clusters to have substantial numbers of blue stragglers (see Piotto et al. 2004 for a census), although as in open clusters the observed fraction of blue stragglers varies significantly between clusters. Specific environmental factors such as cluster mass,

binary fraction, age, density, and amount of dynamical evolution likely influence the characteristics of the population (Sollima et al. 2008; Chatterjee et al. 2013; Leigh et al. 2013).

The much denser environment of globular clusters mean that dynamical processes are expected to be more influential than in open clusters. Yet observational studies reveal that there is no correlation between the fraction of blue stragglers (or the overall number) and cluster collision rate (Piotto et al. 2004; Davies et al. 2004) as would be expected if blue stragglers were primarily produced through collisions. Davies et al. (2004) argue that this lack of correlation suggests collisions are not the dominant formation mechanism in globular clusters, and internal binary evolution processes (i.e. mass transfer and mergers) play the more significant role. Such an interpretation is bolstered by evidence that the number of blue stragglers is best correlated with overall cluster mass, such that proportionally more blue stragglers are found in lower mass globular clusters (Knigge et al. 2009). This result may stem from the fact that lower mass globular clusters have higher binary fractions, and therefore lower mass clusters should produce more blue stragglers through binary evolution channels. If binary evolution is responsible for producing most blue stragglers as these studies suggest, one would expect blue straggler numbers are even more strongly correlated with cluster binary fraction than cluster mass. However, Leigh et al. (2013) determine this is not the case, and blue straggler numbers are not more strongly correlated with binary fraction than with cluster mass. They suggest this result may still be compatible with blue straggler formation through binary evolution, but only if cluster binary fraction is so tightly correlated with cluster mass that cluster mass is actually a better predictor of the cluster's true binary fraction than the binary fractions estimated from photometric studies (Milone et al. 2012).

Additionally, some clusters appear to have two distinct sequences of blue stragglers,

one bluer and one redder (Dalessandro et al. 2013; Ferraro et al. 2009) . It has been suggested that this is evidence for both mass-transfer and collision channels contributing to the population, with the bluer sequence well reproduced by collisional models (Sills, Karakas & Lattanzio 2009) and the redder sequence better matching mass transfer models (Xin et al. 2015).

Cluster simulations do require substantial contributions from mass-transfer channels to produce observed numbers of blue stragglers (for example, 25% in globular cluster 47 Tuc, and perhaps up to 60% in lower density globulars; Mapelli et al. 2004; Chatterjee et al. 2013). It seems likely that even in dense globulars, both mass-transfer and collisions contribute to blue straggler populations. Mass transfer could be the dominant mechanism in all clusters, and certainly seems to be so in open clusters and perhaps low-density globulars, but the relative significance of each production mechanism and how this may vary based on environment is still a subject of ongoing research.

1.2.3 Blue Stragglers in the Field

Blue stragglers are easy to pick out in cluster environments based on their CMD location bluer and brighter than the main sequence turnoff. Given the age spread amongst the field population, blue stragglers cannot be identified in the same way. Nevertheless, if blue stragglers frequently form as the result of mass transfer rather than through dynamical channels, significant populations of blue straggler analogs should exist in the field. Such stars have indeed been identified using other techniques, primarily abundance studies.

Populations of blue stars with low metallicity and high velocity have been discovered in the Milky Way (Preston & Sneden 2000; Santucci et al. 2015). While their abundances and kinematics suggest they belong to an old halo or thick disk population, their blue colors indicate younger ages. The high binary fraction among these stars (Preston &

Sneden 2000; Carney et al. 2001, 2005) is similar to that found in NGC 188 and other old open clusters, with similar low eccentricities and secondary masses consistent with white dwarf companions (Carney et al. 2005). These stars are thought to be field blue stragglers formed through mass transfer.

Other studies have detected both field dwarfs and giants with s-process enrichment, particularly barium excesses. Barium and other s-process elements are synthesized in AGB stars. Large surface abundances of these elements indicate accretion of material from an AGB companion during Case C or Case D mass transfer. Examples of these s-processed enriched stars are the carbon enhanced metal poor stars with s-process enrichment (Hansen et al. 2016; Jorissen et al. 2016) and barium stars (Jorissen et al. 1998; Escorza et al. 2017). Again, these stars have a very high binary fraction, low eccentricities, and secondary masses compatible with white dwarf companions (McClure & Woodsworth 1990; Jorissen et al. 1998; Lucatello et al. 2005; Van der Swaelmen et al. 2017). Notably, some cluster blue stragglers are found to have s-process enrichment, but many do not (Milliman et al. 2016; Shetrone & Sandquist 2000), so blue straggler and s-process enhanced populations are not identical. While there is clearly an overlap with the cluster blue stragglers, s-process enhanced stars may be just one subset of the overall blue straggler population. Other abundance signatures have been suggested to indicate recent mass-transfer or mergers, including carbon and oxygen depletion in Case B mass-transfer products (e.g. Ferraro et al. 2006) and lithium anomalies in Case A merger products (Shetrone & Sandquist 2000; Andronov et al. 2006). Understanding the enrichment signatures of mass transfer is an ongoing area of research (Merle et al. 2016).

1.3 Other Stars in the Early Stages of Binary Evolution

Blue stragglers are far from the only early-stage binary evolution products that may be produced by mass transfer, mergers, and collisons. There are also the yellow stragglers, sub-subgiants, and main sequence-white dwarf binaries, all stars with equal potential to illuminate aspects of binary evolution physics.

1.3.1 Yellow Stragglers

It stands to reason that blue stragglers, which are understood to be core hydrogen burning stars, will eventually exhaust their core hydrogen and evolve into giants, moving to the red in the a CMD (Sills, Karakas & Lattanzio 2009). In several clusters, stars are observed that fall in between the blue straggler domain and the red giant branch (Geller et al. 2015, 2008). These stars have been called "yellow giants" or "yellow stragglers." While some could be explained as the combined light of a binary system (e.g. a blue straggler-red giant binary Mathieu et al. 1990; Janes & Smith 1984), others are thought to be the evolved counter parts to the blue stragglers. In at least one case, a yellow straggler has a hot white dwarf companion, indicating it is indeed a product of mass transfer (Landsman et al. 1997).

With the recent advent of asteroseismology, masses can now be well determined for large samples of giants. In the two older open clusters observed with Kepler, NGC 6819 and NGC 6791, asteroseismic studies reveal giant stars with masses substantially above normal for the clusters (Brogaard et al. 2012; Stello et al. 2011; Corsaro et al. 2012; Handberg et al. 2017). These stars sometimes appear slightly bluer than the main locus of the giant branch, and sometimes blend with rest of the giant branch or the red clump. Much like the yellow stragglers, these stars are likely evolved blue straggler stars , though they would be difficult to detect from CMD studies alone due to the normal photometric scatter in cluster giant

branches. This should be as expected, as the RGB temperature is only weakly impacted by mass. Only stars evolving through the Hertzsprung gap or giants that are extremely overmassive would show up as distinct CMD outliers. We discuss these stars at length in Chapter 2, and in particular the asteroseismic study of a yellow straggler binary in M67.

Globular clusters are too distant, crowded, and faint for similar asteroseismic studies of their giant branches to be possible. However, globular cluster CMDs do show evolved stars located between the horizontal branch and base of the AGB, a location core-helium-burning evolved blue stragglers are predicted to occupy (Ferraro et al. 1999; Beccari et al. 2006). Recently Ferraro et al. (2016) proposed a method to infer masses using chemical abundance signatures, determining one of these outliers in the CMD of globular cluster 47 Tuc has a mass more than 0.5 $M_{\odot}$ above the cluster turnoff. This result supports the hypothesis that at least some of these stars are evolved blue straggler stars.

1.3.2 Sub-subgiants

Sub-subgiants (SSGs) are stars found redder and/or fainter than the subgiant and giant branch in a region not easily populated by stellar evolutionary tracks or the combined light of normal cluster stars. The first sub-subgiants were identified in open cluster M67 (Belloni et al. 1998; Mathieu et al. 2003) and globular cluster 47 Tuc (Albrow et al. 2001). Over 70 SSGs have now been cataloged in both open and globular clusters[2] (Geller et al. 2017). SSGs are generally found to X-ray sources, photometric variables, and where binary information is known, short-period binary systems. Their evolution thus may be related to

[2]Particularly in globular clusters, these stars are also sometimes called "red stragglers." In this work, we prefer the term sub-subgiants for stars fainter than the subgiant branch, and red stragglers to describe stars to the red of the RGB, though these terms have sometimes been used interchangeably and both may form through the same mechanisms.

their status as close binary systems.

Mathieu et al. (2003) suggest SSGs may be products of close stellar encounters involving binaries, or stars with enhanced extinction (i.e. due to the presence of circumstellar material). Other authors invoke mass transfer and stellar collision events to form SSGs (Hurley et al. 2005; Albrow et al. 2001). In at least one case, a sub-subgiant has a pulsar companion, and it appears to be an undermassive giant evaporating due to the pulsar wind (Cohn et al. 2010; D'Amico et al. 2001; Ferraro et al. 2003; Bogdanov et al. 2010). Despite this speculation, no detailed models of SSG formation mechanisms had been presented in the literature prior to the publication of the work described in this thesis.

I put forth the first detailed formation models for these stars in Chapter 3, focusing on reproducing the observed stellar and binary characteristics of the sub-subgiants in M67 and NGC 6791. One hypothesis for formation is significant mass loss from a subgiant or giant star, either through standard Roche lobe overflow, or due to rapid envelope stripping, e.g. during dynamical encounters. The other is inhibition of convection in subgiants and giants due to the strong magnetic fields present in in short-period, tidally synchronized binaries with subgiant or giant primaries.

1.3.3 Main sequence-White dwarf binaries

It is worth noting that not all mass transfer or mergers must produce blue stragglers with temperatures and luminosities above the cluster turnoff. Lower luminosity analogues to the blue stragglers could be produced in theory, e.g. through mass accretion onto an initially lower-mass secondary, through highly non-conservative mass transfer, or through mergers of low-mass main sequence stars that produce stars with masses below the turnoff mass.

Many main-sequence-white dwarf (MS-WD) binaries have been identified in the field.

Very close MS-WD binaries can be detected in time-series photometric surveys if they are eclipsing (Parsons et al. 2015; Almenara et al. 2012; Breton et al. 2012), or from X-ray and transient surveys in cases where there is active accretion and/or outbursts (i.e. novae and cataclysmic variables) (Fornasini et al. 2014; Strope et al. 2010; Szkody et al. 2011). These systems are generally predicted to result from common envelope evolution, and are therefore early-stage binary evolution products and relatives of the blue stragglers. Recently, identification of large samples of nearby very wide MS-WD binaries has also been possible by looking for proper motion pairs in large photometric and proper motion surveys (Fouesneau et al. 2018), though these systems are so wide the two components are not expected to have ever interacted. MS-WD binaries with intermediate periods (orbits of tens to thousands of days, as would result from stable Case B/C/D mass transfer) are challenging to detect because they are neither close enough to be accreting or eclipsing, nor wide enough to be individually resolved. These binaries have been detected primarily from UV surveys, where hot white dwarf companions create significant UV excesses in the combined light (e.g. Jeffries & Stevens 1996; van Roestel et al. 2018; Parsons et al. 2016; Li et al. 2014; Rebassa-Mansergas et al. 2010, 2017). This method can detect a wide range of orbital periods, but is biased toward detecting cool primaries (K- and M-dwarfs) with very young and hot white dwarf companions, a combination which maximizes contrast in the UV between the two components. These K and M stars would be below the turnoff of even the oldest globular clusters, making them low-luminosity blue straggler analogs. These types of studies have generally been conducted in the field, where large samples of fairly nearby stars are available from surveys like GALEX, SDSS, or ROSAT. The resulting large samples of of MS-WD binaries are an important source of observational constraints for mass-transfer models, and particularly common envelope evolution.

In clusters, our knowledge of the analogous population is fairly limited. While X-

ray studies with Chandra and XMM as well as HST studies have identified samples of interacting white dwarf binaries (e.g. Edmonds et al. 1999; Belloni et al. 1998; Cool et al. 2013; Rivera Sandoval et al. 2018), samples of wider MS-WD are less developed. Targeted UV studies have identified individual clusters stars with very young white dwarf companions (Landsman et al. 1997, 1998; Subramaniam et al. 2016; Gosnell et al. 2015), largely targeting blue straggler stars, but the full population of cluster stars with white dwarf companions remains unknown. In Chapter 4, we pilot the use of a new method to identify recent mass transfer products in M67 based on stellar rotation rates.[3]

1.4 The Old Open Cluster M67

As discussed above, close binary systems evolve along different evolutionary pathways than single stars as the result of different types of mass exchange that occur in these systems. The primary aim of this thesis it to investigate the population of stars in the open cluster M67 that are following these alternative binary evolution channels. M67 is a very well studied old open cluster with a wealth of photometric and spectroscopic observations, making it ideally suited to such an in-depth study.

1.4.1 Observations

M67 (NGC 2682) is located at $\alpha = 8^h51^m23^s.3$, $\delta = +11°49'02''$. With a solar metallicity and age of 4 Gyr (Nissen et al. 1987; Demarque et al. 1992; Montgomery et al. 1993; Carraro et al. 1994; Fan et al. 1996; Balaguer-Núñez et al. 2007; Stello et al. 2016), it is one of the few old, metal rich clusters in the nearby galaxy. It is also relatively close

[3]Note this method may also detect merger/collision products that are rapidly rotating, stars which usually are not detectable below the cluster turnoff because they do not have distinctive companions or clear abundance tracers to indicate their history.

(800-900 pc, Janes & Smith 1984; Nissen et al. 1987; Montgomery et al. 1993; Sarajedini et al. 2009; Stello et al. 2016, with low extinction ($A_V = 0.12$), and a reddening of 0.041 (Taylor 2007).

M67 has been the subject of many photometric studies from the X-ray (Belloni et al. 1998; van den Berg et al. 2004; Mooley & Singh 2015), to the ultraviolet (Landsman et al. 1998), optical (Montgomery et al. 1993; Nissen et al. 1987; Anthony-Twarog 1987; Fan et al. 1996), and infrared (Cohen et al. 1978; Sarajedini et al. 2009). Several ground-based time-series photometric observations have also been done (Sandquist et al. 2003; Gilliland & Brown 1992; Stassun et al. 2002; van den Berg et al. 2002). Abundance studies have also been done in the cluster using spectroscopy and narrow-band imaging (Pancino et al. 2010; Friel et al. 2010; Önehag et al. 2014; Canto Martins et al. 2011; Souto et al. 2018). Kinematics for the cluster have also been studied, with several proper motion and radial-velocity studies available (Girard et al. 1989; Mathieu et al. 1990; Milone 1992; Yadav et al. 2008; Geller et al. 2015).

1.4.2 The WIYN Open Cluster Study

M67 is a foundational cluster of the WIYN Open Cluster study (Mathieu 2000). WOCS's goal is to establish a database of spectroscopic, photometric, and astrometric information for a selection of galactic open clusters spanning a range in age and metallicity. The collaboration has published several papers on M67, including photometry (Sarajedini et al. 2009), proper motions (Yadav et al. 2008), and analysis of abundances and activity indicators (Giampapa et al. 2006; Sills & Deliyannis 2000; Jacobson et al. 2011).

Most crucial for this thesis, Geller et al. (2015) published a comprehensive membership study of the cluster, incorporating memberships probabilities from several proper-motion studies and 30 years of radial-velocity observations from WOCS as well as measurements

pre-dating WOCS taken using the Havard-Smithsonian Center for Astrophysics Speedometers as well as other contemporaneous observations. This study covers a 30′ radius from the cluster center, extending to a limiting magnitude of V= 16.5, including the red giant branch, blue straggler region, and FGK-type main sequence stars. The study allows for clean separation of the cluster members from the field stars, and enables the identification of blue stragglers, yellow stragglers, and sub-subgiants in the cluster CMD (Figure 1.1).

1.4.3 The K2 M67 Study

Recently, M67 has been the focus of a dedicated observation campaign by the repurposed *Kepler* mission K2. The cluster was observed as part of K2 Campaign 5 using a combination of a $25' \times 25'$ "superstamp" region centered on the cluster in which data from all pixels were downloaded and processed, as well as individual targets outside the cluster center. The observations are primarily "long cadence" light curves, with measurements taken every 30 minutes. A few targets were also targeted for "short cadence" light curves, with measurements taken every 1 minute. Campaign 5 took data between 27 April 2015 and 10 July 2015. M67 was re-observed during K2 Campaign 16 (7 December 2017-5 February 2018). The field of view was only slightly different, allowing re-observation of most M67 stars observed in Campaign 5, and doubling the time baseline for the M67 light curves. M67 is also scheduled for more observations in Campaign 18 (2018 May 12- 2018 August 2) if the Kepler spacecraft continues to be operational. At the time of writing, only Campaign 5 data are processed and available. Campaign 16 light curves are scheduled for release in Summer 2018.

K2 observations of M67 have been quite valuable, particularly for studies of rotation and asteroseismology. Several stellar rotation and gyrochronology studies of M67 have been conducted as a result of the K2 observations (Barnes et al. 2016; Gonzalez 2016; Nardiello

et al. 2016), as well as an asteroseismic analysis of the cluster's red giant branch (Stello et al. 2016), and a detailed analysis of a new eclipsing binary system in the cluster (Sandquist et al. 2018). In this work, we use K2 light curves for an asteroseismic analysis (Leiner et al. 2016, Chapter 2) and to derive rotation periods for post-interaction main-sequence population of the cluster (Leiner et al. in prep, Chapter 4). No doubt these light curves will continue to yield new insights into stellar and binary evolution for many years to come.

1.5 Summary and Thesis Outline

Blue stragglers – stars brighter and bluer than the main sequence turnoff formed via binary mass-transfer, mergers, and stellar collisions – are one outcome of the early stages of binary evolution. Other early-stage binary-evolution products may include other outliers in the CMD such as yellow stragglers and sub-subgiants. In the field, white dwarf companions are found around all types of main-sequence stars including M-dwarfs, suggesting mass transfer can occur onto even very low-mass stars, but these are more difficult to detect in clusters because they blend photometrically with standard main-sequence populations. Similarly, evolved blue stragglers may exist in clusters, but have gone undetected because they fall within the photometric scatter of the red giant branch. In this thesis I seek to move beyond the blue stragglers to understand these other understudied products of binary evolution. To do so, I use the old open cluster M67 as an exemplar, studying the non-standard populations found in the cluster with a combination of stellar/binary evolution modeling, archival spectra, astrometry, photometry and light curves from the K2 M67 campaign. In Chapter 2, I perform an asteroseismic analysis on a yellow straggler in M67, producing the first precise mass and radius estimates for a yellow straggler star. In Chapter 3, I focus on the sub-subgiants in M67 as well as another old open cluster NGC 6791, developing the first detailed theoretical models of possible formation mechanisms. In

Chapter 4, I use rotation information from Kepler/K2 to identify candidate post-interaction stars on the M67 main-sequence. Finally, in Chapter 5 I summarize the significance of these results and discuss future directions of binary stellar evolution research in clusters and beyond.

References

Aarseth, S. J. 2001, NewA, 6, 277

Abate, C., Pols, O. R., Izzard, R. G., Mohamed, S. S., & de Mink, S. E. 2013, A&A, 552, A26

Albrow M. D., Gilliland R. L., Brown T. M., Edmonds P. D., Guhathakurta P., Sarajedini A., 2001, ApJ, 559, 1060

Almenara, J. M., Alonso, R., Rabus, M., et al. 2012, MNRAS, 420, 3017

Andronov, N., Pinsonneault, M. H., & Terndrup, D. M. 2006, ApJ, 646, 1160

Anthony-Twarog, B. J. 1987, AJ, 93, 647

Bailyn, C. D. 1992, ApJ, 392, 519

Balaguer-Núñez, L., Galadí-Enríquez, D., & Jordi, C. 2007, A&A, 470, 585

Barnes, S. A., Weingrill, J., Fritzewski, D., Strassmeier, K. G., & Platais, I. 2016, ApJ, 823, 16

Beccari, G., Ferraro, F. R., Lanzoni, B., & Bellazzini, M. 2006, ApJ, 652, L121

Belloni, T., Verbunt, F., & Mathieu, R. D. 1998, A&A, 339, 431

Benz, W., & Hills, J. G. 1987, ApJ, 323, 614

Bogdanov S., van den Berg M., Heinke C. O., Cohn H. N., Lugger P. M., Grindlay J. E., 2010, ApJ, 709, 241

Breton, R. P., Rappaport, S. A., van Kerkwijk, M. H., & Carter, J. A. 2012, ApJ, 748, 115

Brogaard K. et al., 2012, A&A, 543, A106

Canto Martins, B. L., Lèbre, A., Palacios, A., et al. 2011, A&A, 527, A94

Carney, B. W., Latham, D. W., Laird, J. B., Grant, C. E., & Morse, J. A. 2001, AJ, 122, 3419

Carney, B. W., Lee, J.-W., & Dodson, B. 2005, AJ, 129, 656

Carraro, G., Chiosi, C., Bressan, A., & Bertelli, G. 1994, A&AS, 103, 375

Chatterjee, S., Rasio, F. A., Sills, A., & Glebbeek, E. 2013, ApJ, 777, 106

Chen, H.-L., Woods, T. E., Yungelson, L. R., Gilfanov, M., & Han, Z. 2014, MNRAS, 445, 1912

Chen, X., & Han, Z. 2008a, MNRAS, 384, 1263

Chen, X., & Han, Z. 2008, MNRAS, 387, 1416

Cohen, J. G., Persson, S. E., & Frogel, J. A. 1978, ApJ, 222, 165

Cohn H. N. et al., 2010, ApJ, 722, 20

Cool, A. M., Haggard, D., Arias, T., et al. 2013, ApJ, 763, 126

Corsaro, E., Stello, D., Huber, D., et al. 2012, ApJ, 757, 190

D'Amico N., Possenti A., Manchester R. N., Sarkissian J., Lyne A. G., Camilo F., 2001, ApJ, 561, L89

Davies, M. B., Piotto, G., & de Angeli, F. 2004, MNRAS, 349, 129

Dalessandro, E., Ferraro, F. R., Massari, D., et al. 2013, ApJ, 778, 135

Demarque, P., Green, E. M., & Guenther, D. B. 1992, AJ, 103, 151

Edmonds, P. D., Grindlay, J. E., Cool, A., et al. 1999, ApJ, 516, 250

Eggleton, P. P. 1983, ApJ, 268, 368

Escorza, A., Boffin, H. M. J., Jorissen, A., et al. 2017, A&A, 608, A100

Fan, X., Burstein, D., Chen, J.-S., et al. 1996, AJ, 112, 628

Ferraro, F. R., Lapenna, E., Mucciarelli, A., et al. 2016, ApJ, 816, 70

Ferraro F. R., Sabbi E., Gratton R., Possenti A., D'Amico N., Bragaglia A., Camilo F., 2003, ApJ, 584, L13

Ferraro, F. R., Sabbi, E., Gratton, R., et al. 2006, ApJ, 647, L53

Ferraro, F. R., Beccari, G., Dalessandro, E., et al. 2009, Nature, 462, 1028

Ferraro, F. R., Messineo, M., Fusi Pecci, F., et al. 1999, AJ, 118, 1738

Fornasini, F. M., Tomsick, J. A., Bodaghee, A., et al. 2014, ApJ, 796, 105

Fouesneau, M., Rix, H.-W., von Hippel, T., Hogg, D. W., & Tian, H. 2018, ArXiv e-prints, arXiv:1802.06663

Fregeau, J. M., Cheung, P., Portegies Zwart, S. F., & Rasio, F. A. 2004, MNRAS, 352, 1

Friel, E. D., Jacobson, H. R., & Pilachowski, C. A. 2010, AJ, 139, 1942

Geller, A. M., Hurley, J. R., & Mathieu, R. D. 2013, AJ, 145, 8

Geller, A. M., Latham, D. W., & Mathieu, R. D. 2015, AJ, 150, 97

Geller, A. M., & Mathieu, R. D. 2011, Nature, 478, 356

Geller, A. M., Mathieu, R. D., Harris, H. C., & McClure, R. D. 2008, AJ, 135, 2264

—. 2009, AJ, 137, 3743

Geller, A. M., Leiner, E. M., Bellini, A., et al. 2017, ApJ, 840, 66

Giampapa, M. S., Hall, J. C., Radick, R. R., & Baliunas, S. L. 2006, ApJ, 651, 444

Gilliland, R. L., & Brown, T. M. 1992, AJ, 103, 1945

Girard T. M., Grundy W. M., Lopez C. E., van Altena W. F., 1989, AJ, 98, 227

Gonzalez, G. 2016, MNRAS, 463, 3513

Gosnell, N. M., Mathieu, R. D., Geller, A. M., et al. 2015, ApJ, 814, 163

—. 2014, ApJ, 783, L8

Handberg, R., Brogaard, K., Miglio, A., et al. 2017, MNRAS, 472, 979

Hansen, C. J., Nordström, B., Hansen, T. T., et al. 2016, A&A, 588, A37

Heggie, D. C. 1975, MNRAS, 173, 729

Hills, J. G., & Day, C. A. 1976, Astrophys. Lett., 17, 87

Hjellming, M. S., & Webbink, R. F. 1987, ApJ, 318, 794

Hurley, J. R., Tout, C. A., & Pols, O. R. 2002, MNRAS, 329, 897

Hurley J. R., Pols O. R., Aarseth S. J., Tout C. A., 2005, MNRAS, 363, 293

Hut, P., & Bahcall, J. N. 1983, ApJ, 268, 319

Ivanova, N., Heinke, C. O., Rasio, F. A., Belczynski, K., & Fregeau, J. M. 2008, MNRAS, 386, 553

Ivanova, N., Justham, S., Chen, X., et al. 2013, The Astronomy and Astrophysics Review, 21, 59

Jacobson, H. R., Pilachowski, C. A., & Friel, E. D. 2011, AJ, 142, 59

Janes, K. A., & Smith, G. H. 1984, AJ, 89, 487

Jeffries, R. D., & Stevens, I. R. 1996, MNRAS, 279, 180

Jorissen, A., Van Eck, S., Mayor, M., & Udry, S. 1998, A&A, 332, 877

Jorissen, A., Van Eck, S., Van Winckel, H., et al. 2016, A&A, 586, A158

Knigge, C., Leigh, N., & Sills, A. 2009, Nature, 457, 288

Kulkarni, S. R., Ofek, E. O., Rau, A., et al. 2007, Nature, 447, 458

Landsman, W., Aparicio, J., Bergeron, P., Di Stefano, R., & Stecher, T. P. 1997, ApJ, 481, L93

Landsman, W., Bohlin, R. C., Neff, S. G., et al. 1998, AJ, 116, 789

Latham, D. W. 2007, Highlights of Astronomy, 14, 444

Leigh, N., Knigge, C., Sills, A., et al. 2013, MNRAS, 428, 897

Leiner, E., Mathieu, R. D., Stello, D., Vanderburg, A., & Sandquist, E. 2016, ApJ, 832, L13

Leonard, P. J. T. 1989, AJ, 98, 217

Li, L., Zhang, F., Han, Q., Kong, X., & Gong, X. 2014, MNRAS, 445, 1331

Lidov, M. L. 1962, Planet. Space Sci., 9, 719

Lombardi, C., Rasio, F. A., & Shapiro, S. L. 1995, ApJ, 445, L117

Lucatello, S., Tsangarides, S., Beers, T. C., et al. 2005, ApJ, 625, 825

Mapelli, M., Sigurdsson, S., Colpi, M., et al. 2004, ApJ, 605, L29

Mathieu, R. D. 2000, in ASP Conf. Ser., Vol. 198, Stellar Clusters and Associations: Convection, Rotation, and Dynamos, ed. R. Pallavicini, G. Micela, & S. Sciortino, 517

Mathieu R. D., van den Berg M., Torres G., et al., 2003, AJ, 125, 246

Mathieu, R. D., & Geller, A. M. 2009, Nature, 462, 1032

Mathieu, R. D., Latham, D. W., & Griffin, R. F. 1990, AJ, 100, 1859

McClure, R. D., & Woodsworth, A. W. 1990, ApJ, 352, 709

McCrea, W. H. 1964, MNRAS, 128, 147

McMillan, S., Hut, P., & Makino, J. 1990, ApJ, 362, 522

Merle, T., Jorissen, A., Van Eck, S., Masseron, T., & Van Winckel, H. 2016, A&A, 586, A151

Milliman, K. E., Leiner, E. L., Mathieu, R. D., & Tofflemire, B. M. 2016, AJ, arXiv:1408.0239

Milliman, K. E., Mathieu, R. D., & Schuler, S. C. 2015, AJ, 150, 84

Milliman, K. E., Mathieu, R. D., Geller, A. M., et al. 2014, AJ, 148, 38

Milone, A. A. E. 1992, PASP, 104, 1268

Milone, A. P., Piotto, G., Bedin, L. R., et al. 2012, A&A, 540, A16

Mohamed, S., & Podsiadlowski, P. 2012, Baltic Astronomy, 21, 88

Montgomery, K. A., Marschall, L. A., & Janes, K. A. 1993, AJ, 106, 181

Mooley, K. P., & Singh, K. P. 2015, MNRAS, 452, 3394

Naoz, S., & Fabrycky, D. C. 2014, ApJ, 793, 137

Nardiello, D., Libralato, M., Bedin, L. R., et al. 2016, MNRAS, 455, 2337

Nissen, P. E., Twarog, B. A., & Crawford, D. L. 1987, AJ, 93, 634

Önehag, A., Gustafsson, B., & Korn, A. 2014, A&A, 562, A102

Paczyński, B. 1971, ARA&A, 9, 183

Paczynski, B. 1976, in IAU Symposium, Vol. 73, Structure and Evolution of Close Binary Systems, ed. P. Eggleton, S. Mitton, & J. Whelan, 75

Pancino, E., Carrera, R., Rossetti, E., & Gallart, C. 2010, A&A, 511, A56

Parsons, S. G., Rebassa-Mansergas, A., Schreiber, M. R., et al. 2016, MNRAS, 463, 2125

Parsons, S. G., Agurto-Gangas, C., Gänsicke, B. T., et al. 2015, MNRAS, 449, 2194

Passy, J.-C., Herwig, F., & Paxton, B. 2012, ApJ, 760, 90

Pavlovskii, K., & Ivanova, N. 2015, MNRAS, 449, 4415

Perets, H. B., & Fabrycky, D. C. 2009, ApJ, 697, 1048

Piotto, G., De Angeli, F., King, I. R., et al. 2004, ApJ, 604, L109

Preston, G. W., & Sneden, C. 2000, AJ, 120, 1014

Raghavan, D., McAlister, H. A., Henry, T. J., et al. 2010, ApJS, 190, 1

Rebassa-Mansergas, A., Gänsicke, B. T., Schreiber, M. R., Koester, D., & Rodríguez-Gil, P. 2010, MNRAS, 402, 620

Rebassa-Mansergas, A., Ren, J. J., Irawati, P., et al. 2017, MNRAS, 472, 4193

Rivera Sandoval, L. E., van den Berg, M., Heinke, C. O., et al. 2018, MNRAS, 475, 4841

Sana, H., Gosset, E., Nazé, Y., Rauw, G., & Linder, N. 2008, MNRAS, 386, 447

Sandquist, E. L., Latham, D. W., Shetrone, M. D., & Milone, A. A. E. 2003, AJ, 125, 810

Sandquist, E. L., Mathieu, R. D., Quinn, S. N., et al. 2018, AJ, 155, 152

Santucci, R. M., Placco, V. M., Rossi, S., et al. 2015, ApJ, 801, 116

Sarajedini, A., Dotter, A., & Kirkpatrick, A. 2009, ApJ, 698, 1872

Shetrone, M. D., & Sandquist, E. L. 2000, AJ, 120, 1913

Sills A., Karakas A., Lattanzio J., 2009, ApJ, 692, 1411

Sills, A., Adams, T., & Davies, M. B. 2005, MNRAS, 358, 716

Sills, A., Adams, T., Davies, M. B., & Bate, M. R. 2002, MNRAS, 332, 49

Sills, A., Faber, J. A., Lombardi, Jr., J. C., Rasio, F. A., & Warren, A. R. 2001, ApJ, 548, 323

Sills, A., & Deliyannis, C. P. 2000, ApJ, 544, 944

Sollima, A., Lanzoni, B., Beccari, G., Ferraro, F. R., & Fusi Pecci, F. 2008, A&A, 481, 701

Souto, D., Cunha, K., Smith, V. V., et al. 2018, ArXiv e-prints, arXiv:1803.04461

Stassun, K. G., van den Berg, M., Mathieu, R. D., & Verbunt, F. 2002, A&A, 382, 899

Stello D., Meibom S., Gilliland R. L., et al., 2011, ApJ, 739, 13

Stello, D., Vanderburg, A., Casagrande, L., et al. 2016, ApJ, 832, 133

Strope, R. J., Schaefer, B. E., & Henden, A. A. 2010, AJ, 140, 34

Subramaniam, A., Sindhu, N., Tandon, S. N., et al. 2016, ApJ, 833, L27

Szkody, P., Anderson, S. F., Brooks, K., et al. 2011, AJ, 142, 181

Taylor, B. J. 2007, AJ, 133, 370

Tout, C. A., & Eggleton, P. P. 1988, MNRAS, 231, 823

Tylenda, R., Hajduk, M., Kamiński, T., et al. 2011, A&A, 528, A114

van den Berg, M., Stassun, K. G., Verbunt, F., & Mathieu, R. D. 2002, A&A, 382, 888

van den Berg, M., Tagliaferri, G., Belloni, T., & Verbunt, F. 2004, A&A, 418, 509

Van der Swaelmen, M., Boffin, H. M. J., Jorissen, A., & Van Eck, S. 2017, A&A, 597, A68

van Roestel, J., Kupfer, T., Ruiz-Carmona, R., et al. 2018, MNRAS, 475, 2560

Webbink, R. F. 1976, ApJ, 209, 829

Woods, T. E., & Ivanova, N. 2011, ApJ, 739, L48

Xin, Y., Ferraro, F. R., Lu, P., et al. 2015, ApJ, 801, 67

Yadav, R. K. S., Bedin, L. R., Piotto, G., et al. 2008, A&A, 484, 609

Chapter 2

An Evolved Blue Straggler in M67 from K2 Mission Asteroseismology

A version of this chapter has previously appeared in the Astrophysical Journal Letters

Leiner, et al. 2016, ApJ, 832, L13

Abstract

Yellow straggler stars (YSSs) fall above the subgiant branch in optical color-magnitude diagrams, between the blue stragglers and the red giants. YSSs may represent a population of evolved blue stragglers, but none have the direct and precise mass and radius measurements needed to determine their evolutionary states and formation histories. Here we report the first asteroseismic mass and radius measurements of such a star, the yellow straggler S1237 in the open cluster M67. We apply asteroseismic scaling relations to a frequency analysis of the *Kepler* K2 light curve and find a mass of 2.9 ± 0.2 $M_\odot$ and a radius of 9.2 ± 0.2 $R_\odot$. This is more than twice the mass of the main-sequence turnoff in M67, suggesting S1237 is indeed an evolved blue straggler. S1237 is the primary in a spectroscopic binary. We update the binary orbital solution and use spectral energy distribution (SED) fitting to constrain the color-magnitude diagram (CMD) location of the secondary star. We find that the secondary is likely an upper main-sequence star near the turnoff, but a slightly hotter blue straggler companion is also possible. We then compare the asteroseismic mass of the primary to its mass from CMD fitting, finding the photometry implies a mass and radius more than 2σ below the asteroseismic measurement. Finally, we consider formation mechanisms for this star and suggest that S1237 may have formed from dynamical encounters resulting in stellar collisions or a binary merger.

2.1 Introduction

In color-magnitude diagrams (CMDs) of open clusters, stars are observed between the blue straggler stars (BSSs) and the red giant branch (RGB). We call these yellow straggler stars (YSSs). In M67, a ∼4 Gyr, solar-metallicity open cluster (Taylor 2007; Montgomery, Marschall & Janes 1993), there are four 3D kinematic members found in this CMD region. Three are binary systems, and one is a single star (Geller, Latham & Mathieu 2015). While some YSSs might be explained as the combined light of two cluster stars (e.g., a red giant-blue straggler binary), many may be evolved BSSs (Mathieu, Latham & Griffin 1990). These stars would be post-main-sequence stars more massive than the main-sequence turnoff (MSTO).

BSSs are thought to form from mass transfer in binary systems (McCrea 1964; Gosnell et al. 2014), stellar collisions during dynamical encounters (Leonard 1989), or binary mergers induced by Kozai cycles (Perets & Fabrycky 2009). In M67, one of the four YSSs has a helium white dwarf (WD) companion, suggesting it is an evolved BSS formed from mass transfer (Landsman et al. 1997).

Asteroseismic analysis of *Kepler* stars have uncovered red giants in open clusters more massive than the cluster standard (Stello et al. 2011; Brogaard et al. 2012; Corsaro et al. 2012). These stars are called evolved blue straggler stars (E-BSSs). They fall in or near their clusters' red clumps, but YSSs may be bluer examples of the E-BSSs, making them more identifiable in cluster CMDs. Mass measurements for YSSs are needed to confirm this hypothesis.

Recent data from the *Kepler* K2 mission allow for the asteroseismic measurement of stellar masses and radii in M67 (Stello et al. 2016b), providing an exciting opportunity to

study the YSSs in this cluster. Here we report the first determination of an asteroseismic mass and radius for the primary star in the M67 binary YSS S1237 (Sanders 1977). We summarize radial-velocity (RV) and X-ray observations of S1237, and use the spectral energy distribution (SED) to constrain the mass of the secondary star. We compare the asteroseismic mass to the primary mass implied from its CMD position, and comment on possible formation pathways for this star.

2.2 Asteroseismic Measurements

M67 was observed during Campaign 5 of the *Kepler* K2 mission, providing high-precision 75-day light curves for targets in the cluster. Light curves were obtained using the method of Vanderburg & Johnson (2014).

The light curve of YSS S1237 shows solar-like oscillations and our seismic analysis followed the same approach as Stello et al. (2016b). We processed the light curve of S1237 as in Stello et al. (2015) and used the pipeline of Huber et al. (2009) to extract

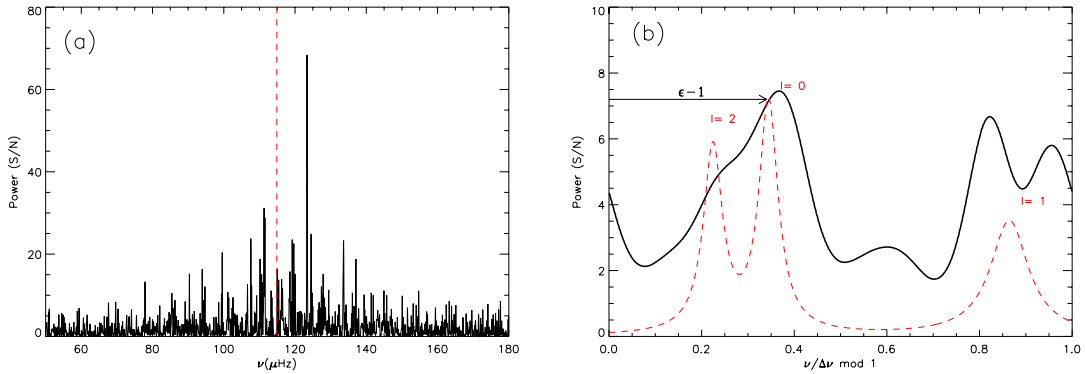

Figure 2.1 : **(a)** Background corrected power spectrum of S1237. The dashed red line shows the location of $\nu_{\rm max}$. **(b)** Folded and smoothed spectrum of the central $\pm 2\Delta\nu$ range around $\nu_{\rm max}$ (black curve). The red dashed line shows an empirical model representing the average of a large ensemble of red giants used to measure ϵ and determine the location of the different modes (Stello et al. 2016a,b). The arrow indicates the offset from zero of the radial modes.

the large frequency separation ($\Delta\nu$)) and frequency of maximum power ($\nu_{\rm max}$) from the Fourier frequency spectra of the light curve. From these global frequencies, we used the asteroseismic scaling relations, $\Delta\nu \propto \sqrt{M/R^3}$ and $\nu_{\rm max} \propto M/(R^2\sqrt{T_{\rm eff}})$ (e.g. Kjeldsen & Bedding 1995), to determine a mass and radius for the star.

$$\frac{M}{M_\odot} = \left(\frac{\Delta\nu}{\Delta\nu_\odot}\right)^{-4}\left(\frac{\nu_{\rm max}}{\nu_{\rm max_\odot}}\right)^{-3}\left(\frac{T_{\rm eff}}{T_{\rm eff_\odot}}\right)^{\frac{3}{2}} \tag{2.1}$$

$$\frac{R}{R_\odot} = \left(\frac{\Delta\nu}{\Delta\nu_\odot}\right)^{-2}\left(\frac{\nu_{\rm max}}{\nu_{\rm max_\odot}}\right)\left(\frac{T_{\rm eff}}{T_{\rm eff_\odot}}\right)^{\frac{1}{2}} \tag{2.2}$$

The $\Delta\nu$ scaling relation needs a small metallicity- and temperature-dependent correction (e.g. White et al. 2011). To derive this correction factor, $f_{\Delta\nu}$, we adopt $T_{\rm eff} = 4997 \pm 91$ K and [Fe/H]$= 0.072 \pm 0.033$ (from APOGEE[1]; Holtzman et al. 2015), which we feed into the correction interpolator of Sharma et al. (2016). We derive two correction factors, one assuming the star is helium-core burning (HeB) and the other assuming it is an RGB star. We obtain R = 9.27 $\pm$ 0.19 $R_\odot$ and M = 2.97 $\pm$ 0.24 $M_\odot$ for a HeB star, or R = 9.21 $\pm$ 0.19 $R_\odot$ and M = 2.94 $\pm$ 0.24 $M_\odot$ for an RGB star (Table 2.1). The errors on mass and radius come from propagating errors on $T_{\rm eff}$, $\Delta\nu$,and $\nu_{\rm max}$ through Equations 2.1 and 2.2.

Our results seem to indicate this is a HeB star. A 2.6-2.9 $M_\odot$ star with this radius would be in the Hertzsprung Gap, and thus is unlikely to be observed. The power spectrum also shows broader peaks and more blended $l = 0$ and $l = 2$ modes than typical of RGB stars. We show the full power spectrum in Figure 2.1a, as well as the central $\pm 2\Delta\nu$ around $\nu_{\rm max}$ folded on $\Delta\nu$ and smoothed with a Gaussian as in Stello et al. (2016a) (Figure 2.1b). The folded spectrum shows a broad series of multiple peaks around the location of the dipole ($l = 1$) mode. This is indicative of a large period spacing between dipole mixed

[1]http://www.sdss.org/surveys/apogee/

Table 2.1 : Parameters for S1237

General		
RA	8:51:50.20	
Dec.	11:46:07.0	
EPIC ID	211408357	
WOCS ID[1]	1015	
Sanders ID[2]	S1237	
Updated Binary Orbital Parameters		
Period (P) (days)	698.4	$\pm$0.3
Eccentricity (e)	0.087	$\pm$0.015
Amplitude (K) (km s^{-1})	5.024	$\pm$0.071
f(m) ($M_\odot$)	0.0091	$\pm$0.0004
Old Binary Orbital Paramters[3]		
Period (P) (days)	697.8	$\pm$0.7
Eccentricity (e)	0.105	$\pm$0.015
Amplitude (K) (km s^{-1})	5.03	$\pm$0.07
f(M)) ($M_\odot$)	0.0091	$\pm$0.0004
Measured $\Delta\nu$-scaling		
$\nu_{\rm max}$ (μHz)	114.89	$\pm$2.06
$\Delta\nu$ (μHz)	8.32	$\pm$0.11
Radius ($R_\odot$)	9.11	$\pm$0.18
Mass ($M_\odot$)	2.87	$\pm$0.23
Surface gravity (log g)	2.98	$\pm$ 0.01
Corrected $\Delta\nu$-scaling assuming RGB		
$f_{\Delta\nu}$	1.0057	
Radius ($R_\odot$)	9.21	$\pm$ 0.19
Mass ($M_\odot$)	2.94	$\pm$ 0.24
Corrected $\Delta\nu$-scaling assuming HeB		
$f_{\Delta\nu}$	1.0089	
Radius ($R_\odot$)	9.27	$\pm$ 0.19
Mass ($M_\odot$)	2.97	$\pm$ 0.24

[1]from Geller, Latham & Mathieu (2015)

[2]from Sanders (1977)

[3]from Mathieu, Latham & Griffin (1990)

modes (Bedding et al. 2011) and of a larger coupling between the envelope and core of the star (Dupret et al. 2009), both suggestive of a HeB star. In Figure 2.1b we also measure ϵ, the offset from zero of the radial modes ($l = 0$), by correlating the spectrum with a model profile following Stello et al. (2016a). We find $\epsilon = 1.34$, outside the range for an RGB star (Stello et al. 2016a, Fig. 2).

2.3 Other Observations

2.3.1 Updated Orbit

Updating the orbital solution from Mathieu, Latham & Griffin (1990) with additional RVs from the WIYN Open Cluster Study (WOCS; Mathieu 2000), we find the orbital parameters do not change significantly (see Table 2.1). The system is a near-circular 698-day period spectroscopic binary.

The system is single-lined in the WOCS spectra ($R \sim 15,000$). Given the small amplitude of the orbit and the fact that any MS companion would be more than 2 magnitudes fainter than a ~ 9.0 $R_\odot$ giant primary, we do not expect to see the features of the secondary at the signal to noise of the WOCS spectra,. Higher resolution, high signal-to-noise spectra may allow detection of the secondary. For a primary of 2.9 $M_\odot$, the binary mass function ($f(m_1, m_2) = 0.0091$) indicates a secondary with $m_2 \geq 0.46$ $M_\odot$.

2.3.2 X-ray Observations

S1237 has a 0.3-7 KeV luminosity of $L_x = 5.5 \times 10^{29}$ ergs s^{-1}, comparable to what is expected from rapid rotation (van den Berg et al. 2004). However, WOCS spectra of the primary provide an upper limit on the v sin i of 10 km s^{-1} set by the instrumental broadening and the binary is too wide for rapid rotation to be expected from tidal synchronization. Belloni, Verbunt & Mathieu (1998) also detect S1237 as an X-ray source

and find no satisfactory explanation. We discuss a possible explanation for this X-ray emission in Section 2.6.

2.3.3 SED Fitting

We have assembled an SED from existing UBVI photometry (Montgomery, Marschall & Janes 1993), the Two-Micron All Sky Survey (2MASS; Skrutskie et al. 2006), Wide Field Infrared Explorer (WISE; Wright et al. 2010), and the Galaxy Evolution Explorer (GALEX; Martin et al. 2005).

We use χ^2 minimization to fit the observed SED to a grid of models. We first fit a model of the primary to the 2MASS and WISE data. These IR measurements should be dominated by the flux from the primary, whereas the optical and UV flux may be contaminated by flux from a MS secondary. We model the primary with a 4500-5500 K giant spectrum (Castelli & Kurucz 2004) in steps of 50 K in order to bracket the the APOGEE $T_{\rm eff}$ of 4997 ± 91 K. We use a grid of radii between 8.0-10.0 $R_\odot$ in 0.1 $R_\odot$ increments. We fix the surface gravity to log g= 3.0 from asteroseismic scaling (Table 1). We use distances of either 800, 850, or 900 pc based on the range given in the literature (Geller, Latham & Mathieu 2015). We adopt E(B-V)= 0.041 (Taylor 2007) and the extinction curve of Cardelli, Clayton & Mathis (1989).

The best-fit SED temperature and radius only fall within the 3σ errors on the APOGEE temperature and the asteroseismic radius if we use a distance of 900 pc. Using 900 pc, we find a best-fit of 8.8 $R_\odot$and 4900 K (see Figure 2.2b). Using this model for our primary, we find a significant flux excess over the model in all of the bluer bands (FUV, NUV, U, B, V) indicating the presence of a secondary (see Figure 2.2a). Fixing the primary to these best-fit values, we model the secondary using a fixed surface gravity of log g= 4.5 (typical for a MS star), a grid of temperatures between 5000-8000 K in steps of 250 K, and

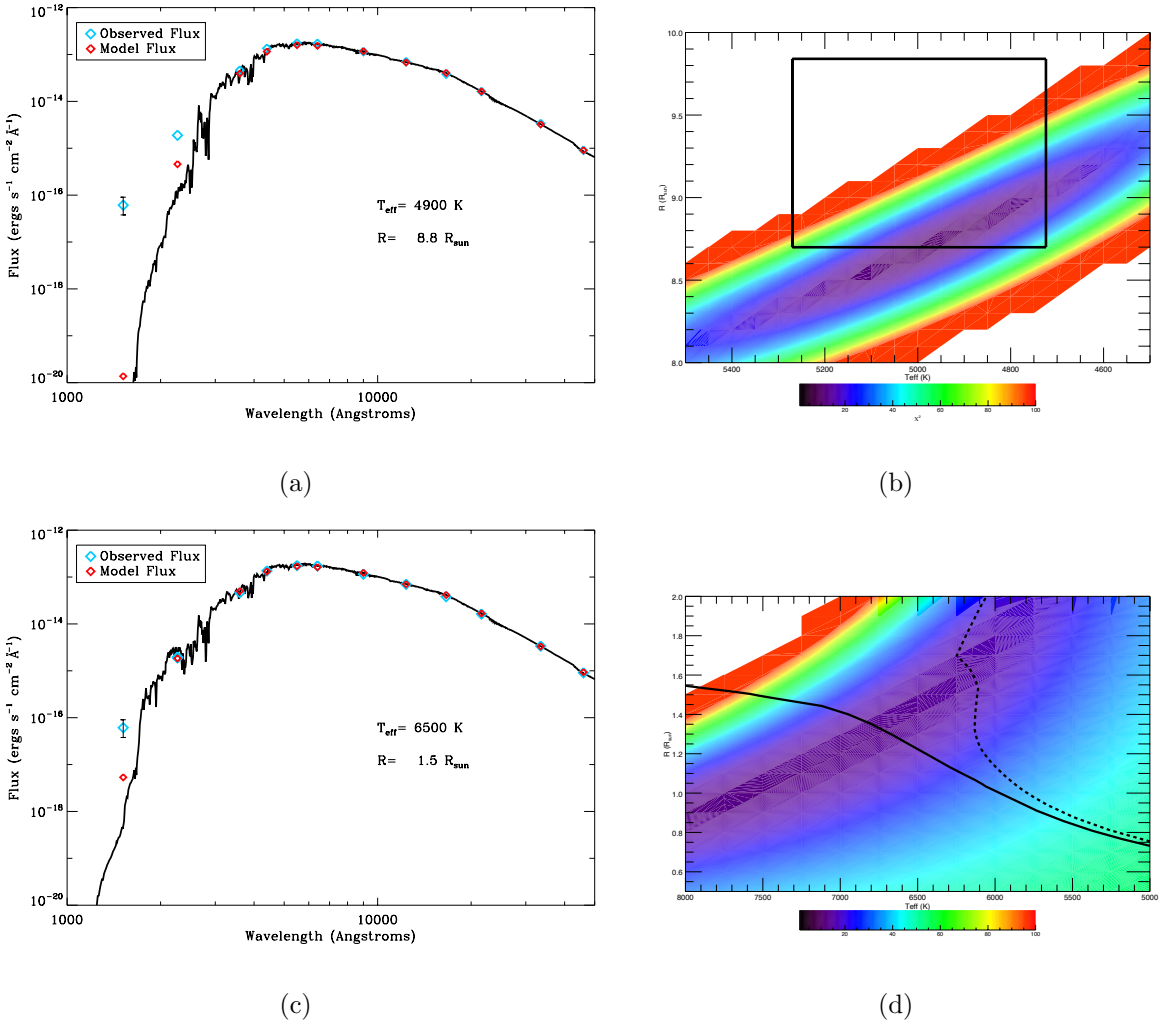

Figure 2.2 : **(a)** The observed SED of S1237 (blue points) compared to our best fitting model of a 8.8 $R_\odot$, 4900 K giant (black line). The red points indicate the model flux when the SED is convolved with the filter transmission functions. **(b)** A χ^2 map resulting from fitting a grid of models for the primary to the 2MASS and WISE observations of S1237. The color indicates the χ^2 value from smallest (purple) to largest (red). The black box bounds the area within 3σ of the APOGEE $T_{\rm eff}$ and the asteroseismic radius. **(c)** The observed SED of S1237 compared to a model of the combined light of a 4900 K, 8.8 $R_\odot$ giant and a 6500 K, 1.5 $R_\odot$ MS star. **(d)** A χ^2 map resulting from fitting a grid of models containing a 4900 K, 8.8 $R_\odot$ giant and various MS secondaries.. The solid black line indicates the zero-age main-sequence, and the dashed black line is a 4 Gyr isochrone.

secondary radii between 0.5 $R_\odot$-2.0 $R_\odot$ in steps of 0.1 $R_\odot$.

We find that a variety of secondary models result in χ^2 values near the minimum with temperatures of 6250-8000 K and radii of 0.5-1.8 $R_\odot$, but if we restrict the radius to fall between the ZAMS radius and the radius at 4 Gyr for a given temperature, we find the best fit to be a ∼6250-6750 K, 1.2-1.6 $R_\odot$ star (Figure 2.2c, d). This range includes both stars on the upper main-sequence in M67, as well as blue straggler stars near the MSTO. For simplicity, we assume the star is on the upper MS when considering formation scenarios, but the possibility that the secondary is a blue straggler is worth follow up, i.e. with higher resolution spectra that could detect the secondary.

We note there is a GALEX FUV excess in the SED (Figure 2.2c), but we do not consider this excess to be meaningful. Castelli-Kurucz models have poor resolution in the FUV, and a few unresolved emission lines can change the flux substantially. In fact, MS stars near the turn off in M67 have widely varying GALEX FUV fluxes, and several are observed to have comparable FUV magnitudes.

2.4 Photometric versus Asteroseismic Mass

In Figure 2.3 we decompose the light of the binary to show the location of the primary and the secondary in a CMD. We show two possible deconvolutions: an MS secondary and a BSS secondary. The secondary is fixed to either a 6750 K BSS (red circle), or a 6250 K MS star near the turnoff (orange circle). The primary is a $\sim$ 4900 K giant.

We compare the CMD position of the primary and secondary to evolutionary tracks using Modules for Experiments in Stellar Astrophysics (MESA; Paxton et al. 2015). We use the test suite case `1M_pre_ms_to_wd` changing only the mass and turning off RGB and AGB wind mass loss. The CMD location of the primary is fainter than expected from MESA models for a giant with a mass and radius within 1σ of the asteroseismic measurements.

To bring the photometry and asteroseismology into agreement requires using a distance at the highest range of those determined in the literature for M67 (900 pc), and a primary mass and radius of ~ 2.4 $M_\odot$ and ~ 8.8 $R_\odot$, more than 2σ below the asteroseismic values. The BSS and MSTO secondary fall on evolutionary tracks for a ~ 1.4 and ~ 1.3 $M_\odot$ star, respectively.

While using a distance of 900 pc to M67 creates the best agreement between the asteroseismic mass and the photometry for S1237, Stello et al. (2016b) find an asteroseismic distance to M67 of 816 ± 11 pc based on the entire sample of red giants in M67. Using 816 pc results in a photometric mass and radius for the primary more than 3σ below the asteroseismic values. Depending on the distance used, the asteroseismic results may be $15 - 30\%$ and $\sim 5\%$ higher than the photometric mass and radius, respectively.

Some recent studies comparing *Kepler* masses and radii from uncorrected asteroseismic scaling relations and RGB eclipsing binaries have found systematic differences between the two measurements (e.g. Brogaard et al. 2016, Gaulme et al. 2016) similar to the size of the discrepancy we find. We have used corrected scaling relations, which should provide better agreement (Sharma et al. 2016), and Stello et al. (2016b) find that the average RGB mass in M67 from corrected scaling relations is consistent with eclipsing binary results for the cluster. However, the scaling relations have not been well validated by independent measurements (e.g. comparison to eclipsing binaries or cluster isochrones) for HeB stars at masses as large as 2.9 $M_\odot$, and it is therefore possible that the corrections that work for lower mass stars can not be extrapolated to stars of such high mass. This uncertainty is not reflected in our errors. We encourage more tests of the scaling relations for massive HeB stars to shed light on this possible discrepancy.

Alternatively, S1237 may be following a non-standard evolutionary track due to past mass transfer, a merger, or a stellar collision. However, models of the evolution of mass-

transfer products predict they return to close-to-normal evolution soon after mass transfer has ceased (Tian et al. 2006). Models of stellar collision products are bluer and brighter than standard evolutionary tracks due to enhanced mixing enriching the star in helium, although this difference is minor on the giant branch (Sills et al. 1997; Sills, Karakas & Lattanzio 2009). Our results indicate the opposite: the star is less luminous and redder than expected given its asteroseismic mass. APOGEE C, N, and Fe abundances do not appear unusual, but a more careful abundance analysis may prove interesting.

2.5 Formation Pathways

2.5.1 Time Since Formation

Using MESA we estimate the primary's age to be 450 Myr if it is a 2.9 $M_\odot$ HeB star. This is likely an overestimate, as it assumes the primary begins with a core that has not burned through any hydrogen. In reality, this star likely formed by adding material to a lower mass MS star to create a BSS. The MS progenitor would already have gone through $\sim$3.5 Gyr of evolution, perhaps resulting in a core substantially depleted of hydrogen. This translates to a shorter lifetime for the star once it becomes a BSS.

If we consider a 2.4 $M_\odot$ star, $\sim$2 σ lower than the asteroseismic value but consistent with the mass implied from its CMD position, the lifetime is $\sim$750 Myr. This longer lifetime would result in a more massive MSTO at the time of formation, and the lower mass makes it more plausible that the star formed from mass transfer or a merger. We discuss this in greater detail in the following sections.

2.5.2 Mass Transfer

The M67 MSTO is 1.3 $M_\odot$($1.31 \pm .05$ $M_\odot$; Gokay et al. 2013; Stello et al. 2016b), and would have been only slightly more massive 450 Myr ago. Mass transfer between two such

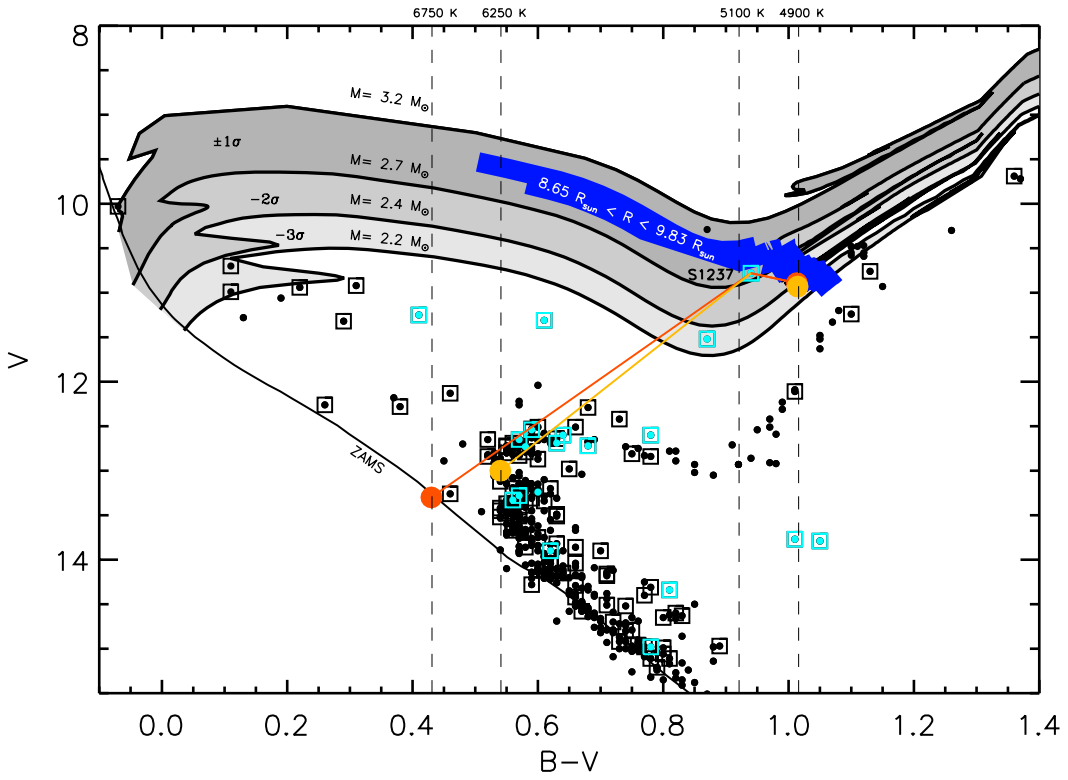

Figure 2.3 : A CMD of M67. We plot X-ray sources from Belloni, Verbunt & Mathieu (1998) and van den Berg et al. (2002) in light blue and all other 3D kinematic members in black. Binaries are boxed (Geller, Latham & Mathieu 2015). We use d= 900 pc and E(B-V)= 0.041. Also shown are MESA evolutionary tracks for a 3.2, 2.7, 2.4, and 2.2 $M_{\odot}$. The shaded regions between these tracks indicate the offset from the asteroseismic mass: the darkest gray is within 1σ, medium gray within 2σ, and lightest gray within 3σ. The blue region indicates the points on the evolutionary tracks where the star has a radius within 3σ of the asteroseismic values. We show two examples of the possible photometric deconvolution, one with a BSS secondary (red circles) and one with a MS secondary near the turnoff (orange circles). The dashed vertical lines show the 1σ range in temperature from APOGEE spectra for the primary and SED fitting for the secondary (Torres 2010).

stars would not create a star within the 1σ uncertainty on the mass of S1237 (2.97 ± 0.24 $M_{\odot}$). If we consider a 2.4 $M_{\odot}$ primary the star could have formed from two 1.4 $M_{\odot}$ stars (the turnoff mass 750 Myr ago) and a mass transfer origin is worth considering.

The result of mass transfer from an AGB star would be a blue/yellow straggler-WD binary, and thus some mass would be locked up in a WD companion. Given the typical

carbon-oxygen WD mass of 0.5-0.6 $M_\odot$, we would expect a primary with $M \leq 2.3$ $M_\odot$, even under the unrealistic assumption of totally conservative mass transfer. A lower mass helium WD is not possible because the orbital period of 698 days is too wide to be the result of RGB mass transfer (Rappaport et al. 1995). Additionally, the SED shows no clear evidence of a hot WD companion, though an older ($t \gtrsim 300$ Myr), cool WD would be compatible with the FUV photometry. The system requires a MS companion to explain the SED, so including a WD would require the system to be a triple, e.g. a giant- WD binary with a wide MSTO tertiary. The orbital solution and residuals show no indication of perturbation by such a third body.

Mass transfer leading to a merger between two MS stars could create a $\sim 2.6 - 2.7$ $M_\odot$ star without a WD remnant. Such mergers may happen when magnetic braking shrinks the orbit of a close binary, but MS mergers may also result from angular momentum loss during a dynamical encounter or Kozai-cycle oscillations (see Sections 2.5.3 and 2.5.4).

2.5.3 Dynamical Encounters

At least three turnoff mass stars are needed to make a 2.9 $M_\odot$ primary, and another is required for the secondary. A binary-binary, single-triple, binary-triple, or triple-triple encounter could provide the four stars needed to create S1237. If we consider a 2.4 $M_\odot$ primary it is possible to form the primary from just 2 stars, making a single-binary encounter viable.

Table 2.2 : Encounter Probabilities

Mass ($M_\odot$)	τ_{S1237} (Myr)	τ_{2+2} (Myr)	Ψ_{2+2}	τ_{1+3} (Myr)	Ψ_{1+3}	τ_{3+2} (Myr)	Ψ_{3+2}	τ_{2+1} (Myr)	Ψ_{2+1}	τ_{3+3} (Myr)	Ψ_{3+3}
2.4	750	400	0.85	1300	0.44	890	0.57	940	0.55	3300	0.20
2.9	450	400	0.68	1300	0.29	890	0.40	–	–	3300	0.13

Leigh & Sills (2011) present a method to estimate BSS production rates from stellar collisions. We use their equations and parameters for M67 to calculate encounter rates and present them in Table 2.2. We also list the Poisson probability (Ψ) that at least one encounter of each type would have occurred within the lifetime of S1237, calculated using:

$$\Psi_{n+m} = 1 - e^{\frac{-\tau_{S1237}}{\tau_{n+m}}} \tag{2.3}$$

Here τ_{S1237} is the lifetime from Section 2.5.1, and τ_{n+m} is the encounter rate.

These rates suggest a few encounters can have occurred within the lifetime of S1237, so Leigh & Sills (2011) indicate a collisional origin is possible. We note that post-encounter binaries most commonly have higher predicted eccentricities than S1237 (Fregeau et al. 2004). Theory predicts S1237 should not have tidally circularized (Verbunt & Phinney 1995), so if S1237 was collisionally formed the low eccentricity is unusual.

One collision is sufficient to create a $M < 2.7$ $M_\odot$ primary, but to create a 2.9 $M_\odot$ primary requires at least 2 collisions to occur during the encounter. Scattering experiments show that binary-binary encounters have significant probability ($\sim 5 - 10\%$) of producing two or more collisions due to the increased cross-section for interaction after the adiabatic expansion of the initial collision product (Fregeau et al. 2004).

Alternatively, S1237 could have undergone multiple collisional encounters. N-body simulations of M67 have produced multiple 'super-BSSs' with masses more than twice the turnoff mass after back-to-back dynamical encounters (Hurley et al. 2001). While the rates suggest such massive BSSs should be rare, we know they are produced in open clusters. In addition to S1237, M67 hosts BSSs S977 (a.k.a. F81) and S1082 (Sanders 1977). S977 has a CMD location indicative of a star more than twice the turnoff mass, and S1082 is a triple BSS system with a combined dynamically-measured mass of ~ 5.8 $M_\odot$ (Sandquist

et al. 2003). Multiple collisions seems to be the most plausible mechanism to create these massive systems.

2.5.4 Kozai mechanism

Studies (Perets & Fabrycky 2009; Naoz & Fabrycky 2014) have proposed that Kozai-cycle-induced mergers of an inner binary in a hierarchical triple may form BSSs.

Naoz & Fabrycky (2014) run a large set of Monte Carlo models to determine the effect of Kozai cycles on the final orbital configuration of hierarchical triples. They find the triples that lead to inner binary mergers resemble S1237 in several ways. First, they find that mergers most often originate in triples with outer orbital periods ($P_{\rm out}$) of $10^3 - 10^5$ days, consistent with the 698-day period of S1237. Second, they find a peak in the mass ratio ($\frac{m_3}{m_1+m_2}$) between the tertiary and inner binary of 0.4-0.5. Assuming $m_1 + m_2 = 2.9$ $M_\odot$ and $m_3 = 1.3$ $M_\odot$, S1237 has a ratio of 0.45. Third, merged systems with $P_{\rm out} < 3000$ days have a fairly flat eccentricity distribution from 0.0 to 0.5 (Naoz & Fabrycky 2014), consistent with the low orbital eccentricity of S1237 (e= 0.087).

The vast majority of these systems merge in less than 10 Myr (Naoz & Fabrycky 2014). Therefore, if S1237 was a primordial triple we would expect it to have undergone a Kozai induced merger and evolved to a stellar remnant long ago. However, an initially stable primordial triple may be perturbed by a passing star leading to later-in-life Kozai oscillations. Alternatively, a hierarchical triple could have formed dynamically a few hundred Myr ago, and quickly undergone a Kozai induced merger to create S1237. In either scenario, the maximum mass for the merger product would be twice the turnoff mass, or $2.6 - 2.7$ $M_\odot$, just outside the 1σ error on the asteroseismic mass. To produce a 2.9 $M_\odot$ star would require that one of the stars in the inner binary was already a BSS.

2.6 Summary and Discussion

We present asteroseismic measurements of a binary YSS in M67 from *Kepler* K2 data. Using $\Delta\nu$-corrected scaling relations, we find the primary star is a 2.9 $M_\odot$, 9.2 $R_\odot$, helium-burning star. This is more than twice the mass of the MSTO.

SED fitting determines the secondary is near the MSTO, either a normal MS star or a BSS. The SED and stellar models are only marginally consistent with asteroseismology, requiring a primary mass and radius 2-3 σ lower than the asteroseismic measurements. This suggests that S1237 is either redder and less luminous than a standard for its mass, or the asteroseismic mass and radius are too large by at least ~ 20 and $\sim 5\%$, respectively. We encourage testing the asteroseismic scaling relations for massive helium burning stars for possible discrepancies.

Observed X-ray emission from this star has not been explained. Given the masses of the primary and secondary M_1= 2.9 $M_\odot$, M_2=1.3 $M_\odot$), the mass function indicates the orbit is inclined at $\sim 20^\circ$. If the spin and orbital axes are aligned, the giant primary may be rapidly rotating without observable line broadening or seismic frequency splitting (Beck et al. 2012), thereby explaining the X-rays. Alternatively the X-ray emission may arise from a rapidly rotating secondary. Many X-ray sources in M67 with similar X-ray luminosities are rapid rotators located near the MSTO (see Fig. 2.3). Most are tidally synchronized close binaries, which is not the case for S1237, but rapid rotation is also expected after a recent stellar collision or mass transfer event.

We review possible formation models and suggest that a binary encounter leading to one or more collisions or mergers is a possible formation pathway. Collisions may have taken place during the dynamical encounter itself, or perhaps a Kozai-induced merger of an inner binary in a dynamically formed triple occurred shortly afterward.

This is the first asteroseismic mass measurement for a YSS and the second YSS for which a formation pathway has been suggested. S1040, another YSS in M67, has a helium WD companion, suggesting it formed through mass transfer (Landsman et al. 1997). These two examples indicate that YSSs are likely evolved BSSs, and that like the BSSs there are multiple mechanisms to create them.

2.7 Appendix

Since the publication of this chapter in the Astrophysical Journal Letters, additional analysis while an NSF East Asia and Pacific Science Initiative (EAPSI) Fellow at the University of Sydney has revised the mass measurement of the yellow straggler. While scaling relations result in a mass of 2.9 $M_{\odot}$, requiring a collision of at least 3 typical main-

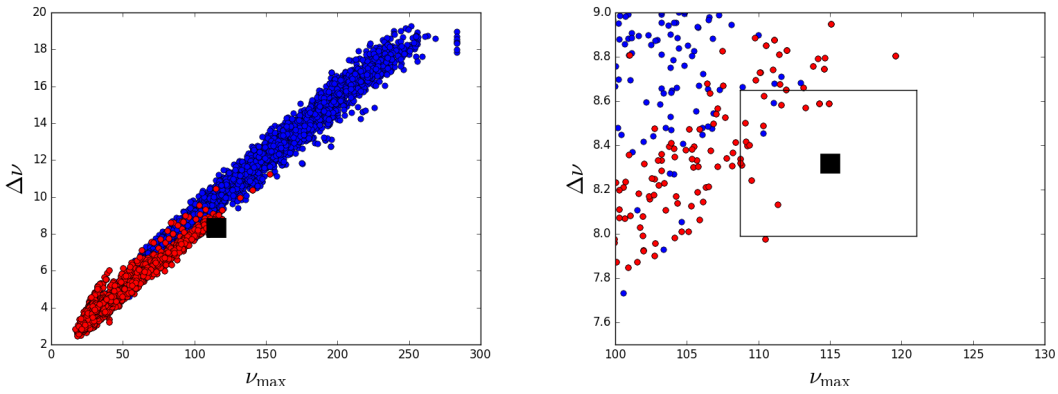

Figure 2.4 : (left panel) The frequency measurements of WOCS 1015 compared to a large sample of Kepler giants. Blue points are Kepler RGB stars and red points are Kepler helium burning giants classified using the algorithm of Hon, Stello & Yu (2017). The black square is the location of WOCS 1015. (right panel) The same diagram, but zoomed in on the region around WOCS 1015. The black box indicates the 3σ errors on the $\Delta\nu$ and $\nu_{\rm max}$ measurements of WOCS 1015. While WOCS 1015 is offset from the main locus of Kepler observations, several other Kepler giants fall within the 2-3 σ errors on the $\Delta\nu$ and $\nu_{\rm max}$ measurements, suggesting WOCS 1015 may be similar to the Kepler stars in this region. These stars are generally determined to be slightly lower mass ($\sim$ 2.4 $M_{\odot}$) helium burning giants.

sequence stars in M67, more detailed modeling suggests that 2.3-2.5 $M_{\odot}$ is a better estimate of the stellar mass of the primary. There are two new arguments for this lower revised mass.

First, a comparison of the measured frequencies of WOCS 1015 to the rest of the Kepler sample of giants shows that the measured $\Delta\nu$ and $\nu_{\rm max}$ are offset from the main locus of red clump and RGB measurements among the entire Kepler sample. We show a comparison between the measured frequencies of the Kepler sample and WOCS 1015 in

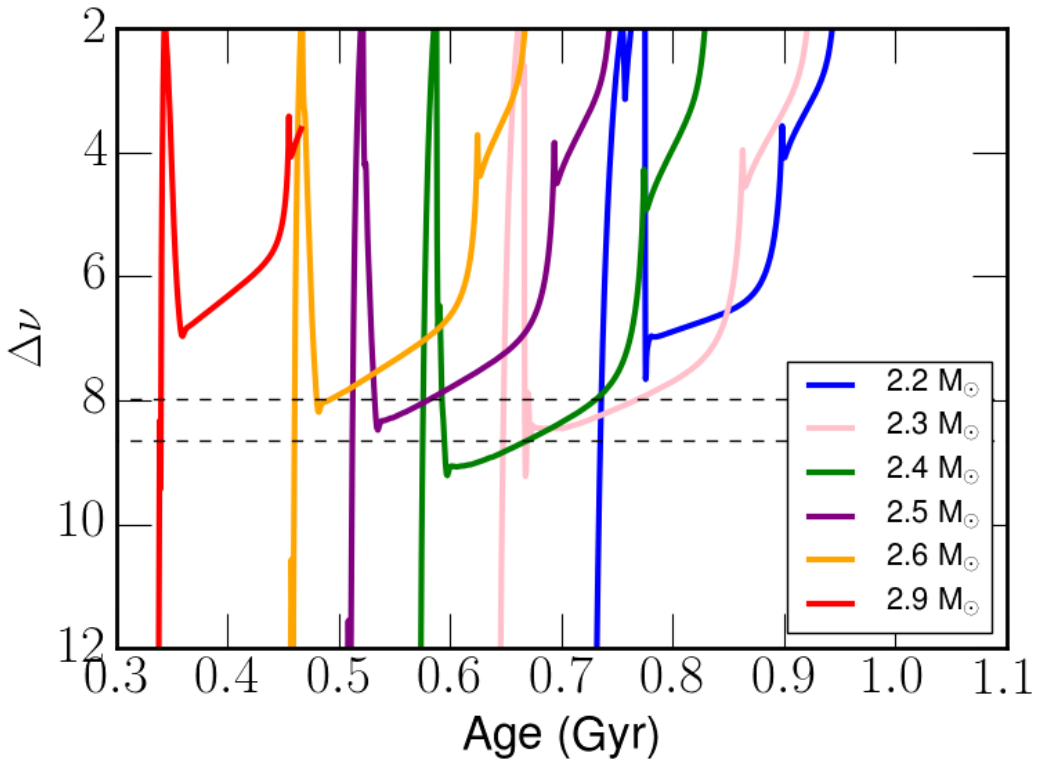

Figure 2.5 : Here we show MESA evolutionary tracks for solar metallicity stars of varying masses (colored lines). The y-axis show $\Delta\nu$, which becomes smaller with increasing density, and the x-axis shows the age. Every track starts with a steep decrease in $\Delta\nu$ corresponding to the first ascent of the RGB. The stars then contract back to the red clump (the steep increase in $\Delta\nu$) when core helium burning commences. The core helium-burning evolution of the star corresponds to the more gradual decrease in $\Delta\nu$. The black dashed lines show the 3σ errors on the $\Delta\nu$ measurement of WOCS 1015. While all tracks pass briefly through this $\Delta\nu$ region on the RGB, only 2.3-2.5 $M_{\odot}$tracks (purple, green, pink) spend significant time in this domain during their helium-burning evolution.

Figure 2.4. Other Kepler giants, however, lie within the $2-3\sigma$ measurement errors on the characteristic frequencies of WOCS 1015. The closest matches to WOCS 1015 in this sample are ~ 2.4 $M_{\odot}$ red clump stars.

Second, more detailed modeling with MESA (Paxton et al. 2015) reveals that the $\Delta\nu$ values measured for WOCS 1015 are in line with those expected for 2.3-2.5 $M_{\odot}$ helium-burning giants, but well outside of the range expected for a 2.9 $M_{\odot}$ helium-burning giant. We show the results of this modeling in Figure 2.5. All the evolutionary tracks in Figure 2.5 briefly pass through $\Delta\nu$ values matching the observed values while on the first ascent of the giant branch, but they spend only a few million years in this $\Delta\nu$ domain. Only the 2.3-2.5 $M_{\odot}$ giants spend substantial time ($\sim 50-150$ Myr) in this $\Delta\nu$ region during their helium-burning evolution. Timescale arguments alone therefore point to a mass of 2.3-2.5 $M_{\odot}$ rather than 2.9 $M_{\odot}$. Combined with our argument that the oscillation frequencies of WOCS 1015 indicate a core helium burning giant (Figure 2.1), we conclude WOCS 1015 has a mass of 2.3-2.5 $M_{\odot}$.

This additional asteroseismic analysis is much more in line with the photometric analysis, which also indicates the star is a core helium-burning giant with a mass of ~ 2.4 $M_{\odot}$. M67 has been re-observed in K2 Campaign 16, with the new data release planned for Summer 2018. Additional observations are planned for Campaign 18 (May-August 2018) if the telescope continues to operate. With these additional observations we will be able to substantially refine the measured $\Delta\nu$ and $\nu_{\rm max}$ values, resulting in an improved stellar mass and radius measurement for this star. If these new measurements agree with the finding that WOCS 1015 is a ~ 2.4 $M_{\odot}$ giant, the photometry and asteroseismology will be brought into good agreement.

As we discuss in this chapter, this slightly lower mass is fully compatible with formation via an efficient stellar merger or collision between two turnoff mass stars in

M67, and does not require invoking a 3-body merger. Given the large mass, it remains unlikely the system could have formed via mass-transfer.

E.L. and R.M. are supported by NASA Grant NNX15AW69G. E.L. is also funded by the Wisconsin Space Grant Consortium. A.V. is supported by the NSF Graduate Research Fellowship, Grant No. DGE 1144152.

References

Beck P. G. et al., 2012, Nature, 481, 55

Bedding T. R. et al., 2011, Nature, 471, 608

Belloni T., Verbunt F., Mathieu R. D., 1998, A&A, 339, 431

Brogaard K. et al., 2016, ArXiv e-prints

Brogaard K. et al., 2012, A&A, 543, A106

Cardelli J. A., Clayton G. C., Mathis J. S., 1989, ApJ, 345, 245

Castelli F., Kurucz R. L., 2004, ArXiv Astrophysics e-prints

Corsaro E., Stello D., Huber D., et al., 2012, ApJ, 757, 190

Dupret M.-A. et al., 2009, A&A, 506, 57

Fregeau J. M., Cheung P., Portegies Zwart S. F., Rasio F. A., 2004, MNRAS, 352, 1

Gaulme P., et al. 2016, in prep.

Geller A. M., Latham D. W., Mathieu R. D., 2015, AJ, 150, 97

Geller A. M., Mathieu R. D., 2011, Nature, 478, 356

Gokay G., Gurol B., & Derman, E. 2013, AJ, 146, 123

Gosnell N. M., Mathieu R. D., Geller A. M., et al., 2014, ApJ, 783, L8

Holtzman J. A. et al., 2015, AJ, 150, 148

Hon Mark, Stello Dennis, Yu Jie, 2017, , 469, 4578

Huber D., Stello D., Bedding T. R., Chaplin W. J., Arentoft T., Quirion P.-O., Kjeldsen H., 2009, Communications in Asteroseismology, 160, 74

Hurley J. R., Tout C. A., Aarseth S. J., Pols O. R., 2001, MNRAS, 323, 630

Kjeldsen H., Bedding T. R., 1995, A&A, 293

Landsman W., Aparicio J., Bergeron P., Di Stefano R., Stecher T. P., 1997, ApJ, 481, L93

Leigh N., Sills A., 2011, MNRAS, 410, 2370

Leonard P. J. T., 1989, AJ, 98, 217

Martin D. C. et al., 2005, ApJ, 619, L1

Mathieu R. D., 2000, in ASP Conf. Ser., Vol. 198, Stellar Clusters and Associations: Convection, Rotation, and Dynamos, Pallavicini R., Micela G., Sciortino S., eds., p. 517

Mathieu R. D., Latham D. W., Griffin R. F., 1990, AJ, 100, 1859

McCrea W. H., 1964, MNRAS, 128, 147

Montgomery K. A., Marschall L. A., Janes K. A., 1993, AJ, 106, 181

Naoz S., Fabrycky D. C., 2014, ApJ, 793, 137

Paxton B. et al., 2015, ApJS, 220, 15

Perets H. B., Fabrycky D. C., 2009, ApJ, 697, 1048

Rappaport S., Podsiadlowski Ph., Joss P. C., Di Stefano R., Han Z., 1995, MNRAS, 273, 731.

Sanders W. L., 1977, A&AS, 27, 89

Sandquist E. L., Latham D. W., Shetrone M. D., Milone A. A. E., 2003, AJ, 125, 810

Sharma S., Stello D., Bland-Hawthorn J., Huber D., Bedding T. R., 2016, ApJ, 822, 15

Sills A., Karakas A., Lattanzio J., 2009, ApJ, 692, 1411

Sills A., Lombardi, Jr. J. C., Bailyn C. D., Demarque P., Rasio F. A., Shapiro S. L., 1997, ApJ, 487, 290

Skrutskie M. F. et al., 2006, AJ, 131, 1163

Stello D., Cantiello M., Fuller J., Garcia R. A., Huber D., 2016a, PASA, 33, e011

Stello D., et al. 2016b, ApJ, accepted.

Stello D. et al., 2015, ApJ, 809, L3

Stello D., Meibom S., Gilliland R. L., et al., 2011, ApJ, 739, 13

Taylor B. J., 2007, AJ, 133, 370

Tian B., Deng L., Han Z., Zhang X. B., 2006, A&A, 455, 247

Torres G., 2010, AJ, 140, 1158

van den Berg M., Stassun K. G., Verbunt F., Mathieu R. D., 2002, A&A, 382, 888

van den Berg M., Tagliaferri G., Belloni T., Verbunt F., 2004, A&A, 418, 509

Vanderburg A., Johnson J. A., 2014, PASP, 126, 948

Verbunt F., Phinney E. S., 1995, A&A, 296, 709

White T. R., Bedding T. R., Stello D., Christensen-Dalsgaard J., Huber D., Kjeldsen H., 2011, ApJ, 743, 161

Wright E. L. et al., 2010, AJ, 140, 1868

Chapter 3

On the Origin of Sub-subgiants: Binary Mass-transfer, Envelope Stripping, and Magnetic Activity

A version of this chapter has previously appeared in the Astrophysical Journal

Leiner, Mathieu & Geller, 2017, ApJ, 840, 67

Abstract

Sub-subgiant stars (SSGs) lie to the red of the main-sequence and fainter than the red giant branch in cluster color-magnitude diagrams (CMDs), a region not easily populated by standard stellar evolution pathways. While there has been speculation on what mechanisms may create these unusual stars, no well-developed theory exists to explain their origins. Here we discuss three hypotheses of SSG formation: (1) mass transfer in a binary system, (2) stripping of a subgiant's envelope, perhaps during a dynamical encounter, and (3) reduced luminosity due to magnetic fields that lower convective efficiency and produce large star spots. Using the stellar evolution code MESA, we develop evolutionary tracks for each of these hypotheses, and compare the expected stellar and orbital properties of these models with six known SSGs in the two open clusters M67 and NGC 6791. All three of these mechanisms can create stars or binary systems in the SSG CMD domain. We also calculate the frequency with which each of these mechanisms may create SSG systems, and find that the magnetic field hypothesis is expected to create SSGs with the highest frequency in open clusters. Mass transfer and envelope stripping have lower expected formation frequencies, but may nevertheless create occasional SSGs in open clusters. They may also be important mechanisms to create SSGs in higher mass globular clusters.

3.1 Introduction

Optical color-magnitude diagrams reveal that 25% of the evolved stars in older open clusters do not fall along standard single-star evolutionary tracks. These stars include the well-known blue stragglers, but also the yellow giants and sub-subgiants.

Sub-subgiant stars (SSGs) were first identified in the color-magnitude diagram (CMD) of the open cluster M67 (Belloni, Verbunt & Mathieu 1998; Mathieu et al. 2003). These two SSGs fall to the red of both the main-sequence and main-sequence binary track and well below the subgiant branch. Both SSGs have high membership probabilities based on both proper-motion and radial-velocity (RV) data, leaving a negligible probability that both are field interlopers.

Broadly speaking, the populations of SSGs in globular and open clusters share similar characteristics. They fall to the red of the main sequence and below the subgiant and giant branch on optical CMDs, a region that can not be easily populated by either single-star evolutionary theory or by any combination of two normal cluster stars. They are also typically X-ray sources with $L_x \sim 10^{30} - 10^{31}$ erg s^{-1} and photometric variables with periods between 1 and 20 days. Where binary status is known, they are often found to be close binary systems with orbital periods on the order of 1-10 days. Similar X-ray sources and photometric variables are also found to red of the RGB. We call these stars "red stragglers" rather than sub-subgiants, though the two types may be related and have similar formation mechanisms. Geller et al. 2017a give a census of the open cluster and globular cluster red stragglers and SSGs known from the literature.

No well-developed theory has yet been presented for the origin and evolutionary status of these non-standard stars. Mathieu et al. (2003) suggest they may be products

of close stellar encounters involving binaries, or stars with enhanced extinction (i.e. due to the presence of circumstellar material). Other authors invoke mass transfer and stellar collision events to form SSGs (Hurley et al. 2005; Albrow et al. 2001).

While many SSGs are kinematic cluster members, most do not have binary orbital information (Geller et al. 2017a). The sample of SSGs with both high quality 3D kinematic memberships and known orbital solutions for the binaries is small, consisting of 6 stars in two open clusters in the WIYN Open Cluster Study (WOCS; Mathieu 2000): 4 SSGs (3 binaries and one single star) in NGC 6791 (Platais et al. 2011; Milliman et al. 2016) and 2 binaries in M67 (Mathieu et al. 2003). We use this sample to guide the formation of an origin theory that matches the observed properties of this sample. We focus on three hypotheses for SSG formation: mass transfer in a binary system, stripping of a subgiant's envelope, or a reduced luminosity due to the presence of a strong magnetic field.

3.2 Sub-subgiant Sample and Observations

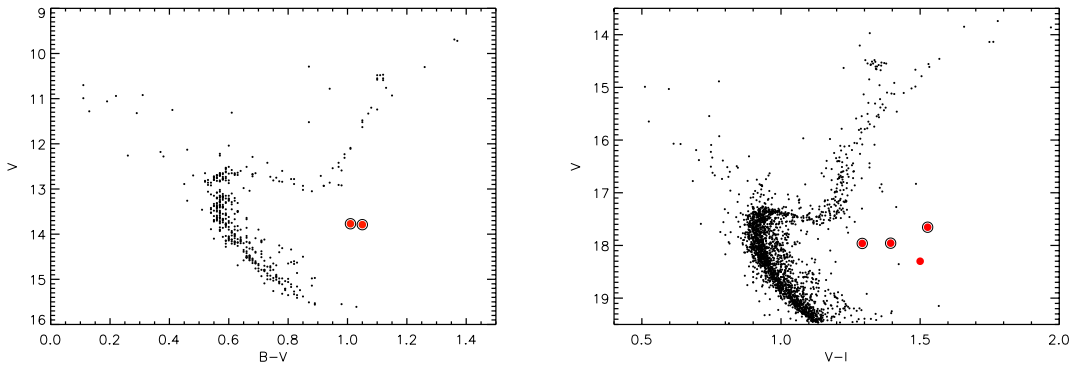

Figure 3.1 : (left) A BV color-magnitude diagram of M67 showing all 3D kinematic members (Geller, Latham & Mathieu 2015). The sub-subgiants are shown with red circles. **(right)** A VI CMD showing proper-motion members of NGC 6791 (Platais et al. 2011). The SSGs confirmed to be 3D kinematic members of NGC 6791 are shown in red circles (Milliman et al. 2016). The binary SSGs in both plots are circled in black.

3.2.1 M67 and NGC 6791 Cluster Properties

Our sample of six SSGs is drawn from two WOCS open clusters: M67 and NGC 6791. CMDs for both clusters are shown in Figure 3.1 with the locations of the SSGs highlighted.

Located at $\alpha = 8^h51^m23^s.3$, $\delta = +11°49'02''$ (J2000), M67 is an old, solar-metallicity open cluster (e.g. Montgomery, Marschall & Janes 1993; Taylor 2007). Distance measurements for the cluster range from 800-900 pc, with reddening measurements ranging from E$(B-V) = 0.015$ to 0.056 (Geller, Latham & Mathieu 2015). For this study, we adopt E$(B-V) = .041$ (Taylor 2007) and $(m-M)_0 = 9.7$ (Sarajedini, Dotter & Kirkpatrick 2009). Age determinations put the cluster at around 4 Gyr (e.g. Montgomery, Marschall & Janes 1993; van den Berg et al. 2004) with a main-sequence-turnoff mass of ~ 1.3 M$_\odot$.

Located at $\alpha = 19^h20^m58^s.09$, $\delta = +37°46'31''$ (J2000), NGC 6791 is an old (8 Gyr; Carney, Lee & Dodson 2005; Grundahl et al. 2008) and metal-rich ([Fe/H]=+0.40, Carney, Lee & Dodson 2005) open cluster. Distance measurements put the cluster at around 4 kpc (e.g. Grundahl et al. 2008). The turn-off mass of the cluster is ~ 1.1 M$_\odot$ (Brogaard et al. 2012). For this study we use the distance modulus and reddening values found by Carney, Lee & Dodson (2005): E$(B-V) = 0.14$, $(m-M)_0 = 13.07$.

3.2.2 SSG Cluster Memberships and Orbital Parameters

In Table 3.1 we list the WOCS ID, coordinates, proper-motion membership probabilities (P$_\mu$), and the radial-velocity membership probabilities (P$_{RV}$) for the six SSGs in our sample. We also include the BVI photometry from Stetson, Bruntt & Grundahl (2003) for NGC 6791, and Montgomery, Marschall & Janes (1993) for M67. In the comments section we include other identifiers for these targets from previous studies.

Five of the six SSGs in our sample are binary systems, and for these we also list periods and eccentricities in Table 3.1. One SSG is a double-lined spectroscopic binary

(SB2; WOCS 15028), and the other four are single-lined (SB1s). All but one of these binaries are circular, and they all have short periods ranging from 2.8 to 18.4 days.

While it is possible that any one SSG could be a field contaminant, given the kinematic memberships the probability that all of these systems are field stars is quite low. Mathieu et al. (2003) provide a membership analysis for the M67 SSGs, calculating a 9% probability that one of the 246 3D kinematic members in their sample is a nonmember. The probability of finding 2 nonmembers is just 0.4%. This is within their entire sample of kinematic members, so the likelihood that the 2 SSGs specifically are field stars is smaller still.

Milliman et al. (2016) provide a similar analysis of the NGC 6791 SSGs. Their analysis, based on the kinematic membership probabilities and the CMD location of the stars, indicates that it is highly unlikely for all four stars to be field contaminants. Specifically, they calculate a 17% probability that one of the four SSGs is a field star, dropping to just 1.8% chance that two SSGs are field stars, 0.13% for 3, and 0.007 % for all 4. We are thus confident that our sample of 6 SSGs cannot be explained simply by field contamination.

3.2.3 SSG Spectral Energy Distributions

In order to measure the physical characteristics of the open cluster SSGs, we pieced together spectral energy distributions (SEDs) from existing optical observations (Montgomery, Marschall & Janes 1993; Stetson, Bruntt & Grundahl 2003) and photometry from the Two-Micron All-Sky Survey (2MASS; Skrutskie et al. 2006), Wide Field Infrared Explorer (WISE; Wright et al. 2010), and Spitzer Space Telescope Infrared Array Camera (Skrutskie, Cutri & Marsh 2007). We used these SEDs to fit a temperature and radius to each star and determine the bolometric luminosities of the systems.

Table 3.1. M67 and NGC 6791 SSGs

Cluster	WOCS ID	α (J2000)	δ (J2000)	P_μ[a](%)	P_{RV} [b]	V	$B-V$	$V-I$	$P_{\rm orb}$[c] (days)	e[c]	Other IDs[d]
M67	15028	08 51 25.30	+12 02 56.3	97	99	13.77	1.01	···	2.823094 ±0.000014	0 ±0	S1113
M67	13008	08 51 13.36	+11 51 40.1	98	98	13.79	1.05	···	18.396 ±0.005	0.26 ±0.014	S1063
NGC 6791	130013	19 21 25.22	+37 45 49.82	99	84	17.65	···	1.53	7.7812 ±0.0012	0.015 ±0.019	15561
NGC 6791	131020	19 20 10.61	+37 51 11.20	96	85	18.30	···	1.50	··· ···	··· ···	83
NGC 6791	147014	19 20 21.48	+37 48 21.60	99	95	17.96	1.35	1.39	11.415 ±0.007	0.05 ±0.04	746
NGC 6791	170008	19 20 38.88	+37 49 04.29	99	63	17.96	1.15	1.29	5.8248 ±0.0008	0.013 ±0.020	3626

[a]Proper motion probabilities come from Girard et al. (1989) for M67 and from Platais et al. (2011) for NGC 6791

[b]RV membership probability from Geller, Latham & Mathieu (2015) for M67 and Milliman et al. (2016) for NGC 6791

[c]Periods ($P_{\rm orb}$) and eccentricities (e) are taken from Milliman et al. (2016) for NGC 6791 and Mathieu et al. (2003) for M67

[d]Comments list Stetson, Bruntt & Grundahl (2003) IDs for NGC 6791 and Sanders IDs (proceeded by an S) for M67

Table 3.2. Photometry for SSGs[a]

Cluster	WOCS ID	α (J2000)	δ (J2000)	P_μ(%)	P_{RV} [b]	V	$B-V$	$V-I$	$P_{\rm orb}$[c] (days)	e[c]	Other IDs[d]
15028[b]	15.3	14.78	13.77	13.09	···	11.671	11.123	10.971	10.84	10.822	10.681
	···	···	···	···	···	±.021	±.023	±.022	±.023	±.021	±.086
13008[b]	15.56	14.84	13.79	···	12.59	11.657	11.058	10.958	10.810	10.855	10.643
	···	···	···	···	···	±.022	±.019	±.018	±.022	±.019	±.101
130013[c]	···	···	17.654	···	16.127	15.197	14.495	14.485	14.16	14.337	
	···	···	±.0052	···	±.0117	±.047	±.050	±.086	±.028	±.043	···
131020[c]	···	···	18.3	···	16.8	15.791	15.040	14.780	···	···	···
	···	···	···	···	···	±.069	±.071	±.101	···	···	···
147014[c]	···	19.305	17.957	···	16.563	15.532	14.810	14.707	14.643	14.77	···
	···	±.0076	±.0028	···	±.01	±.059	±.057	±.101	±.033	±.051	···
170008[c]	···	19.116	17.962	···	16.670	15.795	15.248	15.055	···	···	···
	···	±.0069	±.0012	···	±.0011	±.061	±.08	±.1029	···	···	···

[a]Errors listed are measurement errors, not variability.

[b]UBVR photometry from Montgomery, Marschall & Janes (1993).

[c]BVI photometry from Stetson, Bruntt & Grundahl (2003).

3.2.3.1 SED Fitting

We performed a χ^2-minimization between the observed photometry and a grid of Castelli-Kurucz models (Castelli & Kurucz 2004) convolved with filter transmission functions. We fit only T_{eff} (K) and R ($R_\odot$) while fixing the distance and reddening to cluster values. Altering the distance does significantly affect the values of radius and bolometric luminosity we determine, and so we ran our code using a range of distance values (3900-4100 pc for NGC 6791; 800-900 pc for M67) found in the literature to better determine the range in radius and luminosity.

Photometry used in these SEDs is listed in Table 3.2. Because 5 of the 6 systems are

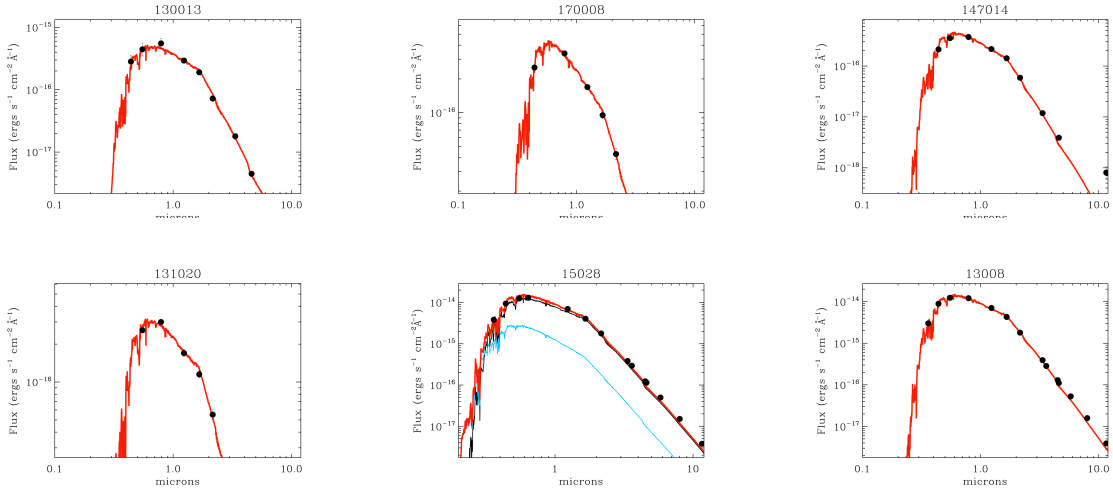

Figure 3.2 : Best-fit SEDs for all six SSGs in M67 and NGC 6791. Observed flux is shown with filled circles. For the SB1s, we assume the flux contribution from the secondary to be negligible and show the flux from the primary in red. For the SB2, 15028, we assume a flux from a main-sequence secondary with R=0.83 and T_{eff} = 5250K based on the analysis of Mathieu et al. (2003). For this star we show the flux contribution from the secondary in blue, the contribution of the primary in black, and the combined light in red.

known photometric variables, the larger source of error in some bandpasses is the intrinsic variability of the system and not the photon statistics. The amplitude of this variability ranges from a few percent in the V band, up to 0.26 mags for WOCS 130013, the most variable SSG (de Marchi et al. 2007; Mochejska et al. 2005; van den Berg et al. 2002). In order to fit the SED we therefore use the amplitude of the variability of the star rather than the photometric errors for the optical photometry. This variability is known for each star in at least the V band. Where the amplitude of variability is known, we use that as our error. If we do not have a measurement of variability in an optical band, we use the V-band variability. Spot modeling predicts that IR observations are much less effected by spot modulation, and therefore for 2MASS, WISE, and Spitzer observations we use the photometric errors for the SED fits. In most cases we expect the amplitude of the variability in these bands to be less than the photometric errors.

Fit parameters for each of the SSGs are given in Table 3.3. For comparison, we also used our code to fit subgiants near the base of the RGB in NGC 6791 and M67: WOCS 10006 in M67 and WOCS 12270 in NGC 6791.

These fits suggest that SSGs are slightly cooler and larger than a typical cluster subgiant. The SSG radii would place them on the lower RGB or near the end of the subgiant branch, but with cooler temperatures and lower luminosities than expected for a typical cluster giant.

We note that a few of the stars show tentative evidence of an IR excess. However, given the large uncertainties on some of the WISE photometry and the variable nature of the stars, its not clear that this excess is significant.

3.3 A Mass-transfer Origin for Sub-subgiants

One hypothesis for SSG formation is that Roche lobe overflow reduces the mass of a subgiant star, lowering its luminosity and moving it into the SSG CMD region. In order to investigate this idea we employ two different stellar evolution codes: Binary Star Evolution (BSE; Hurley, Tout & Pols 2002) and Modules for Experiments in Stellar Astrophysics (MESA; Paxton et al. 2011, 2013, 2015). We use BSE as an efficient tool to search the large progenitor-binary parameter space. We use MESA to produce more detailed models of the evolution of systems BSE indicates may produce SSGs.

3.3.1 BSE Mass Transfer Models

3.3.1.1 Genetic Algorithm

We first used BSE to simulate binaries in clusters with parameters matching those of NGC 6791 and M67 (see Section 3.2.1).The genetic algorithm creates 100 generations of 5000 binaries each, and for each cluster we perform 20 simulations. To begin, we define a sample of 5000 binaries for the first generation with:

- primary masses chosen randomly from a uniform distribution between 0.7 $M_\odot$ (well

Table 3.3. SED Best-fit Parameters for SSGs and Subgiant Comparison Stars

Cluster	WOCS ID	T_{eff} (K)	R ($R_\odot$)	L ($L_\odot$)	Type
M67	15028	4500	2.5-2.9	2.32-3.13	SSG
M67	13008	4500	2.8-3.1	2.92-3.57	SSG
NGC 6791	130013	4250	2.9-3.2	2.50-3.03	SSG
NGC 6791	147014	4500	2.3-2.5	1.97-2.32	SSG
NGC 6791	170008	4750	1.9-2.1	1.67-2.03	SSG
NGC 6791	131020	4250	2.3-2.5	1.56-1.85	SSG
M67	10006	5250	2.4-2.7	3.97-5.02	Subgiant
NGC 6791	12270	5000	1.9-2.1	2.04-2.50	Subgiant

below the MSTO in both clusters) and twice the turnoff mass of the cluster,

- secondary masses chosen randomly from a uniform distribution between 0.1 $M_\odot$ and twice the turnoff mass,
- periods chosen randomly from a uniform distribution between 3 days and 5000 days,
- and eccentricities chosen randomly from a uniform distribution between 0 and 1.

These distributions cover the relevant initial parameter space, but are not meant to reproduce the true shapes of these binary distributions, for example as observed in open clusters.

BSE then evolves these 5000 systems up to the age of the cluster (4 Gyr for M67, 8 Gyr for NGC 6791). We use the default parameters from BSE, but we make two changes to the code: 1) We increase the strength of the convective tidal damping coefficient by a factor of 100 to correspond with the findings of Geller, Hurley & Mathieu (2013), and 2) we fix a bug in the implementation of Equation 32 in Hurley, Tout & Pols (2002)[1]

Once the systems have been evolved to the age of the cluster, we evaluate the fitness of each model. We evaluate fitness based on two criteria: the observed location of a system in a BV CMD, and the period of the final binary system. Specifically, we define the fitness (F) as:

$$F = f_{reg} f_{BV} f_V f_p \tag{3.1}$$

where

$$f_{reg} = \begin{cases} 1 & \text{Star falls redward of the equal-mass binary sequence} \\ 0 & \text{Otherwise} \end{cases} \tag{3.2}$$

[1]Specifically, we change f=MIN(1.d0, (ttid/(2.d0*tc)**2)) to f=MIN(1.d0, (ttid/(2.d0*tc))**2) in two locations in evolv2.f

and

$$f_i = e^{\frac{-(O_i - S_i)^2}{\sigma_i^2}} \tag{3.3}$$

where i=B-V, V, or P, respectively, O refers to the observed color, magnitude or period of the SSGs, and S the color, magnitude, or period of the BSE model.

For M67, we took $O_{B-V} = 0.9$ and $O_V = 13.8$. For NGC 6791 we took $O_{B-V} = 1.25$ and $O_V = 17.7$. For both clusters, we select for short period systems by taking $O_P = 10$ days, and we adopt $\sigma_P = 3$ days, $\sigma_{B-V} = 0.15$, and $\sigma_V = 0.3$.

For a second round of models, we sought to produce systems matching the orbital periods of the SSGs in NGC 6791 and M67. For this we re-ran the genetic algorithm for each cluster, this time taking O_P to be the specific orbital period of each SSG. For 15028, the SB2 SSG, we also included a fitness term for the mass ratio of the system ($\frac{M_2}{M_1} = q$) with O_q=0.7.

After evaluating the fitness of each of the 5000 first-generation models, we take any models with non-zero fitness and these models become "parents" for the next generation of models. Technically we limit the number of parents per generation to 1000, but we rarely find more than a few hundred. Parents are then allowed to "mate" with each other to produce two "children" per parent-parent pair in the next generation. To define the children, we begin with the parent that has the highest fitness value, allow it to mate with all other parents, repeat this process for the parent with the second highest fitness value, and so on until we obtain all parent-parent combinations or we produce 3000 children.

To produce a child we take a random combination of the initial parameters from each parent. Specifically, to determine each initial binary parameter for a child, we draw a random number from a uniform distribution between 0 and 1; if the number is < 0.5, we choose the initial parameter of the first parent, and otherwise we choose the initial parameter from the second parent for the child. If a child duplicates a binary already

in the subsequent generation, we impose a mutation where at least one of the binary initial parameters is chosen randomly from the same respective distribution defining the initial parameters if the first generation, and the number of mutated parameters is chosen randomly.

We take the ≤ 3000 children produced in this manner, and fill the remaining ≥ 2000 spots with binaries whose parameters are chosen from the same distributions as the initial generation. We then evolve this new generation of 5000 binaries with BSE up to the cluster age, and the process is repeated for 100 generations. Through this procedure, we ensure that subsequent generations climb to higher and higher fitness values, retain the best fitting binaries throughout the generations, and introduce a fresh sample of random binaries in each generation to fill out the parameter space.

Note that the genetic algorithm does not uniformly sample parameter space, and therefore can potentially miss a peak in the fitness surface. This is alleviated somewhat by the introduction of binaries with randomly chosen initial parameters into each generation. We ran 20 simulations of the genetic algorithm (with different initial random seeds) and combine the results to further alleviate this issue.

3.3.1.2 Results of BSE Genetic Algorithm

In both sets of runs, those selecting for an orbital period of 10 days and those selecting for specific SSG orbital periods, BSE was able to produce systems in the SSG region of a CMD. Inspection of these results show that there is a family of solutions that create these SSG systems. In M67, the progenitor binaries are generally high-eccentricity systems with periods between 3 and 1000 days, with the longest period binaries requiring eccentricities approaching 1. The secondary star can possess a range of masses between 0.3 and 0.8 $M_{\odot}$, with the majority being drawn from the lower end of this range. The primary star is a

~ 1.3 $M_\odot$ star that begins Roche lobe overflow somewhere on the subgiant branch. This requires that tidal forces circularize and shrink the initial orbit of these systems so that when they evolve through the subgiant branch they have periods of ~ 1 day. We note that our choice of a large tidal strength factor may artificially allow the wide, high eccentricity systems to circularize, but this does not change the conclusion that we require ~ 1 day binaries on the subgiant branch to create SSGs via mass transfer.

The final SSG systems are short period (P < 6.75 days) circular binaries. The highest fitness solutions have reduced the primary mass to $\sim$0.2 $M_\odot$, and increased the secondary mass to $\sim$1.0 $M_\odot$, though a wide range of final primary and secondary masses are produced by the algorithm.

In NGC 6791, results are similar. The progenitor binaries are again high-eccentricity systems with periods from 3 days up to 1000 days, with longer period systems requiring higher eccentricities. Initial primary masses are ~ 1.1 $M_\odot$, with secondaries ranging from 0.3-0.5 $M_\odot$, with the majority drawn from the lower mass end. The final systems are circular binaries periods of just a few days. The longest period system created was a 3.26 day binary.

BSE was unable to produce SSGs with periods above 3.5 days in NGC 6791, or 7 days in M67. These periods are shorter than 5 out of the 6 SSGs in our sample.The only individual SSG that we had some success at reproducing using the genetic algorithm was 15028. This 2.8 day binary falls solidly in the period domain that can be created by mass transfer. However, creating an SSG with the observed mass ratio of this system ($q = 0.7$) proved problematic. The genetic algorithm strongly favored smaller q values for longer period SSGs, with a $q = 0.7$ possible only for shorter period binaries with $P \sim 1$ day.

We note that the algorithm produces longer period SSGs in M67 than in NGC 6791,

which is as expected. The Roche lobe radius is given by Eggleton (1983) as:

$$\frac{r_L}{a} = \frac{0.49q^{\frac{2}{3}}}{0.6q^{\frac{2}{3}} + \ln(1 + q^{\frac{1}{3}})} \tag{3.4}$$

where r_L is the Roche lobe radius, a is the orbital separation, and q is the mass ratio of the binary system. The Roche lobe radius depends only on the mass ratio and the orbital separation of a binary. The stellar radius depends on a star's mass and evolutionary state. Since subgiants in NGC 6791 are lower mass than in M67, they begin with smaller radii. Therefore, for a given mass ratio and orbital separation, NGC 6791 subgiants must reach a more evolved state to exceed their Roche lobes. This means they will have evolved further up the giant branch than their M67 counterparts, and thus not evolve through the SSG domain as they lose mass. In order for an NGC 6791 subgiants to evolve through the SSG region as they lose mass, they must then have smaller orbital separations than are required for M67 subgiants.

The results indicate that, while we do expect mass transfer to create SSG systems, we would expect the observed periods to be in the range of just a few days in both clusters, shorter than most of the observed SSGs. BSE therefore suggests that none of the NGC 6791 SSGs have short enough periods to be mass transfer systems. Similarly, while mass transfer may create a 2.8 day binary like the one observed in M67, the expected mass ratio would be much smaller than the observed $q = 0.7$, and BSE is unable to create the other 18.4 day binary.

3.3.2 Detailed MESA Modeling

The BSE-based genetic algorithm is an excellent tool for exploring a wide range of parameter space, but the stellar evolution and mass transfer calculations are highly parameterized. We therefore also use the more detailed evolution code Modules for Experiments in Stellar Astrophysics (MESA; Paxton et al. 2013) to create SSGs via stable

mass transfer, and compare the results of these MESA models to our observations.

For M67 we initially ran a coarse grid of models with input based on the BSE results . These models all had a primary mass of $M_1 = 1.3$ $M_\odot$ and companion masses in the range 0.3 $M_\odot < M_2 <$ 1.25 $M_\odot$. We evolved each component of the binary up to core hydrogen exhaustion before placing it in a binary with a period between 1 and 10 days and allowing the evolution to proceed. We start from the test suite case `binary_both_stars`, use non-rotating models, and do not include magnetic braking. We used three different mass transfer efficiencies: $\alpha = 0.0, 0.5$, and 1.0. α is defined such that fully conservative mass transfer has $\alpha = 0.0$, and if no mass is transfered $\alpha = 1.0$. Mass and angular momentum are presumed to be lost from the vicinity of the primary in these models.

Models with periods above ~ 2 days began Roche lobe overflow after beginning their ascent up the red giant branch, and mass transfer products did not evolve through the SSG region. In many cases mass transfer was dynamically unstable and we terminated their evolution, as MESA cannot handle these cases. It is generally assumed that binaries undergoing unstable Case B mass transfer enter a common envelope phase that ends with the spiraling in of the binary and an ejection of the common envelope material (Paczynski 1976; Ivanova et al. 2013). The end product of this phase is either a shorter period white dwarf-main sequence binary or a merger to create a single star. If this is correct, we conclude these longer period systems do not create SSGs.

Models with periods less than ~ 2 days began Roche lobe overflow while still on the subgiant branch and did proceed through the SSG region as mass transfer proceeded. For these shorter period models we ran a more detailed grid of models with periods between 0.6 and 2.0 days, $M_1 = 1.3$ $M_\odot$, varying M_2 from 0.3 $M_\odot < M_2 <$ 1.25 $M_\odot$, and using three mass transfer efficiencies $\alpha = 0.0$, 0.5, and 1.0. Our models indicate that systems with initial periods $P < 0.8$ days begin RLO prior to evolution onto the subgiant branch

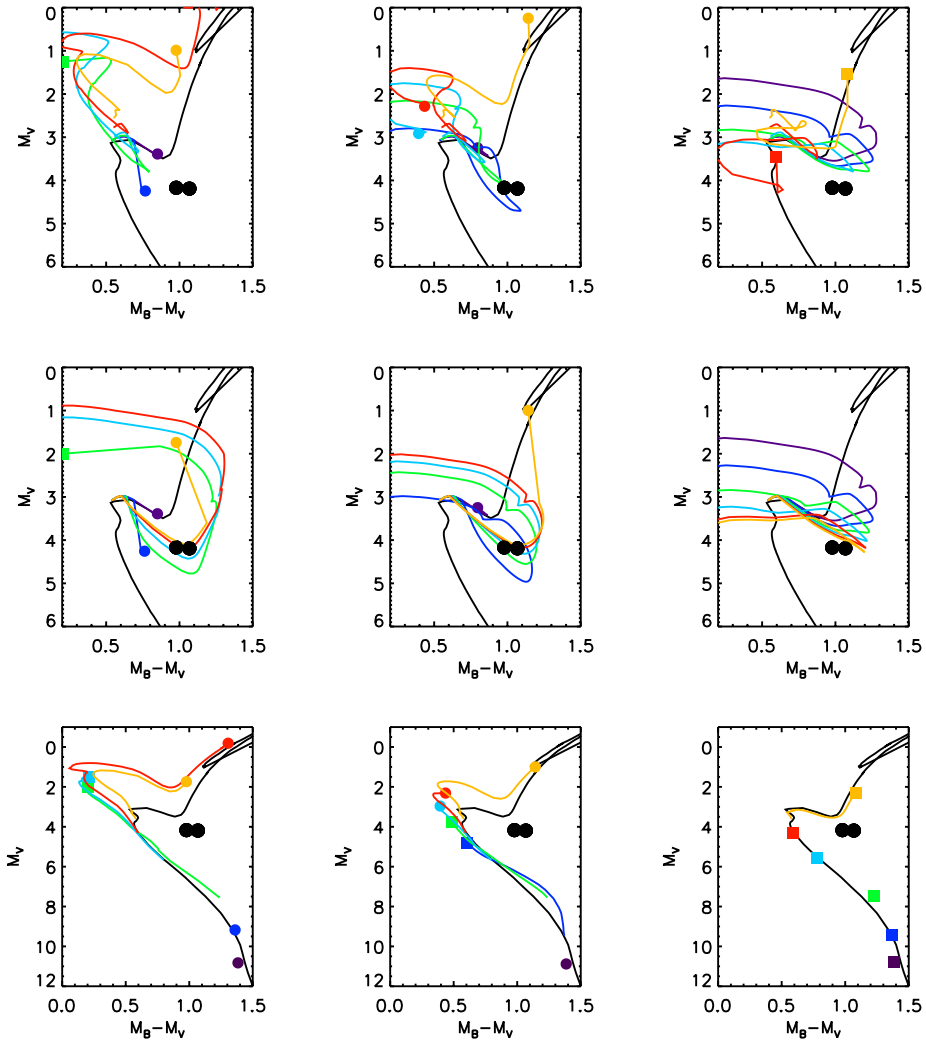

Figure 3.3 : Evolutionary tracks for mass transfer SSGs in M67 given three different mass transfer efficiencies. All models show a 1.3 $M_\odot$ subgiant primary in a 1.0 day binary. Mass of the secondary for each system is indicated by color of the track: 1.25 $M_\odot$ (yellow), 1.1 $M_\odot$ (red), 0.9 $M_\odot$ (light blue), 0.7 $M_\odot$ (green), 0.5 $M_\odot$ (dark blue), 0.3 $M_\odot$ (purple). The first column displays conservative mass transfer, the middle column shows 50% efficient mass transfer, and the last column shows 0% efficient mass transfer. The top row shows the evolution of the combined light of the system, the middle row shows the evolution of the primary only, and the bottom row shows the evolution of the secondary. Mass transfer tracks were all evolved up to 5 Gyr, except in the case the model was terminated due to the onset of dynamically unstable mass transfer and/or common envelope evolution. The colored symbols indicate the end of the evolutionary track, either at 5 Gyr (filled square) or due to the onset of unstable mass transfer (filled circles). The black circles indicate the location of the SSGs. A 4 Gyr isochrone is shown in black (Bressan et al. 2012).

and do not pass through the SSG region. Models with 0.8 days$< P \leq 1.2$ days will often evolve through the SSG region depending on M_2 and mass transfer efficiency. Models with $P > 1.2$ days may have primaries that evolve through the SSG region, but mass transfer is only stable in these systems if they have a near equal-mass secondary. Due to the required mass of the secondary, the combined light of the binary does not pass into the SSG domain. Therefore, it appears that only a very narrow range of systems with periods right around $P = 1.0$ day begin mass transfer at the right time in their evolution, with faint enough companions to move through the SSG domain.

As an example , we show a grid of MESA models with a 1.0 day period, 1.3 $M_\odot$ primary and a range of secondary masses from 0.3 $M_\odot$ to 1.25 $M_\odot$ in Figure 3.3 with the secondary mass indicated by the color of the track. In this grid, for a large range of secondary masses and mass transfer efficiencies, the primary will evolve near the domain of the M67 SSGs (see Figure 3.3, middle row). However, only for models beginning with a fairly low-mass secondary and a moderate degree of non-conservativeness will the combined light of the binary evolve through this region (Figure 3.3, top row). For example, see the top middle plot. Only the model binaries with progenitor secondaries of 0.5 and 0.7 $M_\odot$ are observed in the SSG region during their evolution.

The evolution of the accreting stars in these models is also interesting. We assume the accreting star in these binaries is a main sequence star with initial mass ranging from 0.3 to 1.25 $M_\odot$. For models where mass transfer can proceed stably and we assume a significant fraction of the mass lost from the primary is accreted by the secondary, the secondaries may gain several tenths of a solar mass of material. This accretion causes them to move up the main sequence to a position corresponding to their new larger mass. If the accreting star starts close enough to the main sequence turn off, or we assume a large mass-transfer efficiency, the accreting star may move above the main-sequence turn-off and in to the blue

straggler region (for example, see Figure 3.3, lower left plot). As these accretors begin to evolve off the main sequence, their higher mass causes them to follow an evolutionary track brighter and bluer than the cluster isochrone. Such 'yellow stragglers' have been observed in M67 and other clusters, and are believed to be evolved blue stragglers (Landsman et al. 1997; Leiner et al. 2016; Geller, Latham & Mathieu 2015). In this mass transfer scenario, then, SSGs could be part of the same evolutionary pathway that leads to the formation of other non-standard stars like the blue and yellow stragglers.

We ran another grid for NGC 6791, using a primary of $M_1 = 1.1$ $M_\odot$, varying M_2 from 0.3 $M_\odot < M_2 < 1.0$ $M_\odot$, using three mass transfer efficiencies $\alpha = 0.0$, 0.5, and 1.0, and periods between 0.6 and 10.0 days. Results were similar to those of M67. The models indicate that systems with initial periods $0.6 \leq P \leq 1.0$ days moved through the SSG region during RLO. As in M67, longer period systems began mass transfer on the lower giant branch, and if mass loss proceeded stably the model evolved to the red of the RGB, not down into the SSG region.

We compare this finding to the results of the BSE models. Shown in Figure 3.4 is a histogram of orbital periods of the SSG binaries produced in BSE models of M67 and NGC 6791 (Section 3.3.1). We show both the orbital period of the system at onset of RLO, and the final period of the binary at 4 Gyr when it is observed as an SSG. We also show the shortest and longest period SSG created with MESA with vertical dashed blue lines. Note that our grid of MESA models has a resolution of 0.1 days in period. We conclude that the MESA results are consistent with our findings from BSE that only binaries in ~ 1 day orbits at onset of RLO will move through the SSG region.

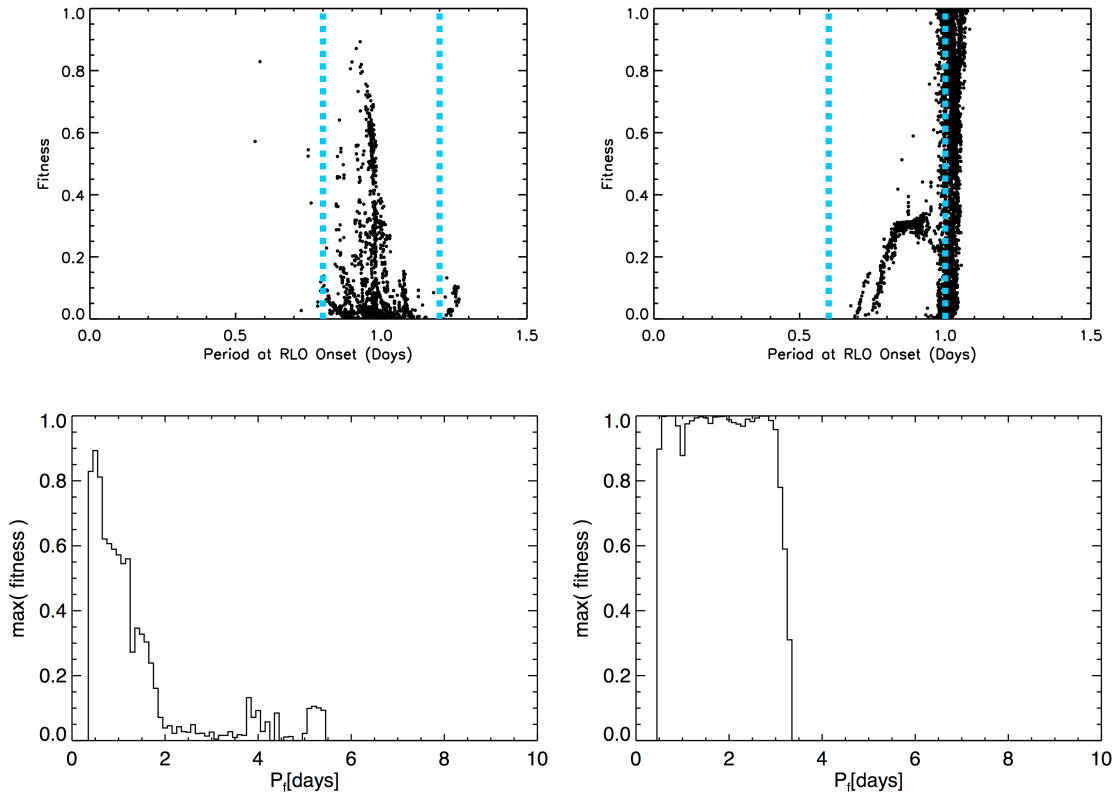

Figure 3.4 : (top)Plots of the fitness of BSE SSG models versus the orbital period at onset of RLO in M67 (top left) and NGC 6791 (top right). The longest and shortest periods that produce SSGs in MESA are also overplotted with dashed blue vertical lines. In both clusters, the highest fitness SSGs are all produced by systems with ~ 1 day orbital periods.**(bottom)** Plots of the maximum fitness of BSE SSG models versus the model SSG's final orbital period at 4 Gyr for M67 (bottom left) or 8 Gyr for NGC 6791 (bottom right)

3.3.3 Frequency of Mass Transfer Formation

Given this period range for SSG formation, we can use the period distribution found by Raghavan et al. (2010) to estimate the number of predicted SSG systems in a cluster. Specifically, Raghavan et al. (2010) fit a Gaussian function to the distribution of orbital periods found in a large sample of binary systems. They find μ_{logP}=5.03 and $\sigma_{logP} = 2.28$. Integrating this function using the upper and lower period bounds found for M67 ($0.8 \leq P \leq 1.2$) and NGC 6791 ($0.6 \leq P \leq 1.0$) we would expect only $\sim 0.3\%$

of binaries to go through this evolution. Assuming a 50% binary fraction and given a population of $\sim$ 30 subgiant stars in M67, and $\sim$ 100 subgiant stars in NGC 6791 (see Section 3.6.4), this results in a Poisson probability of observing one or more mass transfer SSGs in M67 of 4% and in NGC 6791 of 14%. This estimate should be regarded as an upper limit, as period is not the only factor which determines whether a star moves through the SSG region. For example, if the companion mass is very small, mass transfer may be unstable and the system would not evolve as an SSG. Conversely, if the companion is too close to the main sequence turn off, the secondary may overwhelm the lower-luminosity primary and move the system into a more standard region of the CMD or into the blue straggler domain.

Given this small number, it is unlikely, though not impossible that we would observe a mass-transfer SSG in NGC 6791 or M67. However, this mechanism is unlikely to explain all the SSGs observed in M67 or NGC 6791. The Poisson probability of producing 2 SSGs in M67 or 4 in NGC 6791 from mass transfer is negligible.

However, in a larger cluster it may be quite likely to observe at least one mass transfer SSG. In a companion paper, Geller et al. 2017b (in preparation), we investigate in more detail the expected formation frequency of this and other formation mechanisms across a wide range of cluster properties.

3.3.4 Tidally Enhanced Wind

A serious mismatch between mass transfer models and observations is that model mass transfer SSGs have shorter periods than most SSGs observed in M67 and NGC 6791. One method to produce longer period binaries undergoing mass loss is to adopt a model in which the primary can lose substantial mass via a wind while still well within its Roche lobe. The tidally enhanced wind model proposed by Tout & Eggleton (1988) proposes that

tidal interactions and magnetic activity drive a stronger stellar wind in close binary systems than in a typical single star. They assume that the wind can be described by the standard Reimer's wind for RGB stars, multiplied by a factor that has the same dependence on stellar radius (R) and Roche lobe radius (R_L) as a tidal torque. Specifically, their expression is:

$$\begin{gathered}\dot{M}_{Wind} = \dot{M}_{Reimers} \times (1 + B \times min[\frac{R}{R_L}^{6}, \frac{1}{2^6}]) \\ \text{where } \dot{M}_{Reimers} = -4 \times 10^{-13}\left(\frac{RL}{M}\right)\end{gathered} \tag{3.5}$$

where R, L, and M are in solar units and time is in years. Here they assume that wind mass loss saturates when $\frac{R}{R_L} = \frac{1}{2}$. This wind prescription includes a constant multiplicative factor (B) that may be varied to achieve greater or lesser mass loss rates. Tout & Eggleton (1988) calibrate this constant to match the properties of the system Z Her, a detached RS CVn binary with a mass ratio inversion in which the more evolved star is near the end of the subgiant branch and is less massive than its near-turnoff companion. Its orbital period is $P = 4$ days. They find $B = 10^4$ well matches the observed mass loss from the primary.

Using a tidally enhanced wind model can reproduce an SSG similar to 15028 (Figure 3.5). This model has an initial primary mass of 1.3 $M_\odot$, a period of 2.8 days, and a coefficient of $B = 2 \times 10^4$, twice as large as that proposed in Tout & Eggleton (1988). The mass loss rates on the subgiant branch required are on the order of 10^{-9} $M_\odot$ yr^{-1}. The star has a mass of just 0.95 $M_\odot$ when it reaches the CMD location of 15028.

While we have no direct mass measurement of 15028, we do have a mass ratio of $q = 0.7$ from the orbital solution. Given this mass ratio, the 0.95 $M_\odot$ mass from the tidally-enhanced wind model would imply a secondary of 0.67 $M_\odot$, in which case the observed secondary is substantially hotter and more luminous than expected for a 0.67 $M_\odot$ star (Mathieu et al. 2003). Alternatively, assuming the rotational and orbital axes are aligned, a secondary mass of $\sim$ 0.9 $M_\odot$ well matches the photometry, spectroscopic

temperature, and mean density of the secondary star (Mathieu et al. 2003). This would imply a mass of 1.3 $M_\odot$ for the primary, indicating a subgiant that has not lost substantial mass. However, the luminosity ratio of the system is not consistent with the alignment of the axes, and Mathieu et al. (2003) were not able to find a fully self-consistent model for the system.

The SSGs in NGC 6791 are in longer-period orbits than 15028. They also presumably start with smaller radii if they are normal cluster subgiants undergoing mass loss. Therefore, the tidal wind enhancement does not produce a noticeable effect in the models until the stars have evolved substantially up the giant branch. Even increasing the B parameter by a factor of 10 is unable to create observed systems near the location of the NGC 6791 SSGs. Similarly, a tidally enhanced wind model for the 18.4 day binary in M67 also does not produce significant mass loss until the primary is substantially more evolved. These stellar models never move through the SSG region.

Overall the wind prescription of Tout & Eggleton (1988) is unable to reproduce the CMD location of any of the NGC 6791 SSGs or the 18.4 day SSG in M67 using a value of B close to what is typically assumed. These stars are just not close enough to their Roche radii to have large mass loss rates using this model. This wind prescription can create the 2.8 day SSG in M67 by losing ~ 0.4 $M_\odot$ from a subgiant primary, but it is not clear from the observational evidence that this star has lost substantial mass. We conclude that wind mass loss rates are likely not large enough to be the sole reason for the SSGs' under-luminosity.

3.4 Sub-subgiants from Envelope Stripping

Another possibility is that SSGs could be created as a result of removing the envelope of a subgiant star. Rapid envelope mass loss yields a rapid decrease in luminosity, and

subsequent evolution below the current subgiant branch to a lower-mass red giant branch.

Such stripping could occur in a number of ways. One suggestion is that such mass loss may occur if a subgiant star has a close encounter with a passing star. This may occur, for example, during a resonant binary encounter (e.g. Heggie 1975; Bacon, Sigurdsson & Davies 1996). If the impact parameter of the passage is sufficient to disrupt and remove a large fraction of the stellar envelope, but not close enough to lead to a merger, an SSG-like star might result.

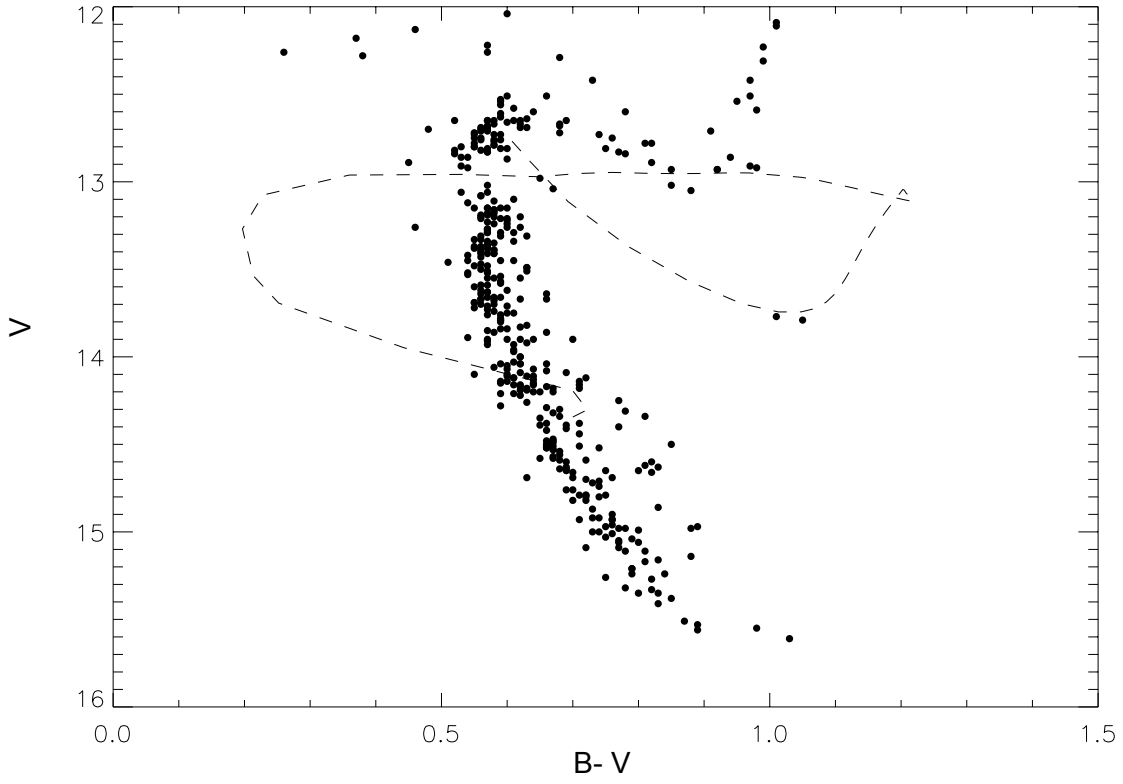

Figure 3.5 : MESA evolutionary track showing the evolution of the combined light of a binary system with a tidally enhanced wind (Tout & Eggleton 1988). The model has a 1.3 $M_\odot$ primary, a 0.9 $M_\odot$ secondary, orbital period of 2.8 days, and a wind coefficient, B, of 2×10^4. We assume no mass gets transferred to the secondary. This model evolves a star through the SSG region, passing through the area occupied by the two M67 SSGs.

3.4.1 MESA models of subgiant mass loss

In order to explore the effect of envelope mass loss on a subgiant, we remove mass from a subgiant star at a high, constant rate using MESA, stopping the mass loss after the star has lost a few tenths of a solar mass of material from its envelope and allowing the star to continue to evolve without further mass loss. In principle, any mass loss rate in which the subgiant can lose a few tenths of a solar mass of material within its subgiant lifetime can move the subgiant into the SSG domain. This requires mass loss rates $\gtrsim 10^{-8}$ $M_\odot$ yr^{-1}. In practice, MESA does not handle dynamical mass loss, and thus the highest mass loss rate for which we achieve numerical stability is 10^{-5} $M_\odot$ yr^{-1}.

As an example, we show an M67 model in which we strip mass from a 1.3 $M_\odot$ subgiant star at a rate of 10^{-5} $M_\odot$ yr^{-1}, stopping the mass loss when the subgiant reaches 0.8, 0.9, 1.0, or 1.1 $M_\odot$. For an NGC 6791 model, we strip mass from a 1.1 $M_\odot$ star, stopping mass loss when the subgiant reaches 0.7, 0.8, or 0.9 $M_\odot$. Plots of the resulting MESA evolutionary tracks are shown in Figure 3.6. The high mass loss rates produce models that are out of thermal equilibrium, causing a rapid drop in luminosity. When mass loss is terminated, the models quickly return to equilibrium and resume evolution along a subgiant/giant track. Due to their newly reduced masses, these tracks are at lower temperature and luminosity than a normal cluster giant. A mass loss rate this large or larger would be required to strip enough envelope material to produce an SSG during a short-duration event like a dynamical encounter. However, lower mass loss rates between 10^{-6} and 10^{-8} $M_\odot$ yr^{-1} could also produce stars in the SSG region if the duration of the stripping event is longer. Lower rates produce a more gradual decline in luminosity and do not drive the star out of thermal equilibrium (similar to the mass transfer models in Fig. 3), but the models still move through the SSG region if they begin mass loss early enough on the subgiant branch

to lose several tenths of a solar mass before beginning their ascent up the giant branch. These models indicate that mass loss of 0.3-0.4 $M_{\odot}$ on the subgiant branch can produce stars in the SSG domain for a wide range of mass loss rates.

3.4.2 Subgiant Collisions

These MESA models indicate that if a subgiant loses significant envelope mass it will move in to the SSG CMD region. We conjecture that one possible mechanism to remove this envelope mass would be a grazing dynamical encounter. In this encounter scenario, another star would have to pass close enough to a subgiant to tidally strip envelope material, but not close enough to lead to a merger.

A similar mechanism has been proposed to explain the depletion of red giants near the Milky Way galactic center (Dale et al. 2009). In this scenario, encounters between RGB stars and black holes can eject the red giant core from the envelope. The core retains only a fraction of the envelope material, creating a giant with a significantly reduced envelope mass. They also find RGB-MS encounters capable of ejecting envelope material if the impact parameter is small enough. Similar models of encounters at the galactic center have found that encounters between RGB stars and MS stars, white dwarfs, or neutron stars can cause significant stripping of a giant envelope, though the amount of mass loss varies substantially between these studies. Depending on the specifics of the encounter and assumptions of the models, some conclude less than 10 % of the envelope mass will be ejected (Bailey & Davies 1999), and others find nearly the entire envelope may be lost (Dale et al. 2009; Alexander 1999). At this stage of evolution, losing even a large fraction of the envelope does not prevent the giant from continuing its evolution up the giant branch, and it does not move into the SSG CMD region (Dale et al. 2009)

Here we suggest similar encounters with subgiants or early giants may create SSGs.

However, no existing studies focus specifically on subgiant encounters. New hydrodynamic simulations for subgiants would be necessary to advance this hypothesis, specifically determining the range of impact parameters that yield substantial mass loss while avoiding common envelope mergers as well as determining the possible orbital parameters for a post-encounter binary.

3.4.3 Frequency of Subgiant Dynamical Encounters

To explore the frequency of such dynamical encounters, we consider the case of the M67 SSGs. Using the encounter rates presented in Leigh & Sills (2011), we find the time between single-binary encounters to be 3.6×10^8 yrs. To get the encounter rate for subgiants, we can scale this rate by the fraction of stars in the cluster that are subgiants or early giants. In M67, we observe ~ 30 subgiants or early giants. Adopting the total number of stars in M67 to be ~ 2000 (Geller, Latham & Mathieu 2015) results in a subgiant fraction of 1.5%. Scaling our single-binary encounter rate by 1.5%, we find a time between single-binary encounters involving a subgiant to be 2.4×10^{10} years. If we assume that all of these encounters lead to an SSG, and that the SSG is observable for its entire subgiant lifetime of ~ 400 Myr in M67, we find the Poisson probability of observing an SSG formed via a single-binary encounter in M67 to be $< 2\%$.

Using the same assumptions, binary-binary encounters also result in a $\sim 2\%$ chance of observing an SSG. While encounters with triples may also play a role, the smaller number of triples makes binary-binary or single-binary encounters the dominant encounter types. More likely only a small fraction of encounters involving subgiants would strip the subgiant's envelope rather than leading to a merger, resulting in a very low probability of observing a dynamically formed SSG in M67.

Dynamically formed SSGs may be more likely to be observed in larger clusters. We

investigate this channel in more detail in the companion paper Geller et al. 2017b, including in globular cluster environments where the larger core densities and higher encounter rates may make this a more likely mechanism.

3.4.4 Other Envelope Stripping Mechanisms

We have proposed two mechanisms that create SSGs via mass loss from a subgiant: 1) mass transfer in a binary system and 2) tidal stripping of a subgiant's envelope during a dynamical encounter. Whether from mass transfer or envelope stripping, the essential finding in Sections 3.3 and 3.4 is that mass loss from a subgiant of several tenths of a solar mass successfully creates stars in the SSG CMD region. Our explorations suggest that neither Roche lobe overflow nor tidal stripping via dynamical encounters produce

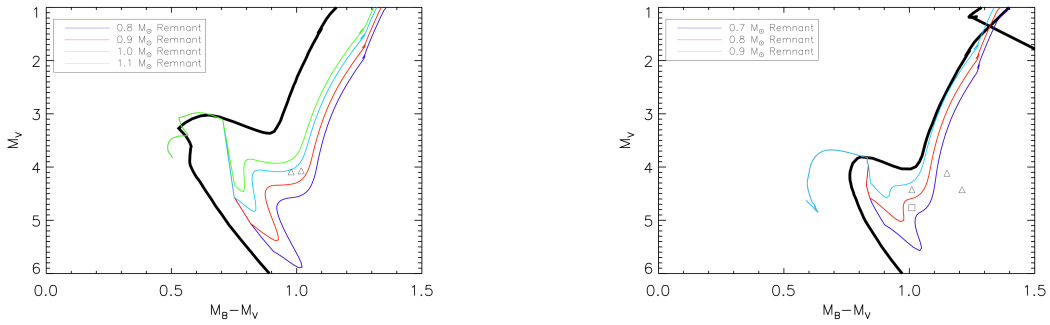

Figure 3.6 : MESA evolutionary tracks showing mass rapidly removed from a subgiant star. **(left)** A 1.3 $M_\odot$ subgiant, mass loss rate of 10^{-5} $M_\odot$ yr^{-1}. Mass loss is terminated when the subgiant star has reached 0.8-1.1 $M_\odot$ and the star is allowed to evolve normally. The plot shows the evolution of this system in colored tracks, with a 4 Gyr Padova isochrone shown in black. The triangles show the locations of the M67 SSGs. **(right)** A 1.1 $M_\odot$ subgiant, mass loss rate of 10^{-5} $M_\odot$ yr^{-1}. Mass loss is terminated when the subgiant star has reached a mass between 0.7 $M_\odot$ and 0.9 $M_\odot$ and the star is allowed to evolve normally. The plot shows the evolution of this system in colored tracks, with an 8 Gyr Padova isochrone shown in black. The triangles show the locations of the NGC 6791 binary SSGs. The square is the NGC 6791 single SSG.

SSGs with high enough frequency to explain the observations. However, we have not fully explored all mechanisms of stellar mass loss, and there may be other ways for a subgiant to lose substantial envelope mass. For example, if a binary system with a subgiant primary went through a period of common envelope evolution, ejecting some but not all of a giant's envelope material before the mass loss stabilized, the remaining system might resemble an SSG. Hurley et al. (2005) create an SSG in an N-body simulation of M67 using a similar mechanism. In their model, two stars merge in a common envelope event, ejecting 0.29 $M_{\odot}$ masses of material in the process. The resulting star lies below the subgiant branch. As a second example, an SSG with a millisecond pulsar companion has been found in the globular cluster NGC 6397 (Cohn et al. 2010; D'Amico et al. 2001; Ferraro et al. 2003; Bogdanov et al. 2010). The SSG is a giant that is extremely under-massive (0.22 $M_{\odot}$- 0.32 $M_{\odot}$) because it is being evaporated by the wind from its pulsar companion (Ferraro et al. 2003). While the N-body SSG is not in a binary and open clusters are unlikely to have millisecond pulsars, we encourage further exploration of more mass-loss hypotheses both in open cluster and other environments.

3.5 Main Sequence Collisions

It is also worth noting that dynamical encounters between main sequence stars are common, and can lead to the collision of two main sequence stars to form a single object. Such collision products are out of thermal equilibrium immediately after collision, and become much brighter than the main sequence due to the energy deposition in their envelopes during the encounter (Sills et al. 1997, 2002). As these products settle back into equilibrium, they contract and move back towards the main sequence. This occurs over a thermal timescale of a few Myr, but during this time such a collision product may be found in the SSG CMD domain (Sills et al. 1997). Due to the short duration of this

phase compared to the single-binary and binary-binary encounter rate for M67 derived in Section 3.4.3, the Poisson probability of observing such a collision product is just a few percent. These encounter products are expected to be rapidly rotating single stars, not close binaries. Scattering experiments find that it is difficult for collision products to retain close binary companions (e.g. Geller, Hurley & Mathieu 2013; Leigh & Sills 2011), and thus we do not consider this a likely explanation for the systems in our sample. While we do determine one of the SSGs to be a single star, it is not observed to be rotating rapidly, and thus is unlikely to be a recent collision product. Again, collisions are more common in denser globular clusters, and we explore the frequency of this formation mechanism in Geller et al. 2017b.

3.6 SSGs as Subgiants with Magnetically Inhibited Convection

3.6.1 Evidence for Magnetic Fields in the SSG Sample

Five of the six stars show evidence that they possess strong surface magnetic fields: X-rays from a hot corona, Hα emission from chromospheric activity, and starspots from areas of concentrated magnetic flux that inhibit convection and lower surface temperatures.

Belloni, Verbunt & Mathieu (1998) determine 0.1-2.4 keV X-ray luminosities for the two SSGs in M67 of 7.3×10^{30} ergs s^{-1} using ROSAT observations. van den Berg et al. (2004) find a 0.3-7 keV luminosity of 1.3×10^{31} ergs s^{-1}for WOCS 13008 using Chandra-ACIS, while WOCS 15028 is outside their field of view. van den Berg et al. (2013) obtain Chandra observations of NGC 6791, detecting 3 of the 4 SSGs as 0.3-7 keV X-ray sources with luminosities of 1.27×10^{31} ergs s^{-1}(15561), 4.5×10^{30} ergs s^{-1}(746), and 4.8×10^{30} ergs s^{-1}(3626). These X-ray luminosities are consistent with coronal emission due to magnetic activity.

All five of these SSG X-ray sources are also observed to be photometric variables with periods on the order of a few days. The lowest amplitude variable has ΔV=0.02-0.09 depending on the variability survey (WOCS 170008; Mochejska et al. 2002, 2005; Kaluzny 2003; Bruntt et al. 2003; de Marchi et al. 2007). The largest amplitude variable has ΔV=0.26 (WOCS 130013; de Marchi et al. 2007). In all cases, the variability is attributed primarily to spot activity on the primary star, with perhaps ellipsoidal variations contributing in some cases. Milliman et al. (2016) present an overview of all known measurements of variability in the SSGs in NGC 6791. van den Berg et al. (2002) present variability information for the 2 SSGs in M67. For 4 of these 5 stars, the variability is found to have periods close to (but not exactly at) the orbital period of the system. For the 5th system, 13008 in M67, they find variability, but do not have a time baseline long enough to determine the periodicity of the variability.

Finally, these 5 SSGs are also observed to have Hα emission (Milliman et al. 2016; van den Berg, Verbunt & Mathieu 1999; van den Berg et al. 2013), indicative of chromospheric activity.

These 5 SSGs are the 5 binaries in our sample, all with orbital periods between 2.8 and 18.4 days. Taken together, these observations indicate these 5 SSGs are magnetically active binaries similar to RS CVn systems.

The 6th SSG (WOCS 131020) shows no evidence of X-ray emission, Hα emission, or photometric variability. It is also the only one of the 6 stars that is not observed to be a binary. Because of this lack of evidence for magnetic activity in WOCS 131020, we suggest that the magnetic field hypothesis is not well suited to explaining its existence. Milliman et al. (2016) conclude that while it is unlikely all 4 SSGs in NGC 6791 are field contaminants, it is possible that at least one of them is. Perhaps 131020 is this field contaminant. It is also possible that WOCS 131020 is formed via a different formation

channel that does not yield binarity, rapid rotation, and magnetic activity.

3.6.2 The Impact of Spots on Stellar SEDs

Mathieu et al. (2003) determine spectroscopic temperatures a few hundred K warmer than our best-fit SED temperatures in the M67 SSGs. One possible explanation is that the SSGs are known photometric variables, and spot activity on the primary could skew the SED fits towards lower $T_{\rm eff}$. Here we revisit our analysis of the SSG SEDs from Section 3.2 to analyze the impact of spots on the determination of radius, temperature, and luminosity.

For example, we refit the 15028 SED to include a 3500 K spot while varying the spot covering fraction. We perform this fit using the same approach detailed in Section 3.2.3, but add the spot covering fraction (f_s) as an additional free parameter. The 3500 K temperature is motivated by the known relation between photospheric temperature and spot temperature (Berdyugina 2005). A 4500-5000 K star would have a temperature contrast of $\sim$1000 K according to this relation. Here we model the SED as a combination of two SEDs weighted by the covering fraction (f_s), one representing the temperature of the unspotted photosphere, and the other a 3500 K SED representing the spotted photosphere.

The new best-fit parameters for 15028 including a spot are $T_{\rm eff}$=4750 K, R=3.1 $R_\odot$, with a 3500 K spot (or spots) accounting for 40% of the surface area. Adding a spot to our model provides a slightly better fit to the photometry and is consistent with the spectroscopically determined $T_{\rm eff}$ of 4800 $\pm$ 150 K (Mathieu et al. 2003). Because the spectroscopic temperature was measured in an optical spectral window, the flux from the star would be dominated by the 4750 K surface rather than the 3500 K spot.

Similarly, adding a spot to 13008 changes the best-fit parameters to 4750 K and 3.4 $R_\odot$, closer to the 5000 K spectroscopic temperature (Mathieu et al. 2003).

Mathieu et al. (2003) also find a discrepancy between the radius of 15028 inferred

from optical photometry (R=2.0 $R_\odot$) and the radius inferred from geometry assuming a tidally synchronized rotation rate (R=4.0 $R_\odot$). The best-fit radius assuming a spot is 3.1 $R_\odot$, a substantially larger photometric radius than determined in Mathieu et al. (2003). While this does not fully explain the discrepancy between the photometric and geometric determinations of the radius, it does bring the two radius measurements closer together. Mathieu et al. (2003) also observe a flux ratio between 15028's secondary and primary of 0.35, much higher than the expected ratio of 0.11 given the spectroscopic temperatures and geometric radii of the primary and secondary. Our SED temperature and radius imply an expected V-band luminosity ratio of ~ 0.2, closer to the observations but still lower than observed.

Spot covering fractions for RS CVn have been measured using various methods (e.g. TiO band strength [O'Neal, Saar & Neff 1996; O'Neal, Neff & Saar 1998; O'Neal et al. 2004], Doppler imaging [Hackman et al. 2012].) These measurements find covering fractions around 30-40% and sometimes up to 50% (O'Neal, Saar & Neff 1996; O'Neal, Neff & Saar 1998; O'Neal et al. 2004), in line with the SED best-fits to the M67 SSGs.

We conclude that if SSGs have a substantial spot covering fraction, the best-fit temperatures from our SED fits in Section 3.2.3.1 may be too cool by a few hundred K and our best-fit radii may be too small by a few tenths of a solar radius. We encourage future observational efforts to determine the spot sizes and temperatures in order to better correct for this effect.

3.6.3 Modeling Inhibited Convection

While the interaction between magnetic fields and convection remains unclear, theory suggests that a magnetic field may act to reduce the efficiency of convective energy transport in stars with sufficiently large field strengths (Stein, Brandenburg & Nordlund 1992).

Observational evidence suggests the presence of magnetic fields in M-dwarfs and solar-type binaries can create stars with temperatures and radii that deviate from model predictions. Radius determinations of eclipsing low-mass main-sequence stars ($M \lesssim 1.0\ M_{\odot}$) are inflated by $5-10\%$ from model predictions (Torres & Ribas 2002; Torres et al. 2006; Chabrier et al. 2005; Morales, Ribas & Jordi 2008) and appear redder and cooler than typical low mass stars by a few percent (Hawley, Gizis & Reid 1996). Similar to our sample of SSGs, these stars display evidence of strong magnetic fields including X-ray and Hα emission. Many have modeled these observations as an effect of inhibited convection due to the presence of magnetic fields (Chabrier, Gallardo & Baraffe 2007; Clausen et al. 2009; Feiden & Chaboyer 2013). We suggest a similar effect may be at work in the SSGs.

Fully modeling the effect of magnetic fields on stellar evolution requires a 3D magnetic stellar evolution code and is not currently technically feasible. Instead, two main approaches have been used to produce 1D models of magnetically active stars. One approach is to introduce magnetic perturbations to the stellar structure equations, equation of state, and mixing-length theory of convection (e.g. Feiden & Chaboyer 2012; Lydon & Sofia 1995). The other has been to reduce the mixing length coefficient ($\alpha_{\rm MLT}$; Chabrier, Gallardo & Baraffe 2007). The argument for using a reduced mixing length has been laid out in several papers (Chabrier, Gallardo & Baraffe 2007; Feiden & Chaboyer 2013). In brief, the argument assumes that the star possesses a turbulent dynamo that sources energy directly from convective motions. The moving plasma in a stellar convective region induces a Lorentz force that preferentially opposes the movement of fluid across magnetic field lines. Thus the motion of a convective bubble will be slowed as some of its kinetic energy is diverted into the local magnetic field. For convective motions to be significantly slowed the local Alfven velocity must approach the convective velocity. Given typical solar values, this requires internal magnetic field strengths of the order 10^4 G, comparable to the

equipartition field expected for rapid rotators. The result is a reduced heat flux transported by convection, which can be expressed in the framework of mixing length theory as a smaller characteristic convective length scale, or lowered mixing length coefficient $\alpha_{\rm MLT}$.

Chabrier, Gallardo & Baraffe (2007) simply alter $\alpha_{\rm MLT}$ to fit the observed properties of magnetically active stars. They do not attempt to tie the value of $\alpha_{\rm MLT}$ to a specific magnetic field strength or topology. In complementary work, Feiden & Chaboyer (2013) compare stellar models with reduced mixing length to models using a slightly different implementation of a turbulent dynamo, as well as to models using a magnetically modified Schwarzschild criterion. They also develop an expression relating the reduction in mixing length to a magnetic field strength. They find that the reduced mixing length models produce stellar structure nearly identical to their turbulent dynamo models, and that these models can reproduce the observed radius inflation among low mass main sequence stars using plausible internal magnetic field strengths and surface magnetic fields comparable to the observations.

Given the exploratory nature of this work, we elect to use the simple and easily implemented approach of Chabrier, Gallardo & Baraffe (2007) of altering mixing length to match the observed temperatures and radii of the sub-subgiants. However, the question of how magnetic fields impact stellar structure is far from settled. We consider this a useful first test, and expect future comparisons with sub-subgiant models using other approaches to implementing magnetic fields in stellar evolution codes will be necessary.

Following the approach of Chabrier, Gallardo & Baraffe (2007), we run a 1.3 $M_\odot$ model and a 1.1 $M_\odot$ model in MESA using different mixing length coefficients in order to explore the impact this may have on the star's global properties. MESA's standard mixing length coefficient is $\alpha = 2.0$. Groups that model this reduced convective efficiency in M-dwarf models found they required α to be around 0.5 to reproduce the observed mass-radius

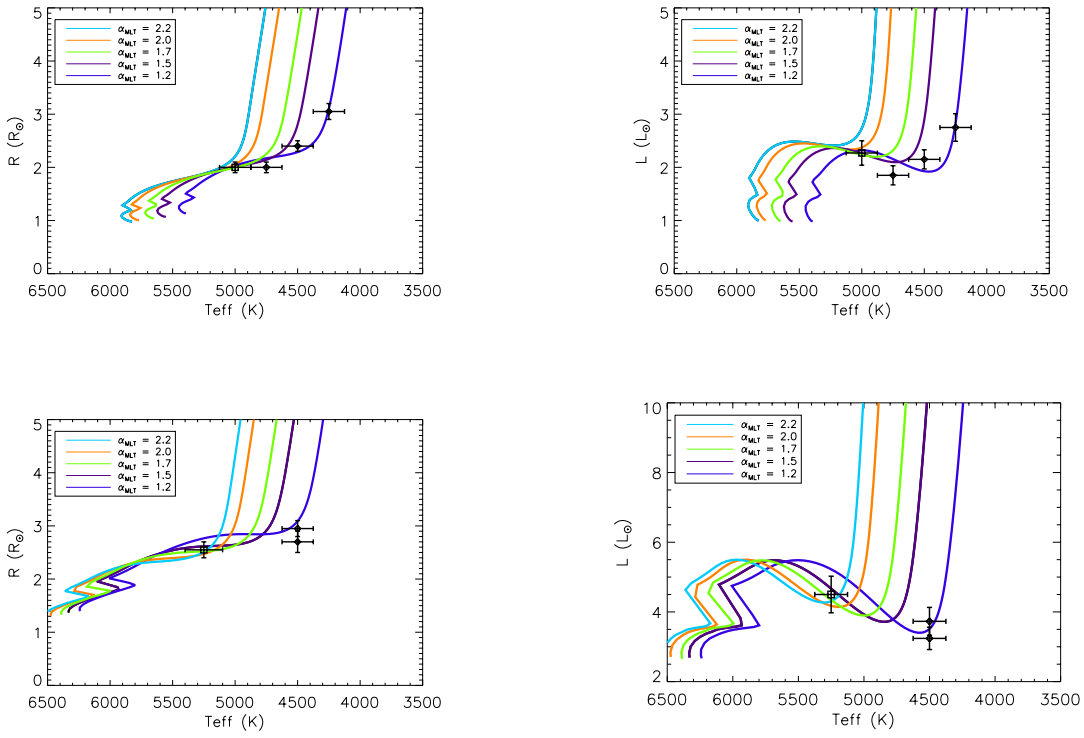

Figure 3.7 : **(a)** an R-T_{eff} plot with MESA models of the evolution of a 1.1 $M_{\odot}$ (the turn-off mass of NGC 6791) star given various mixing length coefficients ($\alpha_{\rm MLT}$). The 3 magnetically active SSGs in NGC 6791 are plotted with diamonds. We do not include the 4th SSG, which does not show signs of magnetic activity. The location of a star at the base of the RGB in NGC 6791 (12270) is plotted for comparison with an open square. **(b)** An HR diagram of the evolution of a 1.1 $M_{\odot}$ star with various mixing length coefficients ($\alpha_{\rm MLT}$) from 2.2 to 1.2. Symbols are as in the diagram on the top left. **(c)** An R-T_{eff} plot with MESA models of the evolution of a 1.3 $M_{\odot}$ (the turn-off mass of M67) star given various mixing length coefficients. M67 SSGs are plotted with diamonds. The location of a normal subgiant in M67 (10006) is plotted for comparison with an open square. **(d)** An HR diagram of the evolution of a 1.3 $M_{\odot}$ star with various mixing length coefficients. Symbols are as in the diagram on the bottom left.

relationship derived from M-dwarf eclipsing binaries when assuming a uniform photospheric temperature. (Feiden & Chaboyer 2013; Chabrier, Gallardo & Baraffe 2007; Morales et al. 2010). A larger mixing length of $\alpha = 1$ was sufficient to reproduce observations when using a two temperature model for the photosphere to account for the effects of starspots to lower surface flux (Chabrier, Gallardo & Baraffe 2007; Morales et al. 2010).

In Figure 3.7 we show the evolution of an SSG using various mixing length parameters in a Hertzprung-Russell (HR) diagram and a R-$T_{\rm eff}$ diagram. Also plotted with diamonds are the SSG best-fit radii, temperatures, and luminosity from the SED fitting assuming an unspotted surface (see Section 3.2.3.1). We compare to the unspotted SED temperature because the MESA models use a single temperature photosphere, and because the spot filling factors for the SSGs are still uncertain. We also plot for comparison the location of a normal cluster star located at the base of the RGB (open square).

The models indicate that lowering mixing lengths creates cooler, larger stars at all points during the evolution of the star, but the luminosity remains unchanged at most stages of evolution regardless of mixing length. However, the altered mixing length does create lower luminosity stars near the end of the subgiant branch and the beginning of the RGB. At this stage in evolution, the expanding shell absorbs enough energy to lower the luminosity for a time. Lowering the mixing length parameter leads to a greater dip in the luminosity here, and this dip occurs at lower $T_{\rm eff}$. The SSGs fall near this dip closest to the $\alpha = 1.2$ track.

We also compare the CMD locations of SSGs to our models with lowered mixing length in Figure 3.8. The color transformation is done using the MESA colors module. This transformation assumes a uniform, unspotted surface temperature for the star. A more accurate treatment of the star would be to include both a lowered mixing length coefficient, and to assume a two (or more) temperature model for the surface flux that

includes contributions from an unspotted photosphere and a spotted region. In fact, the temperature structure may be even more complex, with spots of different temperatures or hot plages surrounding the spots contributing to the emission. We therefore show the CMD to demonstrate the approximate region in which these lowered mixing length models would appear, but caution that the colors may not be accurate for highly spotted stars.

While these models do move through the SSG region in a B-V or V-I CMD, we have less success producing the specific locations of the SSGs in M67 than in the HR diagram. These models predict stars that are redder, but brighter than the observed SSGs. We suggest this discrepancy may be due to our assumption of a single temperature photosphere in the MESA models. A better measurement of the spot temperatures and covering fraction of the SSGs and a stellar evolution code capable of modeling a spotted photosphere would provide more reliable color transformations. In NGC 6791, the models do better at reproducing the observed locations of the magnetically active SSGs. These stars fall between $\alpha = 1.2$ and 1.5, similar to the results in the HR diagram.

The CMD makes clear that changing mixing length becomes most noticeable near the end of the subgiant branch and through the RGB. While the tracks show cooler, more expanded stars on the main sequence and early subgiant branch, the spread in the tracks falls within the scatter of stars that fall on a normal isochrone, and therefore would not be noticed based on CMD position alone. We also expect that the such short-period magnetically active binaries are not observed all the way up the RGB, as they will evolve off the giant branch once they begin Roche lobe overflow. This model therefore predicts we should only observe SSGs in a small region just below or to the red of the lower RGB.

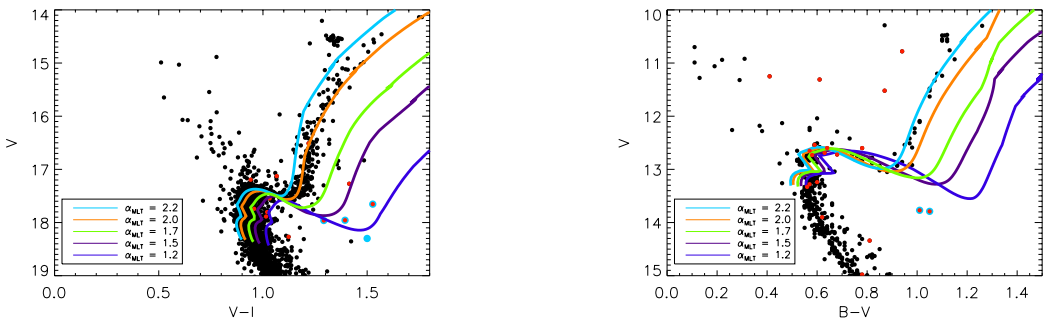

Figure 3.8 : **(left)** A VI CMD of NGC 6791 showing all proper motion members ($P_{PM} \geq 95$) (Platais et al. 2011). X-ray sources from van den Berg et al. (2013) are plotted in red and the 3D kinematic member SSGs are shown with larger light blue circles. Evolutionary tracks show the evolution of a 1.1 $M_{\odot}$ star using varying mixing length coefficients (α_{MLT}) from 2.2-1.2. Colors indicate the different values from α_{MLT} as in Figure 3.7. **(right)** A BV CMD of M67 showing all 3D kinematic members (Geller, Latham & Mathieu 2015). X-ray sources from Belloni, Verbunt & Mathieu (1998) and van den Berg et al. (2004) are shown in red and the two SSGs are shown with larger, light blue circles. Evolutionary tracks show the evolution of a 1.3 $M_{\odot}$ star, again using varying mixing length coefficients with the same values as in Figure 3.7.

3.6.4 Frequency of Formation

1) We start with the assumption that the binary fraction for systems with $P < 10^4$ days in both clusters is 25%. This is the average of binary fractions determined in other WOCS clusters of various ages: M35 (24%, Leiner et al. 2015), NGC 6819 (22%, Milliman et al. 2014) and NGC 188 (29%, Geller & Mathieu 2012).

2) We assume that all binaries with periods less than 18 days (the longest period SSG in our sample) will produce magnetic fields on the subgiant branch that cause them to move through the SSG region. The tidal-circularization period for M67 is observed to be $\sim$ 12 days (Meibom & Mathieu 2005), so this cutoff seems reasonable.

3) We adopt the log-normal period distribution observed by Raghavan et al. (2010).

Integrating this distribution, we find that 11% of binaries with $P < 10^4$ days have $P < 18$ days. Equivalently, we could say that 2.75% of all objects are binaries with $P < 18$ days.

4) We count the number of objects observed in each cluster on the later half of the subgiant branch or the lower RGB. These are the areas predicted by MESA models to appear underluminous due to magnetic fields. In M67, where we have 3D kinematic memberships, we just count the number of stars in this region and find 20. In NGC 6791, we only have proper motion memberships. Here we take all members with $\mathrm{P_{PM}} > 19\%$ from Platais et al. (2011). We correct for field contamination using the result of Tofflemire et al. (2014) that 73% of the $P_{\mathrm{PM}} > 19\%$ stars are confirmed as RV members. We find 100 members in our region of interest.

5) Multiplying our number of stars by 2.75%, we expect to find 0.55 SSGs in M67 and 2.75 SSGs in NGC 6791 formed through this mechanism.

6) We calculate the cumulative Poisson probability to determine our odds of observing SSGs in M67 and NGC 6791.

We find that the chance of observing 1 or more magnetic SSGs in M67 is 42%. The chance of observing 1 or more magnetic SSGs NGC 6791 is 94%. The chance of observing 2 magnetic SSGs in M67 is 9%, while the chance of observing 4 magnetic SSGs in NGC 6791 is 15%. If we assume that only 3 of the 4 SSGs are magnetic since the 4th shows no signs of binarity or magnetic activity, we find a 22% chance of observing 3 magnetic SSGs in NGC 6791.

We conclude that if this magnetic field mechanism can indeed create stars in the SSG CMD region, it is likely that several of the stars in our sample are created in this way.

3.7 Conclusion

Here we put forth three hypotheses of SSG formation: 1) Mass transfer in a binary system, 2) stripping of a subgiant's envelope, and 3) reduced luminosity due to magnetic fields that inhibit convection and produce large stellar spots. We demonstrate that stellar models for each of these methods evolve through the SSG domain.

Models of mass transfer in binaries containing subgiant stars can produce binary systems with combined light in the SSG CMD region. This requires binary systems with orbital periods around 1 day as they evolve along the subgiant branch, as longer period binaries begin RLO once they have started ascending the RGB and do not move through the SSG region. Additionally, the binary must have a small enough secondary that the secondary light does not push the combined light into a more populated CMD region (i.e. the blue straggler domain). Due to these restrictions on period and secondary mass, SSGs formed through mass transfer are expected to be rare, and we would not expect to see many, if any, in open clusters. However, with a larger sample of subgiant stars, e.g. in a massive globular cluster, we may observe SSGs formed in such a way.

Furthermore, mass transfer models produce binaries with shorter periods than the observed orbital periods of the SSGs in M67 and NGC 6791. We test the tidally enhanced wind model of Tout & Eggleton (1988), and find that even with this elevated wind mass loss we cannot achieve the necessary mass loss rates to produce SSGs with the observed periods.

MESA models in which several tenths of a solar mass of material is rapidly stripped from a subgiant's envelope can also produce stars in the SSG domain. We conjecture that this may happen during grazing dynamical encounters in which a star passes close enough to tidally strip material from a subgiant's envelope but avoids merging. Additional scattering

experiments and hydrodynamic simulations are necessary to determine if this mechanism is viable, and if binaries with $\sim$ 10 day orbital periods are an expected end product of such an interaction. As an upper limit on formation rate, we assume that all single-binary or binary-binary encounters with subgiants lead to the formation of SSGs. Even with this very optimistic assumption, the expected rates of formation in open clusters are low enough that we would not expect to observe such stars in M67 or NGC 6791. SSGs may also form as the result of main-sequence collisions during dynamical encounters, but this too should be rare in open clusters. As with mass transfer, this may be a more relevant formation mechanism in massive globular clusters where encounter rates are higher and there are larger populations of subgiant stars, a possibility we investigate in another paper (Geller et al. 2017b, in preparation).

While envelope stripping during dynamical encounters and Roche Lobe overflow perhaps produce SSGs infrequently, clearly substantial mass loss from a subgiant star can create stars in the SSG CMD region. There may be other mass loss mechanisms that we have not explored that create SSGs more frequently, such as common envelope evolution.

Stellar magnetic fields in-and-of themselves may be sufficient to explain the anomalous luminosities and colors of sub-subgiants. Five of our six SSGs show spot variability, X-rays, and Hα emission indicative of surface magnetic activity. Research in the field of low-mass eclipsing binaries suggests magnetic fields can cause inflated radii and lower effective temperatures. The SEDs of the SSGs suggest that the stars do have lower temperatures than normal subgiants in the clusters. Simple 1D models of stars with reduced mixing lengths can fairly well reproduce the observed temperatures, radii, and luminosities of the systems. We have less success matching the models to the SSG CMD locations, which may be a consequence of assuming a single temperature photosphere when performing the color transformation. A stellar evolution code that allows for a multi-temperature photosphere

is necessary to test these results and produce more accurate model colors, as are better measurements of spot temperatures and covering fractions (e.g. using TiO bands).

A calculation of the frequency with which magnetic fields should produce these stars yields an expectation of at least one such star in NGC 6791, and possibly one in M67. The formation frequencies indicate that several of the SSGs in our sample could likely have formed in this way, with a probability of a few percent that all five SSGs showing signs of magnetic activity could have been produced by this mechanism. The sixth SSG shows no signs of magnetic activity or binarity, and we conclude this mechanism is not likely to explain the origin of this system.

Of course, these lowered-mixing length models are simplistic and do not include a physical treatment of the interaction between magnetic fields and convection. Without full 3D magnetic stellar evolution codes, fully implementing all the required physics is impossible, but several other stellar evolution codes use other approaches to model the effects of magnetic fields on evolution (Feiden & Chaboyer 2014; Somers & Pinsonneault 2015). Comparing the results of these codes to our models would be a useful test of our approach.

Finally, the discovery of more SSG SB2 binaries or eclipsing binaries in order to infer masses would be an excellent test. While the magnetic field hypothesis requires SSGs to be similar in mass to normal cluster subgiants, mass-loss mechanisms such as mass transfer in a binary or envelope stripping require significant amounts of mass loss to produce SSGs. A sample of SSG systems in which the mass could be well determined would be a strong test of which hypothesis is best.

Thank you to the anonymous referee for helpful comments and suggestions. This research was supported by a Grant-In-Aid of Research from Sigma Xi, the Scientific

Research Society and by NASA through grants HST-AR-13910 and HST- GO-13354.001-A from the Space Telescope Science Institute, which is operated by AURA, Inc., under NASA contract NAS 5-26555. This work was also funded by the National Science Foundation grant AST-0908082 to the University of Wisconsin-Madison.

References

Albrow M. D., Gilliland R. L., Brown T. M., Edmonds P. D., Guhathakurta P., Sarajedini A., 2001, ApJ, 559, 1060

Alexander T., 1999, ApJ, 527, 835

Bacon D., Sigurdsson S., Davies M. B., 1996, MNRAS, 281, 830

Bailey V. C., Davies M. B., 1999, MNRAS, 308, 257

Belloni T., Verbunt F., Mathieu R. D., 1998, A&A, 339, 431

Berdyugina S. V., 2005, Living Reviews in Solar Physics, 2

Bogdanov S., van den Berg M., Heinke C. O., Cohn H. N., Lugger P. M., Grindlay J. E., 2010, ApJ, 709, 241

Bressan A., Marigo P., Girardi L., Salasnich B., Dal Cero C., Rubele S., Nanni A., 2012, MNRAS, 427, 127

Brogaard K. et al., 2012, A&A, 543, A106

Bruntt H., Grundahl F., Tingley B., Frandsen S., Stetson P. B., Thomsen B., 2003, A&A, 410, 323

Carney B. W., Lee J.-W., Dodson B., 2005, AJ, 129, 656

Castelli F., Kurucz R. L., 2004, ArXiv Astrophysics e-prints

Chabrier G., Baraffe I., Allard F., Hauschildt P. H., 2005, ArXiv Astrophysics e-prints

Chabrier G., Gallardo J., Baraffe I., 2007, A&A, 472, L17

Clausen J. V., Bruntt H., Claret A., Larsen A., Andersen J., Nordström B., Giménez A., 2009, A&A, 502, 253

Cohn H. N. et al., 2010, ApJ, 722, 20

Dale J. E., Davies M. B., Church R. P., Freitag M., 2009, MNRAS, 393, 1016

D'Amico N., Possenti A., Manchester R. N., Sarkissian J., Lyne A. G., Camilo F., 2001, ApJ, 561, L89

de Marchi F. et al., 2007, A&A, 471, 515

Eggleton P. P., 1983, ApJ, 268, 368

Feiden G. A., Chaboyer B., 2012, ApJ, 761, 30

Feiden G. A., Chaboyer B., 2013, ApJ, 779, 183

Feiden G. A., Chaboyer B., 2014, ApJ, 789, 53

Ferraro F. R., Sabbi E., Gratton R., Possenti A., D'Amico N., Bragaglia A., Camilo F., 2003, ApJ, 584, L13

Geller A. M., Hurley J. R., Mathieu R. D., 2013, AJ, 145, 8

Geller A. M., Latham D. W., Mathieu R. D., 2015, AJ, 150, 97

Geller A. M., Mathieu R. D., 2012, AJ, 144, 54

Girard T. M., Grundy W. M., Lopez C. E., van Altena W. F., 1989, AJ, 98, 227

Grundahl F., Clausen J. V., Hardis S., Frandsen S., 2008, A&A, 492, 171

Hackman T., Mantere M. J., Lindborg M., Ilyin I., Kochukhov O., Piskunov N., Tuominen I., 2012, A&A, 538, A126

Hawley S. L., Gizis J. E., Reid I. N., 1996, AJ, 112, 2799

Heggie D. C., 1975, MNRAS, 173, 729

Hurley J. R., Pols O. R., Aarseth S. J., Tout C. A., 2005, MNRAS, 363, 293

Hurley J. R., Tout C. A., Pols O. R., 2002, MNRAS, 329, 897

Ivanova N. et al., 2013, A&A Rev., 21, 59

Kaluzny J., 2003, , 53, 51

Landsman W., Aparicio J., Bergeron P., Di Stefano R., Stecher T. P., 1997, ApJ, 481, L93

Leigh N., Sills A., 2011, MNRAS, 410, 2370

Leiner E., Mathieu R. D., Stello D., Vanderburg A., Sandquist E., 2016, ApJ, 832, L13

Leiner E. M., Mathieu R. D., Gosnell N. M., Geller A. M., 2015, AJ, 150, 10

Lydon T. J., Sofia S., 1995, ApJS, 101, 357

Mathieu R. D., 2000, in ASP Conf. Ser., Vol. 198, Stellar Clusters and Associations: Convection, Rotation, and Dynamos, Pallavicini R., Micela G., Sciortino S., eds., p. 517

Mathieu R. D., van den Berg M., Torres G., et al., 2003, AJ, 125, 246

Meibom S., Mathieu R. D., 2005, ApJ, 620, 970

Milliman K. E., Leiner E. L., Mathieu R. D., Tofflemire B. M., 2016, AJ

Milliman K. E., Mathieu R. D., Geller A. M., Gosnell N. M., Meibom S., Platais I., 2014, AJ, 148, 38

Mochejska B. J., Stanek K. Z., Sasselov D. D., Szentgyorgyi A. H., 2002, AJ, 123, 3460

Mochejska B. J. et al., 2005, AJ, 129, 2856

Montgomery K. A., Marschall L. A., Janes K. A., 1993, AJ, 106, 181

Morales J. C., Gallardo J., Ribas I., Jordi C., Baraffe I., Chabrier G., 2010, ApJ, 718, 502

Morales J. C., Ribas I., Jordi C., 2008, A&A, 478, 507

O'Neal D., Neff J. E., Saar S. H., 1998, ApJ, 507, 919

O'Neal D., Neff J. E., Saar S. H., Cuntz M., 2004, AJ, 128, 1802

O'Neal D., Saar S. H., Neff J. E., 1996, ApJ, 463, 766

Paczynski B., 1976, in IAU Symposium, Vol. 73, Structure and Evolution of Close Binary Systems, Eggleton P., Mitton S., Whelan J., eds., p. 75

Paxton B., Bildsten L., Dotter A., Herwig F., Lesaffre P., Timmes F., 2011, ApJS, 192, 3

Paxton B. et al., 2013, ApJS, 208, 4

Paxton B. et al., 2015, ApJS, 220, 15

Platais I., Cudworth K. M., Kozhurina-Platais V., et al., 2011, ApJ, 733, L1

Raghavan D. et al., 2010, ApJS, 190, 1

Sarajedini A., Dotter A., Kirkpatrick A., 2009, ApJ, 698, 1872

Sills A., Adams T., Davies M. B., Bate M. R., 2002, MNRAS, 332, 49

Sills A., Lombardi, Jr. J. C., Bailyn C. D., Demarque P., Rasio F. A., Shapiro S. L., 1997, ApJ, 487, 290

Skrutskie M. F., Cutri R. M., Marsh K. A., 2007, in Bulletin of the American Astronomical Society, Vol. 39, American Astronomical Society Meeting Abstracts, p. 836

Skrutskie M. F. et al., 2006, AJ, 131, 1163

Somers G., Pinsonneault M. H., 2015, ApJ, 807, 174

Stein R. F., Brandenburg A., Nordlund A., 1992, in Astronomical Society of the Pacific Conference Series, Vol. 26, Cool Stars, Stellar Systems, and the Sun, Giampapa M. S., Bookbinder J. A., eds., p. 148

Stetson P. B., Bruntt H., Grundahl F., 2003, PASP, 115, 413

Taylor B. J., 2007, AJ, 133, 370

Tofflemire B. M., Gosnell N. M., Mathieu R. D., Platais I., 2014, AJ, 148, 61

Torres G., Lacy C. H., Marschall L. A., Sheets H. A., Mader J. A., 2006, ApJ, 640, 1018

Torres G., Ribas I., 2002, ApJ, 567, 1140

Tout C. A., Eggleton P. P., 1988, MNRAS, 231, 823

van den Berg M., Stassun K. G., Verbunt F., Mathieu R. D., 2002, A&A, 382, 888

van den Berg M., Tagliaferri G., Belloni T., Verbunt F., 2004, A&A, 418, 509

van den Berg M., Verbunt F., Mathieu R. D., 1999, A&A, 347, 866

van den Berg M., Verbunt F., Tagliaferri G., Belloni T., Bedin L. R., Platais I., 2013, ApJ, 770, 98

Wright E. L. et al., 2010, AJ, 140, 1868

Chapter 4

Beyond Blue Stragglers: Rotational Identification of Mass-transfer and Collision Products on the M67 Main-Sequence from K2 Campaign 5 Observations

A version of this chapter is in preparation for submission to the Astrophysical Journal

Abstract

At an age of 4 Gyr, typical solar-type stars in M67 have rotation rates of 20-30 days. Using K2 Campaign 5 light curves and the spectral archive of the WIYN Open Cluster Study, we identify eleven three-dimensional kinematic members of M67 with anomalously fast rotation periods of 2-8 days, implying ages of less than 1 Gyr. We demonstrate that post-interaction stars like blue stragglers have similarly rapid rotation rates soon after formation and spin down as they age much as standard main-sequence stars do. We therefore hypothesize that these anomalously fast rotators have been spun up by mass transfer, mergers, or stellar collisions during dynamical encounters within the last Gyr, and thus represent lower-luminosity counterparts to the blue straggler stars. These 11 candidate post-interaction stellar systems have much in common with the blue stragglers including a high binary fraction (73%), a number of long-period, low-eccentricity binary systems, and in at least one case a UV excess consistent with the presence of a hot white dwarf companion. The identification of these 11 systems provides the first picture of the low-luminosity end of the blue straggler distribution, providing new constraints for detailed binary evolution models and cluster population studies. This result also clearly demonstrates the need to properly account for the impact of binaries on stellar evolution, as significant numbers of post-interaction binaries likely exist on cluster main sequences and in the field. These stars are not always easy to identify, but make up $\sim$ 10% or more of the spectroscopic binary population among the solar-type stars in M67.

4.1 Introduction

In color-magnitude diagrams (CMDs) of star clusters, blue straggler stars (BSSs) are found brighter and bluer than the main sequence turnoff. BSSs are thought to form from mass transfer in binary systems (McCrea 1964; Gosnell et al. 2014), stellar collisions during dynamical encounters (Leonard 1989; Sills et al. 2001), or binary mergers induced by Kozai cycles (Perets & Fabrycky 2009; Ivanova et al. 2008).

Blue stragglers are not the only mass-transfer, merger, or collision products that exist in clusters. Evolved counterparts to the blue stragglers (sometimes called 'yellow giants' or 'yellow stragglers') are observed in between the blue straggler region and the red giant branch or detected as over-massive cluster giants via asteroseismology (Landsman et al. 1997; Leiner et al. 2016; Handberg et al. 2017; Corsaro et al. 2012).

In principle, lower-mass blue stragglers could form via mass accretion onto initially lower-mass secondaries, through less efficient mass-transfer processes, or via mergers or collisions of two lower-mass main-sequence stars. Such lower-mass blue stragglers would be hidden within cluster main sequences. Indeed, N-body and population synthesis studies predict that such mass transfer or merger products may be numerous (Andronov et al. 2006; Geller et al. 2013).

Actually detecting these low-mass blue stragglers on the main sequence is challenging. Very close main-sequence-white dwarf (MS-WD) binaries can be detected in time-series photometric surveys if they are eclipsing (e.g. Parsons et al. 2015; Almenara et al. 2012; Breton et al. 2012), or from X-ray and transient surveys in cases where there is active accretion and/or outbursts (i.e. novae and cataclysmic variables; Fornasini et al. 2014; Strope et al. 2010; Szkody et al. 2011). Post-mass-transfer binaries in wider periods (tens

or thousands of days) with hot white dwarf companions can also be identified in UV surveys (e.g. Gosnell et al. 2014; Jeffries & Stevens 1996; van Roestel et al. 2018; Parsons et al. 2016; Li et al. 2014; Rebassa-Mansergas et al. 2010, 2017), but older post-mass transfer systems with fainter, cooler white dwarf companions escape detections in these studies, as do merger and collision products. As a result, the full extent of the post-interaction main-sequence population of clusters is not known. A better census of the post-interaction population requires developing other techniques that may be used to identify these post-interaction stars that blend photometrically with cluster main-sequences.

One method is using stellar abundance measurements. Stellar merger and mass-transfer products are predicted to have spectral signatures including barium, carbon, oxygen, or lithium abundance anomalies. This technique has identified many blue straggler counterparts in the field like carbon-enhanced metal poor stars with s-process enrichment (CEMP-s stars), barium stars, and lithium enhanced giants (e.g. Jorissen et al. 1998; Hansen et al. 2016; Aoki et al. 2008). Detecting these post-interaction systems from abundance signatures requires high-resolution spectra, and known blue stragglers do not always have the observed abundance signatures expected from mass-transfer or collisional formation (Shetrone & Sandquist 2000; Milliman et al. 2016). The observational biases and completeness of abundance detection methods are not well defined.

Here we propose an alternative technique to identify recent mass-transfer and collision products using rotation rates. Recent advances in our understanding of stellar angular momentum evolution have revealed a clearer picture of the rotational evolution of solar-like stars. Observations of young clusters show that on the pre-main-sequence these stars have a wide range of rotation periods. Early in their lives these stars spin down due to magnetic braking (e.g. via a magnetized wind or disc locking; Gallet & Bouvier 2013; Matt & Pudritz 2005), with faster rotators spinning down more quickly due to their stronger magnetic field.

After several hundred Myr, solar-type stars of the same age will converge to the same rotation rate regardless of their initial angular momentum (e.g. Barnes 2003; Gallet & Bouvier 2013; Meibom et al. 2015, 2009; Epstein & Pinsonneault 2014). Thereafter, stellar rotation rates can be used as a proxy for stellar age, a technique known as gyrochronology.

Based on observational and theoretical evidence (Section 4.2), we assume that anomalously rapid rotation rates are observed among all stars that have recently undergone a merger, collision, or mass-transfer event. Therefore, rotation rates from spectroscopic $v\sin i$ measurements or photometric spot modulation may be an effective way to select for recent stellar interaction products. As a test case, we look at stellar rotation rates among stars in the old (4 Gyr) open cluster M67, looking for any main-sequence cluster members with rotation periods much shorter than the typical 20-30 days measured for main sequence stars in the cluster[1] (Barnes et al. 2016; Gonzalez 2016). This study is the first to use rotation to identify the post-interaction population of a cluster, and offers the first glimpse of the low-luminosity end of the blue straggler distribution.

In Section 4.2 we discuss our premise that rapid rotation is a sign of mass-transfer, merger or collision formation, and demonstrate that mass-transfer blue stragglers begin their lives as rapid rotators and spin down with age. In Section 4.3 we discuss the K2 observations of M67 and our technique for light-curve extraction and analysis. In Section 4.4 we discuss each of our candidate post-interaction systems in detail. In Section 4.5 we discuss the overall population characteristics of the anomalously rapid rotators in the cluster that we suggest formed from recent mass transfer or collision events. In Section 4.6 we discuss the significance of these detections and summarize our results.

---

[1]We note that tidally synchronized binaries will be rotating faster than this. These stars are easily excluded from our sample as we explain in Section 4.3.3

4.2 The Rotational Evolution of Mass-transfer Products

In theory, mass transfer in a binary also transports significant angular momentum, resulting in substantial spin-up of the mass accreting star (Packet 1981; de Mink et al. 2013). Similarly, stellar collisions are expected to yield rapidly rotating stellar products (Sills et al. 2002, 2005). These interactions, then, can be seen as resetting the gyro-age clock, giving old stars the rapid rotation rates indicative of youth. Possibly these stars then spin down as they age much like typical main-sequence stars, with their spin down rates determined primarily by their temperatures.

While very little work has been done to systematically compare observed blue straggler rotation rates to these theoretical predictions, observations do confirm qualitatively that many mass-transfer and collision products like the blue stragglers are rotating rapidly (e.g. Carney et al. 2005; Nemec et al. 2017; Jeffries & Stevens 1996; Mucciarelli et al. 2014; Lovisi et al. 2010). These blue stragglers are sometimes observed to have $v\sin i$ measurements as large as 200 km s^{-1}.

To provide a more robust comparison between the rotational evolution of blue straggler stars and other post-mass-transfer systems to models of stellar angular momentum evolution, we assemble a sample of wide ($P_{orb} > 80$ days) post-mass-transfer binaries from the literature consisting of FGK type primaries with detected white dwarf companions. These white dwarf companions all have temperature measurements enabling age estimates for the post-mass-transfer systems from white dwarf cooling models. The primaries in these systems also have rotational measurements from spot modulation or from spectroscopic $v\sin i$ measurements.

Our sample is composed of 12 binaries from the literature containing a white dwarf and a blue straggler or main sequence star, all in close enough orbits to infer mass transfer

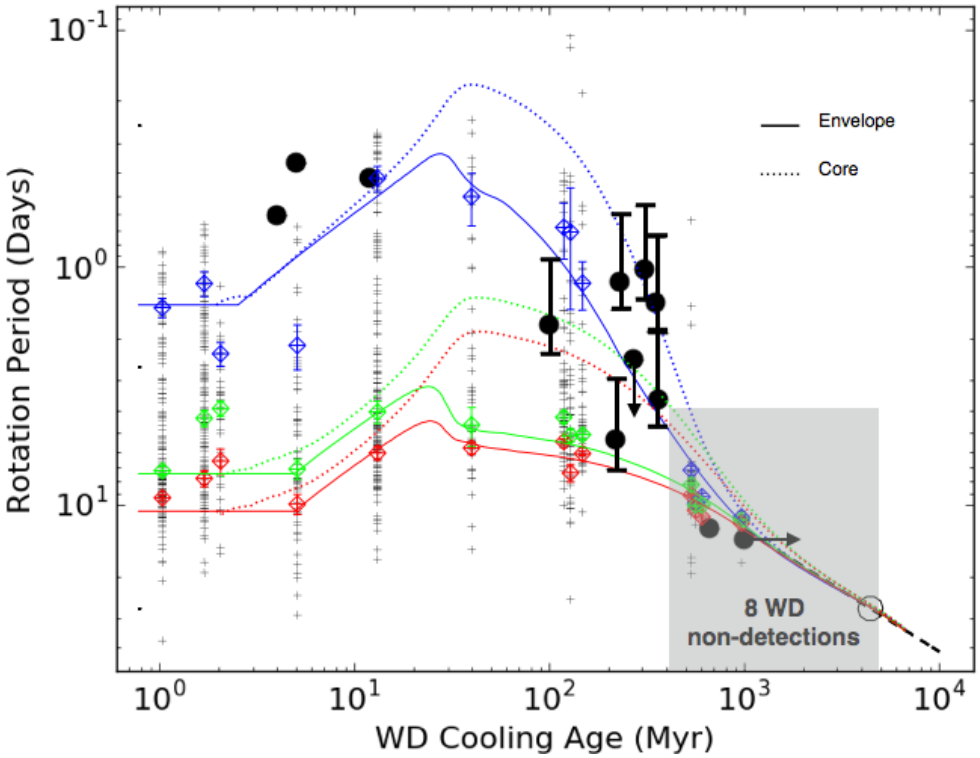

Figure 4.1 : Here we show a modified figure from Gallet & Bouvier (2013) demonstrating that post-mass-transfer binaries spin up to very rapid rotation rates at formation, and then spin down as predicted from standard main-sequence models. The (+) symbols indicate rotation periods among young solar-type stars in clusters in the Gallet & Bouvier (2013) sample. The blue, red, and green diamonds represent the 90th percentile, the 25th percentile, and the median of these observations, respectively. The open circle is the Sun. The colored lines are Gallet & Bouvier (2013) spin-down models for solar-type stars corresponding to the median (green), top decile (blue), and bottom quartile (red) of rotation rates observed among these young stars. We have added blue straggler or main sequence-white dwarf binary systems with measured rotation periods and ages from white dwarf cooling (black circles). Error bars indicate the interquartile range of rotation periods converted from $v\sin i$ measurements. Arrows indicate where the white dwarf age or rotation periods are limits. The gray area indicates the region where the 8 blue stragglers in NGC 188 without detected white dwarf companions must be located in order to have undetectable white dwarf companions and $v\sin i$s below the WOCS measurement limit of 10 km s^{-1}.

would have taken place in their past. This sample includes photometric white dwarf detections to blue stragglers in the old (7 Gyr) open cluster NGC 188 (Gosnell et al. 2015), extreme-UV detections of white dwarf companions to field K-dwarfs (Kellett et al. 1995; Jeffries et al. 1996; Holberg et al. 2014), and Kepler detections of self-lensing binary systems with white dwarfs (Kawahara et al. 2018; Kruse & Agol 2014). These varying detection methods allow us to span an age range from very hot and young (detectable in the field with EUV surveys), to intermediate age (requiring high-precision HST UV photometry), to quite old and cool (photometrically undetectable in binaries with solar-type primaries, but discovered in microlensing surveys).

In Figure 4.1 we compare the white dwarf cooling age of the post-mass-transfer systems to the rotation rate. For uniformity, we adopt the white dwarf temperature estimates from the literature, but determine our own white dwarf cooling ages using the cooling models of Tremblay et al. (2011)[2]. The ages are determined using a bilinear interpolation in $T_{\rm eff}$ and $\log g$. For the white dwarf companions of field K-dwarfs (Kellett et al. 1995; Jeffries et al. 1996; Holberg et al. 2014), we assume surface gravitites of $\log g = 8.0$, corresponding to approximately 0.5 $M_{\odot}$. Due to the high temperatures in these systems, adjusting the mass of the white dwarf by $\pm 0.1 M_{\odot}$ only changes the derived cooling ages by approximately 1 Myr.

For the field stars in our sample we have direct measurements of rotation periods from photometric modulation. We adopt these directly from the literature, except in the case of the detection in Kawahara et al. (2018). They do not determine rotation periods for their self-lensing systems, but we are able to measure a rotation period for one of their systems using the same technique described in Section 4.3.3. For blue stragglers in the cluster NGC 188 we have only $v \sin i$ measurements from the WIYN Open Cluster Study

[2] `http://www.astro.umontreal.ca/~bergeron/CoolingModels`

(see Section 4.3.1). For these systems, we convert the $v\sin i$ measurement to a rotation period using the following method. First, we calculate photometric radii for the blue straggler primaries. To do this, we adopt the temperatures from Gosnell et al. (2015), V-band magnitudes from Sarajedini et al. (1999), and a distance modulus for the cluster of $(m - M)_V = 11.51$. We use this radius to convert the observed rotational $v\sin i$ to a distribution of possible periods assuming a random, uniform distribution of possible inclinations. We adopt the median value of this period distribution in Figure 4.1, and also show error bars corresponding to the interquartile range.

While there is substantial scatter, the rotation rates of the post-mass-transfer binaries fall approximately along the blue curve in Figure 4.1. This curve is a model that describes the spindown of solar-type stars rotating with the fastest rates observed among young clusters (Gallet & Bouvier 2013). It appears that mass transfer has spun up the systems in our sample to rotation periods of < 1 day, comparable to periods observed among the fastest decile of solar-type rotators in young clusters. These stars then spin down at a similar rate to that observed among this fast-rotating young cluster population.

In the Gosnell et al. (2015) NGC 188 sample, 6 of 7 blue stragglers with white dwarf detections also have $v\sin i$'s above the WOCS detection limit of 10 km s^{-1}. There are 8 more binary blue stragglers in the cluster that do not have detected white dwarf companions. Given the 7 stars with detected UV excesses are less than 400 Myr years old, and blue straggler lifetimes are expected to be substantially longer than this, Gosnell et al. (2015) argue that most or all of these 8 non-detections probably also have white dwarf companions that are simply too old and cool to detect. These older systems (> 400 Myr) are all rotating below the 10 km s^{-1}WOCS $v\sin i$ measurement limit. We illustrate these detection limits with the gray shaded region in Figure 4.1. We expect these 8 non-detections to fall somewhere within this gray region. These non-detections thus help to anchor the lower

right portion of the diagram, a region where there are very few known white dwarf-FGK main-sequence binaries because the white dwarfs are too old and cool to detect with UV photometry.

4.3 Observations

4.3.1 WIYN Open Cluster Study

M67 is a well-studied old (4 Gyr) open cluster. It has extensive archival photometry (Montgomery et al. 1993; Fan et al. 1996; van den Berg et al. 2004), proper-motion memberships (Sanders 1977; Girard et al. 1989), and radial-velocity membership information from more than 40 years of high-precision radial velocities obtained on the WIYN 3.5m telescope with the Hydra Multi-Object Spectrograph and with the Harvard-Smithsonian Center for Astrophysics Digital Speedometers. These radial-velocity data are stored in the archive of the WIYN Open Cluster Study (WOCS; Geller et al. 2015; Mathieu 2000). Geller et al. (2015) incorporate both proper motions and radial velocities to determine memberships and binary status for stars in the cluster field out to a radius of $30'$. A subsequent paper will publish orbital solutions for the known binaries (Pollack et al. 2018, in prep). This WOCS synthesis contains members down to a limiting magnitude of V= 16.5, a sample that includes blue stragglers, the subgiant and giant branches, and FGK main-sequence stars. In our analysis, we adopt the most up-to-date membership information and binary orbital parameters from these WOCS papers.

4.3.2 K2 Observations of M67

M67 was observed in Campaign 5 (K2 Guest Observer Program 5031, Mathieu, PI) of the *Kepler* space telescope's extended K2 mission between April and June 2015, using a combination of individual apertures and a 26.5' by 26.5' superstamp of pixels

covering the cluster center. Light curves for both the individual targets and the targets in the superstamp were extracted and corrected for K2 systematic errors using the method of Vanderburg & Johnson (2014) and Vanderburg et al. (2016). While these methods effectively remove systematics caused by the K2 6-hour pointing drift, they leave in long-term instrumental systematics which can impede searches for long-period signals like stellar rotation. To remove these systematics, we used the *Kepler* team's Pre-search Data Conditioning-Maximum A Posteriori (PDC-MAP) software (Stumpe et al. 2014; Smith et al. 2012) to identify and remove common-mode instrumental trends. This process will be described in greater detail by Esselstein et al. 2018 (submitted).

4.3.3 Rotation Measurements

We selected all three-dimensional (3D) kinematic members or likely members of the M67 main sequence observed in K2 Campaign 5. For each star, we created a Lomb-Scargle periodogram using the light–curve processing software `vartools` (Hartman et al. 2008). As a coarse first cut to remove power spectra without significant peaks at short periods, we selected only stars from this sample with measured periods less than 15 days and normalized power of at least 0.1. We cross-referenced these stars with the binary orbital information from Pollack et al. (2018, in prep) to exclude any short-period binaries. We do this because tidal forces spin up the rotation rates of close binaries, explaining any observed rapid rotation. Among the $\sim$ 2800 field eclipsing binaries in the Kepler Eclipsing Binary Catalog, Lurie et al. (2017) find the fraction of tidally circularized binaries drops off at periods greater than 10 days, and the fraction of tidally synchronized binaries drops off dramatically at periods longer than 30 days. These cutoff periods are also compatible with tidal circularization studies in open clusters (Meibom & Mathieu 2005; Meibom et al. 2009). As a conservative cut, we double the Lurie et al. (2017) tidal synchronization limit,

removing any binaries with $P_{\rm orb} < 60$ days from our sample.

We compare this sample to the rotational models of Angus et al. (2015), selecting all stars with rotation rates faster than the 1 Gyr model (Figure 4.2). This age cut allows us to take into account the temperature of the star when determining if rotation rates are unusual, as bluer stars close to the cluster turnoff naturally have slightly faster rotation rates than redder stars further down the main sequence. These rotational models are undefined for stars hotter than $(B-V)_0 = 0.45$. There are a few stars in M67 blueward of this limit, and so for these hotter stars we use a rotation cut of $P_{\rm rot} > 8.0$ day, the approximate rotation rate of a 1 Gyr star near the cluster turnoff. For context, in Figure 4.2 we also show the rotation periods of a sample of normal main-sequence stars in M67 from Barnes et al. (2016). These stars have rotation periods of ~ 25 days.

For this sample of fast rotating stars, we visually examined all the light curves and periodograms to remove any spurious or marginal results. We exclude some lower signal-to-noise systems with multiple peaks. We also exclude any stars with the short-period and multi-periodic variability more consistent with pulsation. We checked the light curves of neighboring stars in the EPIC catalog within 30 arcseconds of each target to determine if the observed periodic signals might originate with a nearby variable star. We also visually examine the CCD images from K2 to check for nearby stars, and cross reference with the 2MASS catalog to check for any stars within 30 arcseconds that may be missing from the EPIC database or too faint to identify in the images. In addition, we adjusted the size of the photometric aperture used to extract the light curve to check that the variability appears to be centered on these sources, and does not become stronger with a larger aperture. Using these techniques we remove several systems where the variability appears to originate with a neighboring star. These steps give us confidence that the remaining stars in our samples are true rotational variables.

As an additional independent check, we also compare these rotation periods to those produced using another light curve production pipeline. Esselstein et al. (submitted) compare periods measured from the Vanderburg & Johnson (2014) light curves we use here and the Oxford pipeline light curves of Aigrain et al. (2015). For most sources, our measured periods agree with the Esselstein et al. period measurements from the Vanderburg light curves and with the Esselstein et al. period measurements from the Oxford pipeline, though a few sources (WOCS 1020, WOCS 2068, WOCS 9005) do not meet their more conservative detection criteria. We discuss these cases in more detail in the next section.

We find 9 stars in our sample that show rotation rates much faster than those of normal main-sequence stars in M67. For specificity, we select stars with rotation rates faster than the 1 Gyr gyrochronology models (Figure 4.2). We show the CMD location of these stars in Figure 4.3. We also show raw light curves, phase-folded light curves, and Lomb-Scargle periodograms for these 9 stars in Figure 4.4. The measurement precision of these periods is generally good to a few percent for periods of several days, up to 10-20% for the longer 20-day periods in our sample. We do not quote these measurement errors because for most of our sources they are misleadingly small. The more significant sources of error will be astrophysical, such as spot migration and differential rotation. We expect these to cause typical rotation period variations on the order of 10%, though in some stars (with more extreme differential rotation, for example) it may be higher (Reinhold & Gizon 2015; Lurie et al. 2017; Balona & Abedigamba 2016).

In addition, we measure $v\sin i$ rates for all 3D kinematic members of the cluster from Geller et al. (2015) (see Geller et al. 2008 for an explanation of our $v\sin i$ measurement technique), again excluding short-period binaries from our sample. The WOCS spectra have a $v\sin i$ measurement limit of 10 km s^{-1}. Typical stars in M67 with rotation rates of 20-30 days would be rotating with surface velocities well below this limit. We therefore

consider any $v\sin i$ measurement above 10 km s^{-1} to be an anomalously rapid rotator. We find that none of the 9 stars discussed above have a $v\sin i > 10$ km s^{-1}. This is not surprising since a rotational velocity of 10 km s^{-1} corresponds to a 4-day rotation period for a turnoff star in the cluster. Given this detection limit, most of the stars in our sample would not have $v\sin i$s above the WOCS velocity resolution limit regardless of inclination angle, and the rest would go undetected if the rotational axes of the systems are somewhat inclined.

We do, however, detect two additional stars with $v \sin i > 10$ km s^{-1}, WOCS 3001 and 11006. These stars have $v\sin i$ measurements of 14.7 km s^{-1}and 18.1 km s^{-1}, respectively. For these stars we convert $v\sin i$ to rotation period using the same technique as discussed in Section 4.2. Using this conversion, we derive rotation periods of $2.6^{3.4}_{1.4}$ days for WOCS 11006 and $3.3^{4.3}_{1.7}$ days for WOCS 3001. We adopt these values in Table 4.1. We also include these two systems in Figures 4.2, 4.3, and 4.4.

Table 4.1 : Stellar and Orbital Properties of Rapid Rotators

EPIC ID	WOCS ID	P_{orb} (days)	Eccentricity	f(m) ($M_\odot$)	V	B-V	P_{rot} (days)	Membership[a]
211411716	4001	139.77	0.36	2.17e-2	15.21	0.79	7.7	BM
211410278	14020	358.9	0.23	2.38e-3	14.58	0.67	4.4	BM
211421624	12020	762	0.056	2.87e-2	14.28	0.59	3.7	BM
211411928	3001[b]	128.14	0.04	1.43e-2	13.26	0.46	3.3[c]	BM
211428722	2068	8567	0.859	6.81e-2	12.19	0.55	20.2 & 3.3	BM
211409959	9005	2769	0.15	3.68e-2	12.65	0.52	4.5	BM
211404255	6025	6265	0.38	2.20e-1	13.70	0.6	2.3	BM
211414427	11006[b]	> 3500	···	···	13.33	0.50	2.6[c]	BLM
211406971	1020	···	···	···	12.70	0.48	5.9	SM
211407130	8010	···	···	···	12.84	0.53	3.6	SM
211427425	7035	···	···	···	13.36	0.57	8.0	SM

[a] Membership classification are explained in Geller et al. (2015). BM= Binary member, BLM= Binary Likely Member, SM= Single Member

[b] These stars are included based on their $v\sin i$ measurements ($v\sin i > 10$ km s^{-1}), not periodic signals in their K2 light curves

[c] Converted from $v\sin i$

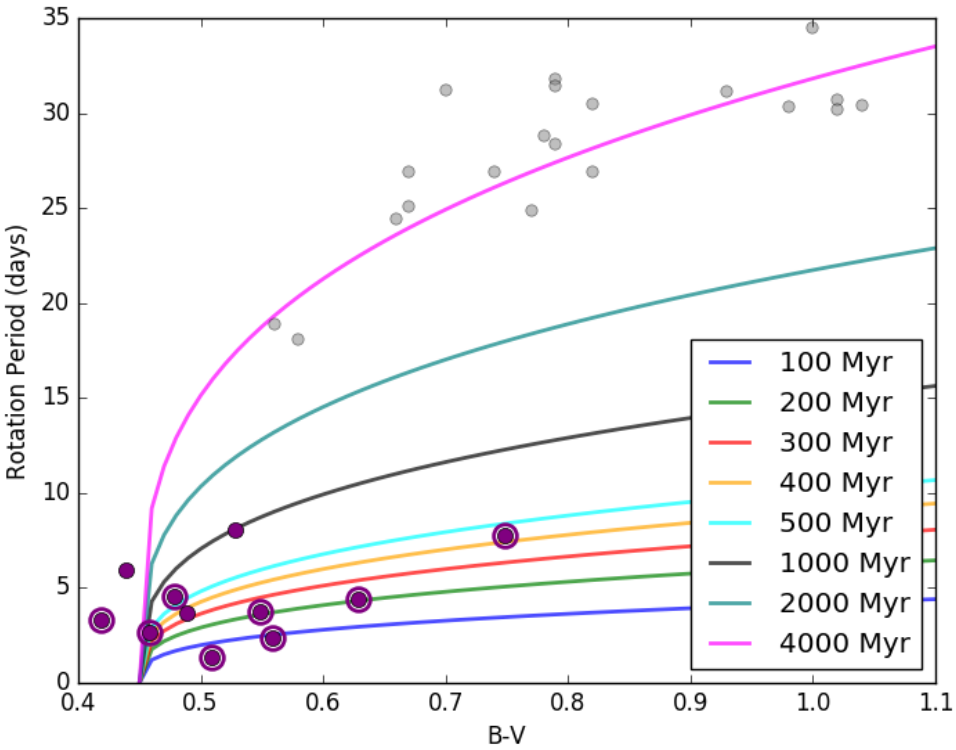

Figure 4.2 : A color-rotation plot comparing the 11 rapid rotators in our sample (purple points) to a sample of normal M67 main-sequence stars with rotation periods from Barnes et al. (2016) (gray points). Binaries are circled as in Figure 4.3. For comparison, we also show gyrochronology models from Angus et al. (2015) for ages ranging from 100 Myr to 4 Gyr.

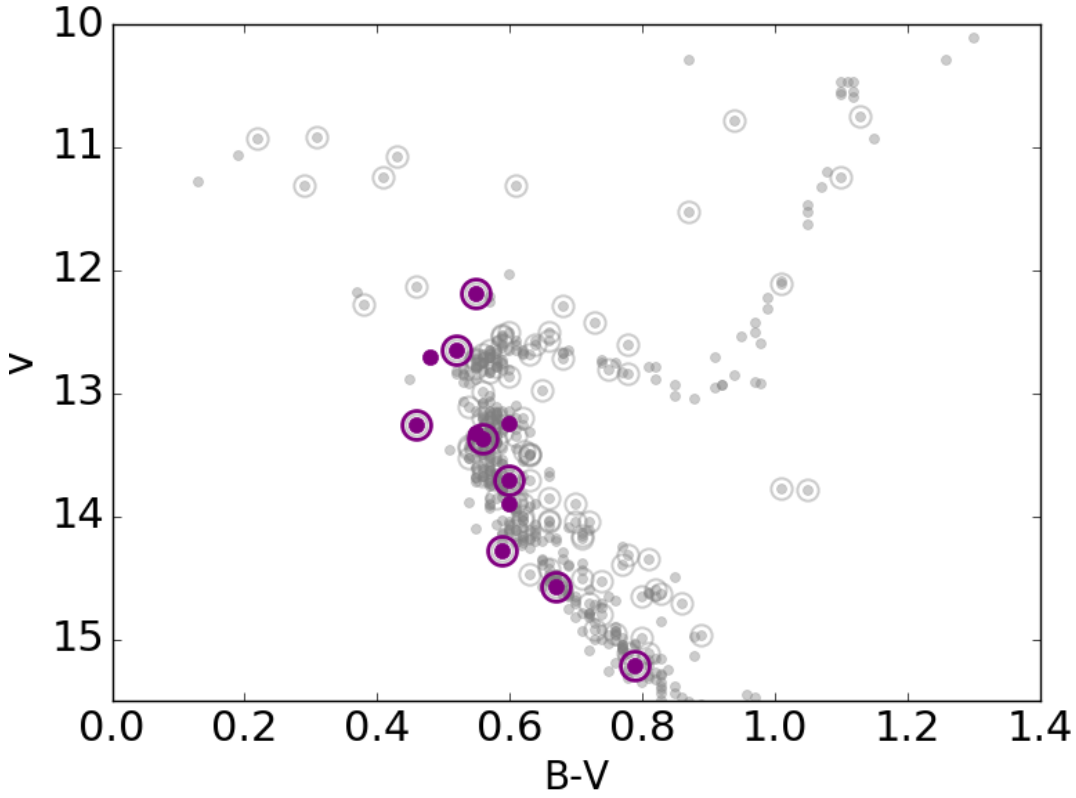

Figure 4.3 : A color-magnitude diagram showing 3D kinematic members of M67, with binary members circled (Geller et al. 2015). Purple points show stars with higher-than-normal rotation rates, which we suggest are products of recent stellar interactions.

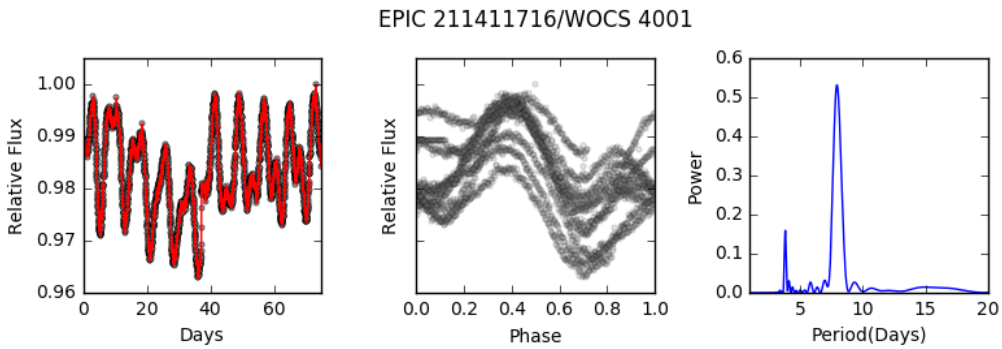

(a) P_{rot}= 7.7 days.

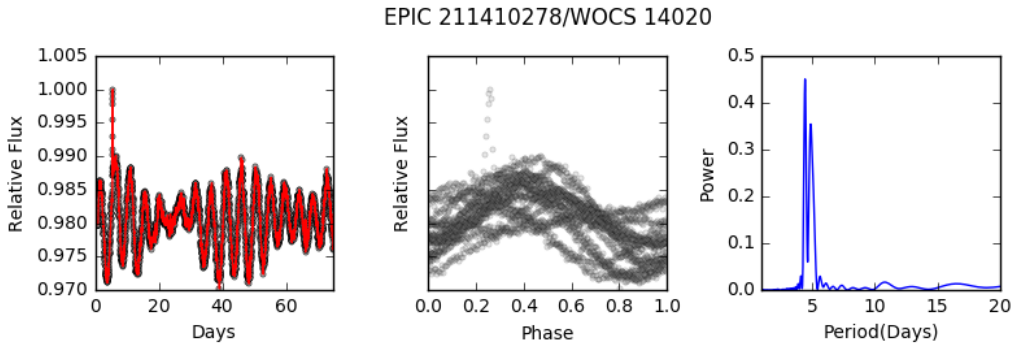

(b) Two signals at P_{rot}= 4.4 and 4.9 days, suggestive of differential rotation.

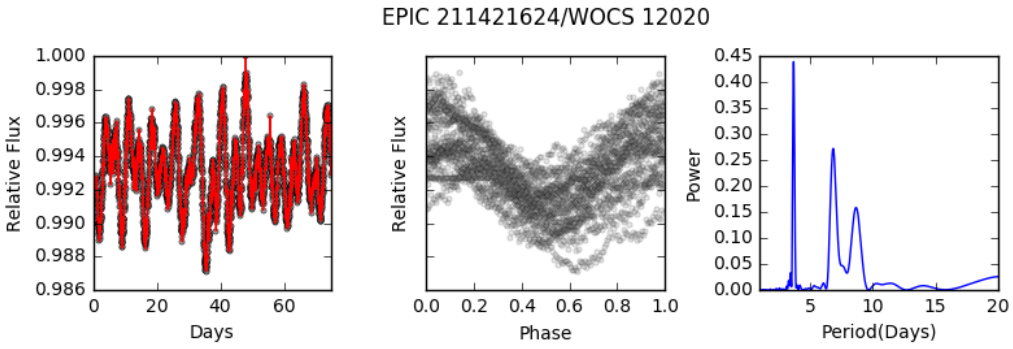

(c) P_{rot}= 3.7 days.

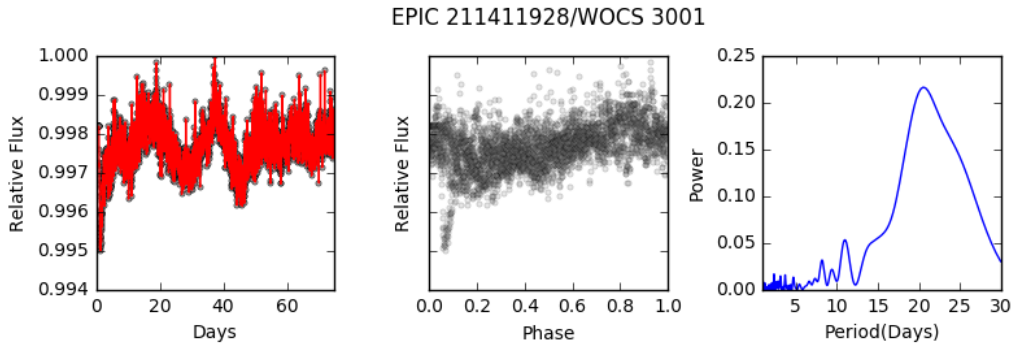

(d) P_{rot}=20.5 days in periodogram; also 3.3 days converted from $v\sin i$. The phased light curve is folded on the 20.5 day period.

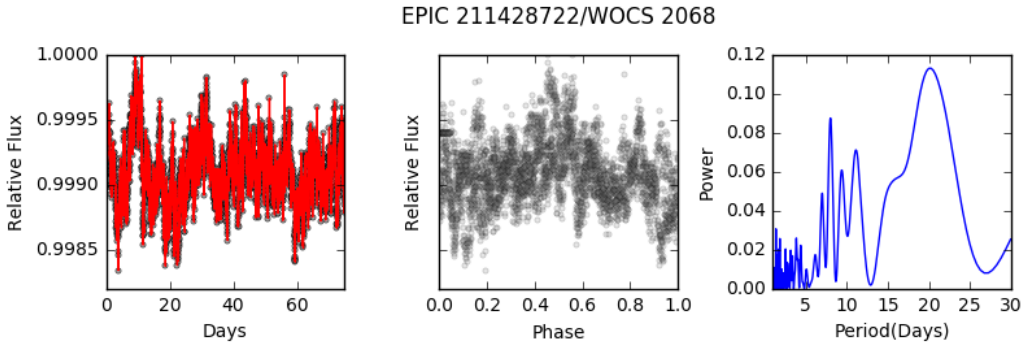

(e) Marginal signal at P_{rot}= 20.3; phased light curve shows an additional signal at 3.3 days.

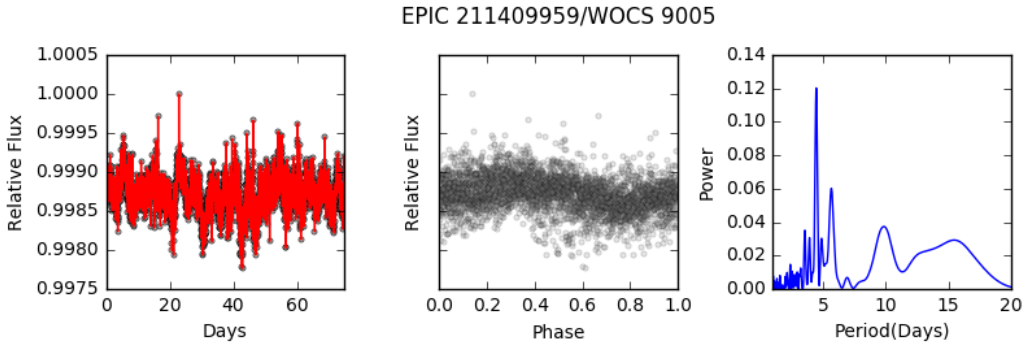

(f) P_{rot}= 4.5 days.

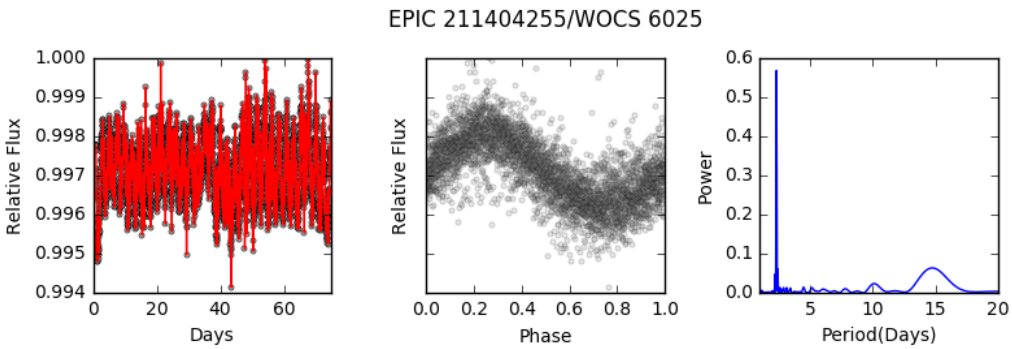

(g) P_{rot}= 2.3 days.

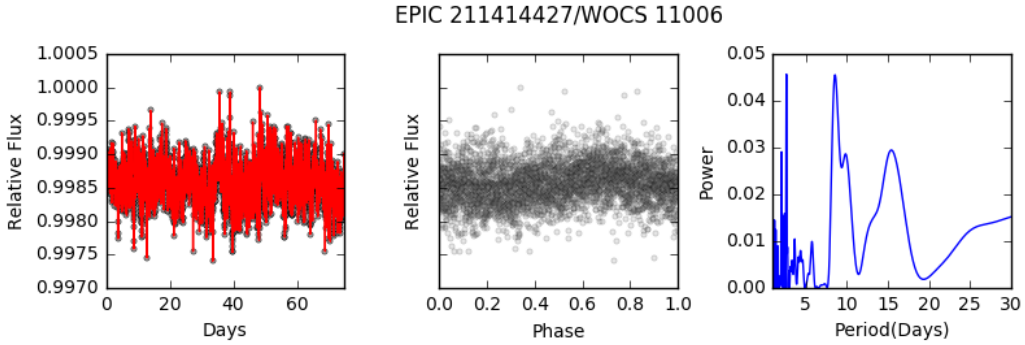

(h) Marginal signal at P_{rot}= 2.6 days, but matches the rotation period converted from $v\sin i$.

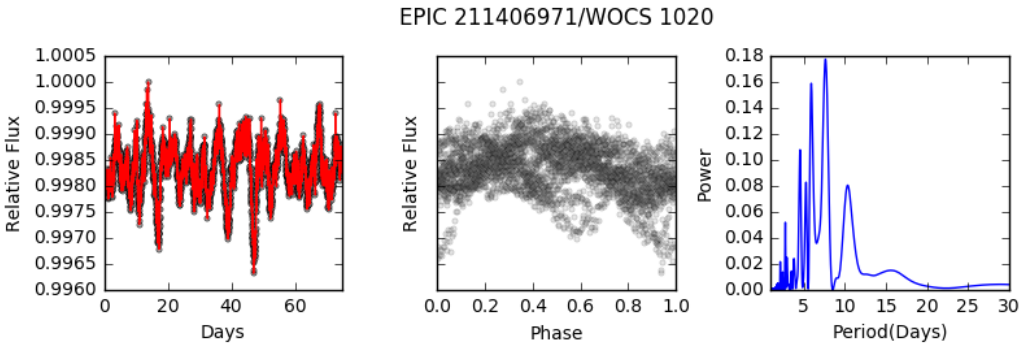

(i) Multiperiodic with the strongest peak at P_{rot}= 5.9 days.

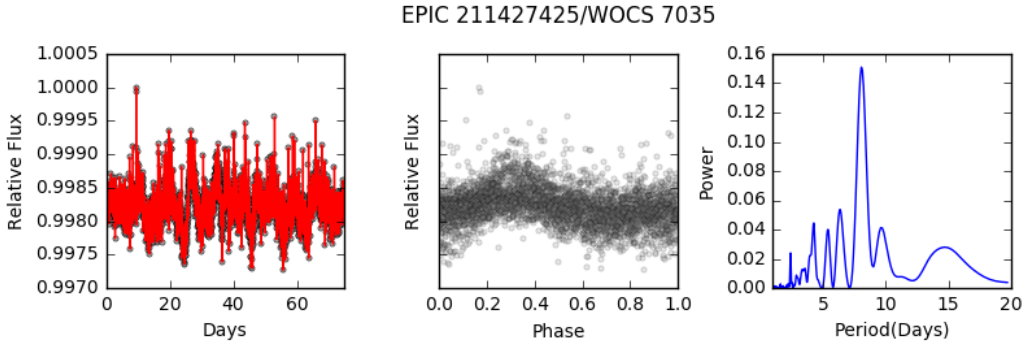

(j) P_{rot}= 8.0 days.

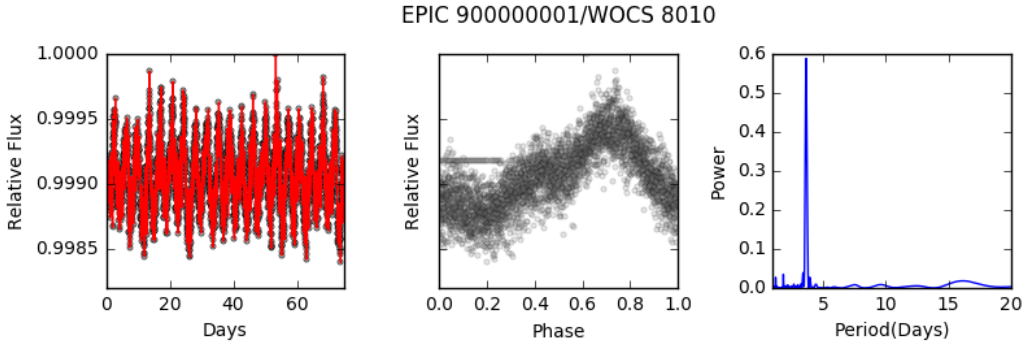

(k) P_{rot}= 3.6 days.

Figure 4.4 : Light curves and periodograms of 11 main-sequence rapid rotators. On the left we show the full K2 Campaign 5 light curve for each star. In the middle we show the phased light curve folded on the dominant period. On the right, we show Lomb-Scargle periodogram for each star.

4.4 Discussion of Individual Stars

In Table 4.1 we list the stellar and orbital properties of the rapidly rotating main-sequence stars. All these rapid rotators are high-probability proper-motion and radial-velocity members of M67. Nevertheless, there is a small probability any individual star in our sample may be a field star whose 3D motion overlaps with the motion of the cluster. However, the probability that more than one of these stars is a field contaminant is negligible (Mathieu et al. 2003).

4.4.1 WOCS 2068

This star is clearly multi-periodic, showing a rotation period of 20 days, as well as a much shorter-period signal of approximately 3 days. In Figure 4.4, we have folded the light curve on the 20-day-period signal. The phase-folded light curve shows additional variability on the 3-day timescale. The Esselstein pipeline also measures a 3-day and 20-day rotation period, though the multi-periodic nature of the star and the relatively low amplitude put it below their formal detection criteria. We show the light curve and power spectrum from the Esselstein analysis in Figure 4.5. Given the consistency of the periods measured in both pipelines and the corresponding variability evident by eye in the light curve, we include this star in our analysis. Additional Campaign 16 and Campaign 18 observations will hopefully allow us to confirm these signals in two more quarters of light curves.

We interpret this light curve as evidence that this binary is composed of two main-sequence stars, one with a 20-day rotation period typical of the solar-type stars in M67. The other star in the system has a very short rotation period. This may indicate the rapidly rotating star is a merger product. In this scenario, the initial system may have

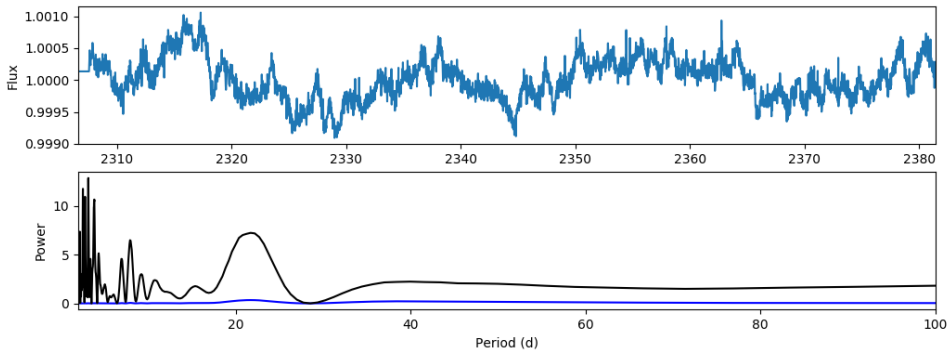

Figure 4.5 : The light curve (top) and power spectrum (bottom) of WOCS 2068 from the pipeline of Esselstein et al. 2018. In the power spectrum, the blue line shows the raw power and the black line shows the normalized power as defined in Esselstein et al 2018. The normalized power spectrum shows the strongest power at ~ 3 days, as well as a signal at 20 days, though the multi-periodic nature of the star and relatively low amplitude put it below their formal detection criteria. The light curve shows variability on both a short and longer timescale that seems to corroborate these measurements.

been a hierarchical triple consisting of a short-period inner binary and a distant triple companion. The inner binary was then driven to a merger, either by magnetic braking or through Kozai-Lidov oscillations. Alternatively, the system may have resulted from a dynamical encounter involving at least one binary star in which two stars collided (e.g. Leonard 1989; Sills et al. 2001)

The orbital solution supports this picture. The system is a long-period, highly eccentric (e=0.859) binary. The mass function indicates that, if the primary is at the turnoff mass of the cluster of 1.3 $M_\odot$, the secondary must be at least 0.7 $M_\odot$, larger than expected if the companion was a C/O white dwarf (see Figure 4.7). It thus is most consistent with a binary comprising 2 main-sequence-stars. The very large eccentricity would be unusual for a post-mass transfer binary (Figure 4.6), but it could be easily explained if the current system resulted from a dynamical interaction. Scattering experiments show that binary systems resulting from dynamical collisions tend to result in very high eccentricity orbits (Fregeau et al. 2004). In contrast, a Kozai-induced merger of an inner binary in a triple

system does not favor any particular eccentricity (Naoz & Fabrycky 2014).

Taking this information together, WOCS 2068 looks most likely to be the result of a recent stellar dynamical encounter that resulted in the collision of two main sequence stars. The current post-interaction binary consists of a rapidly-rotating, post-collision star, and a slowly rotating main-sequence companion in a high eccentricity orbit. A Kozai-induce merger is also possible, though it does not preference the high eccentricity outcome. A mass-transfer origin is not plausible given the main-sequence companion.

4.4.2 WOCS 11006

WOCS 11006 is a single-lined spectroscopic binary. We do not have a final orbital solution, so we cannot derive well-constrained orbital parameters. Our radial-velocity observations cover a time baseline of 10,000 days and indicate the binary system is long-period ($>$ 3500 days, and perhaps as long as 10000 days) with a very large orbital eccentricity. The $v\sin i$ derived from the WOCS spectra is 18.1 km s^{-1}.

The periodogram for this star shows several low-amplitude peaks, including one at 2.6 days and one at 8 days. A stronger peak at 8 days is measured in a nearby companion, and thus this periodic signal may be background contamination. The 2.6 day peak appears to originate with 11006. The Esselstein pipeline also measures a periodic signal of 2.6 days, though it is also below their detection threshold. The signal is low confidence and we would not include this star in our sample based on the periodogram alone. However, the $v\sin i$ conversion suggests a rotation rate of $2.6^{3.4}_{1.4}$ days, providing additional evidence that the photometric rotation period is real. We adopt this 2.6 day rotation period for our analysis.

4.4.3 WOCS 3001

WOCS 3001 is a circular, 128-day single-lined spectroscopic binary that is the bluest star in our sample and notably bluer than the rest of the main sequence (Figure 4.3). Despite its color, it was not included in the Geller et al. (2015) sample of blue stragglers because it fell too close to the blue hook region to be confidently identified as part of the blue straggler population. The detection of this star's elevated rotation rate provides additional evidence that it is indeed a relative of the blue stragglers.

Despite its detection as a rapid rotator with a $v\sin i$ measurement of 14.7 km s^{-1}, WOCS 3001 does not show a rotation signal at short periods in our periodogram. Due to its unusually hot temperature for the cluster, it is near the divide between stars with convective envelopes and those with radiative envelopes. As a result, it is possible the star could be a rapid rotator without significant evidence of spot modulation. The light curve does suggest a 20-day rotation signal, although due to the 75-day time baseline of the K2 observations, the detection of such long-period variability is not secure. Intriguingly, the Esselstein approach measures a signal at 2.3 days and does not detect the 20-day signal. This shorter rotation period would be compatible with the $v\sin i$ measurement, but it is also an unreliable signal below their detection criteria. Given the inconsistencies from these two measurement methods and the low reliability of all the measured signals, we conclude that there is not a clear period evident in the light curves. Perhaps additional K2 Campaign 16 and 18 light curves will allow us to measure a more reliable signal in this star. In the analysis that follows, we adopt a rotation period of 3.3 days, which we derive from the $v\sin i$ measurement using the technique outlined in Section 4.2.

4.4.4 WOCS 14020

WOCS 14020 shows two strong peaks in its periodogram, one at 4.4 days and one 4.9 days. The light curve (Figure 4.4) also shows a clear beating pattern. Given the close spacing of these two peaks, we suggest the two periods are evidence for differential rotation on the star, with two star spots at slightly different latitudes moving in and out of phase with each other (e.g. Reinhold & Gizon 2015).

The spectrum of this star is single-lined, and the mass function sets a minimum companion mass of 0.15 $M_{\odot}$. The lack of flux from a companion in the spectrum combined with the very low mass minimum argues strongly for either a white dwarf or a M-dwarf secondary star. Interestingly, the system is detected in both the GALEX NUV and FUV filters (effective wavelengths of $\lambda_{eff} = 2267$ and 1516 Å, respectively), indicating the system has a large UV excess. We show the spectral energy distribution in Figure 4.8. The GALEX FUV measurement strongly suggests the presence of a hot, faint companion, likely a white dwarf star. The FUV flux excess is consistent with a $\sim 13,000$ K C/O white dwarf. This temperature implies an age of ~ 300 Myr (Tremblay et al. 2011), in general agreement with the age implied from the rotation rate of ~ 200 Myr. Narrow-band UV photometry and/or UV spectroscopy are needed to confirm this detection and provide better temperature and age estimates.

4.4.5 WOCS 4001, 6025, 9005, 12020

These systems are all single-lined spectroscopic binaries. WOCS 6025, 4001, and 12020 have very clear signatures of spot modulation in their light curves at levels of up to a few percent, and strong peaks in their periodograms that are independently confirmed using the period measurement technique of Esselstein et al. WOCS 9005 has lower amplitude variability. The same period is detected using the pipeline of Esselstein et al., but the

amplitude is below their detection threshold. Our visual inspection confirms a single, clean periodic signal in the periodogram and consistent variability in both phased and unphased light curves matching this period. Given that the Esselstein pipeline measures the same period (though below their formal detection criteria) and the visual examination confirms this period, we include it on our sample (Figure 4.4).

All these stars are long-period ($P_{orb} > 100$ day) binaries. All but WOCS 6025 have secondary mass limits consistent with white dwarf companions and thus with being candidate post-mass-transfer systems (Figure 4.7). WOCS 6025 has a large secondary mass limit of 1.1 $M_{\odot}$, more compatible with an F or G main-sequence companion, though the spectra and the spectral energy distribution (SED) of the system do not reveal any evidence of such a main-sequence companion.

4.4.6 WOCS 1020, 7035, 8010

WOCS 8010 and WOCS 7035 both show strong single peaks in their periodograms that are independently confirmed by measurements of Esselstein et al. WOCS 1020 shows at least two strong, closely spaced peaks. Similar to 14020, these may be evidence for two close periods caused by differential rotation and starspots at slightly different latitudes. Additional lower-amplitude peaks may be due to a combination of aliasing and other smaller spot groups. The phased light curve shows variations slightly out of phase with each other, consistent with the interpretation of multiple spots. Esselstein et al. do detect variability in this star with a similar period, but do not classify it as a clean detection due to the multi-periodic nature.

All of these stars are non-velocity variable. If these stars do have companions that have avoided detection, these systems are either quite wide ($P_{orb} \gtrsim 10000$ days), or viewed very close to edge on. Assuming these stars are in fact single stars, they would not have

formed from mass-transfer or Kozai-induced mergers in triple systems, as both scenarios are expected to leave behind binary systems. Instead, they may have formed through dynamical collisions between main-sequence stars (e.g. Sills et al. 2001; Leonard 1989) or a merger of a close main-sequence binary system through internal processes such as magnetic braking (e.g. Andronov et al. 2006). The dynamical scenario most commonly leaves behind binary or higher-order systems (Fregeau et al. 2004), indicating the merger scenario may be most likely.

4.5 Characteristics of Rapid Rotators

In Figure 4.3 we mark the location of these 11 stars in a color-magnitude diagram of M67 members. For reference, we show the rotation periods of these stars compared to standard stars in M67 (Barnes et al. 2016) and those predicted by gyrochronology relations of Angus et al. (2015) (Figure 4.2). We discuss the properties of this sample below.

4.5.1 Binary Fraction

Eight of the 11 systems in our sample are binaries, for a binary fraction of 73% ±31%. For comparison, the spectroscopic binary fractions ($P_{\rm orb} < 10^4$ days) of M67 and other old open clusters are observed to be in the range of 20-30% (Geller et al. 2015; Milliman et al. 2014; Geller et al. 2009). These rapid rotators thus have about 3 times the binary fraction expected for a typical main-sequence population.

Classical blue straggler populations in old open clusters are observed to have similarly high binary fractions. In M67 itself, the blue straggler binary fraction is 80% (Geller et al. 2015). In the 7-Gyr open cluster NGC 188, 76% ±19% of blue stragglers are observed to be spectroscopic binaries within a similar period domain (Mathieu & Geller 2009). Thus the observed high binary fraction among these rapid rotators is consistent with our hypothesis

that they are lower-luminosity analogs of the blue stragglers, and further suggests that they may form through similar binary evolution channels.

4.5.2 Orbital Properties

We show the eccentricity-period distribution of the 8 binaries in our sample in Figure 4.6. For comparison, we also show the eccentricity-period distribution of field barium stars, CEMP-s stars, blue metal poor stars, and blue stragglers in 3 old open clusters NGC

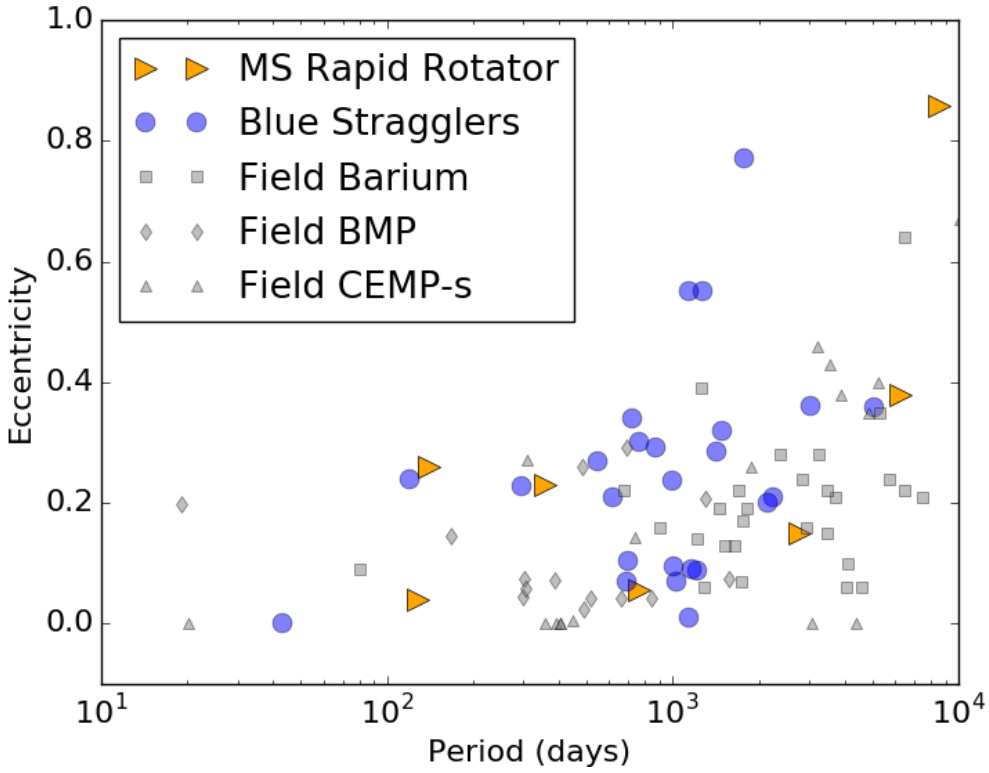

Figure 4.6 : A comparison of the distributions of periods and eccentricities of the M67 main-sequence rapid-rotators (orange triangles) to the the binary blue straggler populations of several old open clusters (blue circles) and post-mass-transfer binaries observed in field (gray symbols), including carbon-enhanced metal poor stars with s-process enrichment (Jorissen et al. 2016; Hansen et al. 2016), blue metal-poor stars (Carney et al. 2005), and barium stars (Jorissen et al. 1998). We do not include WOCS 11006 on this diagram, as we do not have a complete orbital solution, but it appears to be a long-period, high-eccentricity system that would fall in the upper right corner of this diagram.

188 (Geller et al. 2009), M67 (Pollack et al., in prep), and NGC 6819 (Milliman et al. 2014). Most of binaries in our sample of rapid rotators have low eccentricities that fall within the eccentricity-period locus of these post-mass-transfer binaries.

Typical populations of long-period solar-like main-sequence binaries have eccentricities in a gaussian-like distribution about a mean of e= 0.4 (e.g. Meibom et al. 2006; Raghavan et al. 2010). On the other hand, post-mass-transfer binaries show lower eccentricities. Some blue stragglers and the other post-mass-transfer binaries have circularized orbits, and almost all show lower eccentricities than typical solar-type main-sequence binaries at orbital periods of $\sim$ 1000 days (Mathieu & Geller 2009; Jorissen et al. 1998; Hansen et al. 2016; Jorissen et al. 2016; Carney et al. 2005). Two binaries in our sample of rapid rotators (WOCS 3001 and WOCS 12020) do have circular orbits, suggestive that both of these systems have been through mass transfer.

On the other hand, two of the 8 binaries, WOCS 11006 and 2068, have much larger eccentricities and longer periods than typical for post-mass-transfer systems. Such large eccentricities are perhaps more compatible with dynamical formation, as we suggest for WOCS 2068 (Section 4.4.1).

We note that 3 of the binaries in our sample (WOCS 3001, 4001, 14020) have orbital periods of just a few hundred days, shorter than all but three of the observed blue stragglers in NGC 188, M67, and NGC 6819. If these stars are indeed post-mass-transfer binaries, their orbital periods suggest they result from Case B mass transfer (mass transfer from an RGB donor). These 3 short-period systems resemble WOCS 5379 in the cluster NGC 188, a 120-day blue straggler-white dwarf binary that Gosnell et al. (2014) suggest evolved through a common envelope event. Similarly, one of these stars is WOCS 14020, whose UV excess is strongly suggestive of a white dwarf and a mass-transfer origin.

Case B mass transfer is usually found to be unstable (Ivanova et al. 2008; Chen &

Han 2008), leading to common envelope evolution, so these systems could be new tests of the physics of current common envelope models. Additionally, it is interesting that more of these short-period systems show up in this lower luminosity domain than among the blue straggler population. This could hint that they form from binary systems with initially lower-mass secondaries, or that they do not accrete as much mass from their companions and are indicative of more inefficient mass transfer than the blue stragglers. These three systems are excellent candidates to model in more detail, as their evolutionary pathways may help constrain these uncertain aspects of mass-transfer physics.

4.5.3 Companion Masses

For 7 of the 8 binaries in our sample, we have orbit solutions that enable us to determine a binary mass function, f(m). From this function, we can derive lower limits on the mass of the secondary after adopting a mass for the primary. We do this by fitting a stellar evolutionary track to the CMD position of each system, recognizing that standard stellar evolution theory may not be accurate for these stars. We find that the primary stars range in mass from 0.9-1.35 $M_{\odot}$. Using these primary masses, we derive the minimum mass for each secondary star. These secondary mass lower limits are shown in Figure 4.7, plotted against periastron separation.

We find that 5 of the 7 binaries fall well within the period-secondary mass range expected for post-mass-transfer white dwarf-main sequence binaries (Rappaport et al. 1995). Two systems, WOCS 2068 and WOCS 6025, appear to have secondaries more massive than expected if their companions are white dwarfs. This is as expected for WOCS 2068, as the light curve displays two distinct rotation periods, possibly indicating the system is a binary consisting of two main sequence stars. WOCS 6025 also has a substantially more massive companion (> 1.1 $M_{\odot}$) than expected for a white dwarf. The

white dwarf initial-final mass relation predicts such a massive white dwarf would form from a very massive progenitor (> 6 M$_\odot$; Kalirai et al. 2008), far above the 1.3 M$_\odot$ turnoff of M67. This companion is therefore more compatible with a main-sequence star. However, we note that some known white dwarf-main sequence binaries do not fall on the expected Rappaport et al. (1995) relation (e.g. Kawahara et al. 2018, Gosnell et al. 2018, in prep). On their own, the secondary masses cannot definitely confirm or rule out the existence of

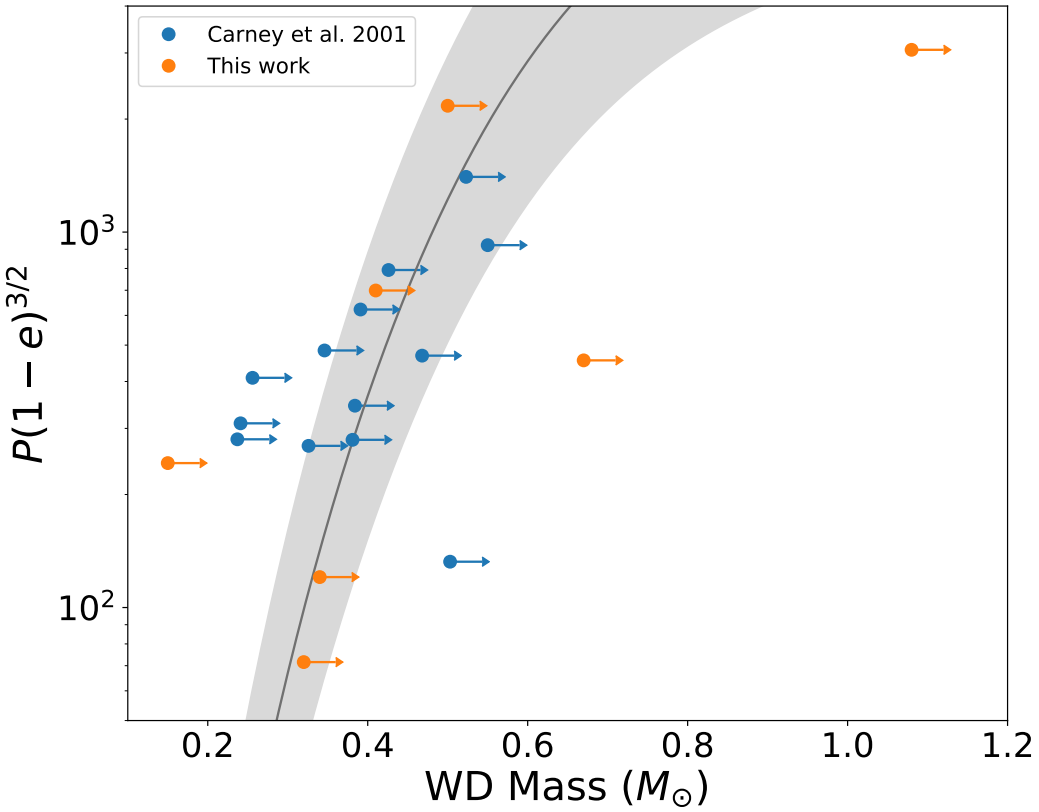

Figure 4.7 : We show the relationship between orbital separation at periastron and secondary mass for a sample of field blue straggler binaries from Carney et al. (2001) (blue points) compared to our sample of rapidly rotating main-sequence binaries (orange points). We also show in gray the Rappaport et al. (1995) theoretical period-white dwarf mass relationship for binaries resulting from stable mass transfer. All points show lower limits on the secondary masses derived from the binary mass functions. WOCS 11006 is not included in the plot, as we have no secure orbital solution.

white dwarf companions for these sources.

4.5.4 UV Excesses Indicative of White Dwarf Companions

To look for evidence of companions to our systems, we examine their spectral energy distributions (SEDs). We include UV photometry from GALEX, IR photometry from 2MASS (Skrutskie et al. 2007) and WISE (Martin et al. 2005), and optical photometry from Geller et al. (2015), originally obtained by Montgomery et al. (1993). Our SED fitting routine is described in Leiner et al. (2016). Briefly, we fit a grid of Castelli & Kurucz (2004) models of varying temperature and radius using χ^2 minimization. We fix the surface gravity to a typical main-sequence value ($\log g = 4.0$), assume solar-metallicity models, and fix the reddening to the cluster value (E(B-V)= 0.041; Taylor 2007). We note that the SED fits are not particularly sensitive to our choice for surface gravity, metallicity, or reddening within a range of reasonable values. We set the distance to 850 pc, the median of the 800-900 pc range found to M67 in the literature (Geller et al. 2015).

We fit SEDs to these stars in three steps: 1) We fit a single, main-sequence model. 2) We fit a combination of 2 main-sequence stars. 3) We fit the flux excluding the GALEX FUV photometry, as this is the only bandpass that would have substantial flux from a hot white dwarf companion. If the best fit comes from Method 1, we characterize the star as being single or having a low-luminosity companion. If the best fit comes from Method 2, the system has a relatively bright main-sequence secondary. If the best fit comes from Method 3, this is indicative of a UV excess not well described by any main-sequence companion. These stars may have hot white dwarf companions contributing to their UV flux, or may have UV flux enhancements due to stellar activity. We show the best fitting model for each star in our sample in Figure 4.8 .

We find that the UV flux of WOCS 2068 can be well described by a combination of

two stars– one near the main-sequence turnoff, and the other a blue straggler of $\sim$ 6800 K. This SED fit is consistent with our interpretation of the photometric variability, that the system consists of one rapidly rotating merger or collision product (the 6800 K blue straggler), and the other a typical main-sequence star.

Several other binaries in our sample also have UV excesses over single-star models that are not resolved by adding a main-sequence companion. These include WOCS 14020, 3001, 12020, 6025, and 11006. WOCS 14020 is the only one of these systems where we consider this UV excess a definitive white dwarf detection. Assuming a typical 0.5 $M_{\odot}$ C/O white dwarf model, the UV excess is most compatible with a $\sim 13,000$ K white dwarf companion corresponding to an age of $\sim$ 300 Myr (Tremblay et al. 2011).

The rest of the binaries with UV excesses are all hotter than WOCS 14020, making it more likely that the wide GALEX FUV passband picks up some flux from the Wien tail of the primary. Due to the low resolution and uncertainties on the spectral models in the UV, it is not clear whether these excesses indicate white dwarf companions. They could, for example, result from elevated UV flux due to chromospheric emission, which might be expected given that these stars are all rapidly rotating. Similar excesses have been discovered in other FGK field stars using GALEX photometry that have been largely attributed to UV emission from stellar activity (Smith et al. 2014). The excesses are nevertheless large enough to be intriguing. While none of the fluxes are large enough to indicate a very young white dwarf ($<$ 150 Myr), they could be compatible with cooler white dwarf companions with ages of $\sim 150 - 300$ Myr. We suggest follow-up observations using more precise, multi-band UV photometry (e.g. HST/WFC3 as in Gosnell et al. 2015) to more definitively address the presence of white-dwarf companions.

Given the temperatures of the primaries and the GALEX detection limits, we might expect to detect white dwarf companions hotter than $\sim$ 13000 K as UV excesses in the

stellar SEDs, corresponding to an age younger than about 300 Myr. Notably, we detect UV excesses only in the binaries with the youngest rotational ages in our sample, all less than 300-400 Myr (Figure 4.2). The binary systems with older inferred gyro-ages (WOCS 4001, WOCS 9005) do not have UV detections. The gyro-ages and UV excesses are therefore both compatible with the hypothesis that 4001 and 9005 formed earlier, and therefore have cooler undetectable WD companions, and the other binaries formed recently enough to have hot, detectable WD companions.

Only one of the single stars, WOCS 1020, has a GALEX FUV detection. The others, WOCS 7035 and WOCS 8010, do not have FUV detections. The non-detection of these stars is as expected, as only WOCS 1020 is hot enough to expect FUV flux above the GALEX detection limit. We show SEDs for all these systems in Figure 4.8. All can be reasonably well fit with single-star SED models.

4.6 Summary and Discussion

We demonstrate that blue stragglers spin up to large rotational velocities at formation, and then spin down as they age approximately as predicted by models for standard solar-type stars. As a result, a mass-transfer event restarts a star's gyro-age clock. This is the first comparison between the spin down of post-mass-transfer solar-type binaries and models of single main-sequence stars, and suggests that gyrochronology is a plausible technique for determining how long ago mass-transfer occurred in blue stragglers and other post-mass-transfer binaries. Crucially, this result enables identification of blue-straggler-type objects within the main-sequence by looking for old stars with fast rotation rates. Though we do not empirically determine the spin down rates of merger or collision products, models and observations both agree these stars are also rapidly rotating soon after formation. These stars thus may also be identifiable using this technique, but it is not clear if gyrochronology

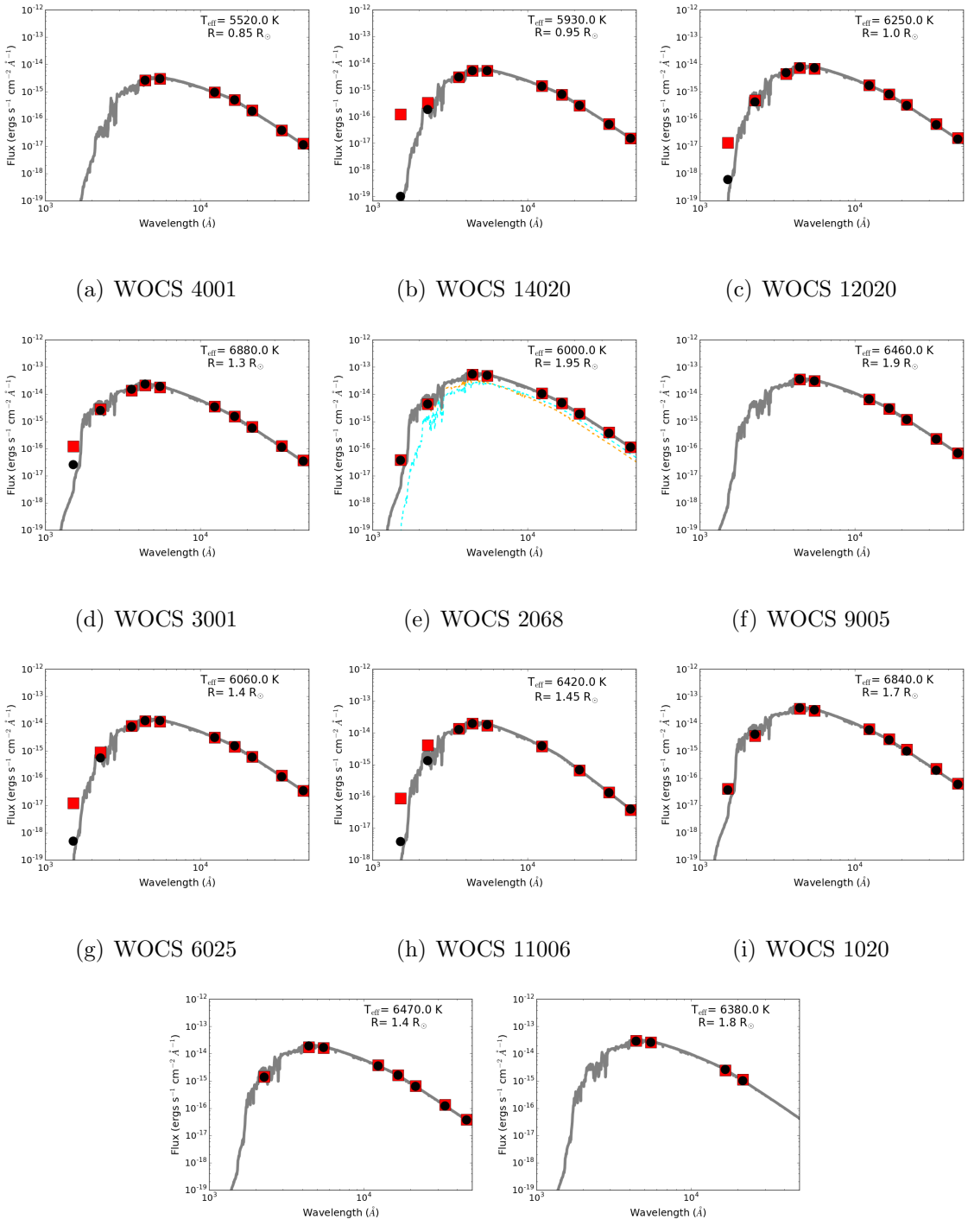

(a) WOCS 4001 (b) WOCS 14020 (c) WOCS 12020

(d) WOCS 3001 (e) WOCS 2068 (f) WOCS 9005

(g) WOCS 6025 (h) WOCS 11006 (i) WOCS 1020

(j) WOCS 7035 (k) WOCS 8010

Figure 4.8 : SEDs of the 11 rapid rotators in M67. We show the best-fit Castelli & Kurucz (2004) spectrum in gray. Black circles are synthetic observations created by convolving the spectrum with filter transmission functions for 2MASS, WISE, GALEX, and Johnson UBV filters. The real observations are shown with red squares. For one system, WOCS 2068, we use a two star model. Here we plot the primary model (6000 K, 1.95 $R_\odot$) in cyan, the secondary model (6800 K, 1.5 $R_\odot$) in orange, and the combined flux in black.

is a reliable predictor of their age.

We pilot the use of this technique in M67 by measuring stellar rotation periods from K2 Campaign 5 light curves as well as the spectral database of the WIYN Open Cluster Study. We find 11 rapid rotators on the M67 main sequence, all with rotation periods less than 8 days. Based on these rotation rates, we hypothesize these stars have been through recent mass-transfer, mergers, or stellar collisions.

These 11 detections have much in common with the blue straggler population of the cluster including: a binary fraction three times higher than the main-sequence spectroscopic binary fraction of M67; a preponderance of long-period, low-eccentricity binary systems; and in at least one case a UV excess indicative of a young white dwarf companion. These results suggest that these 11 sources are mass-transfer, merger, or collision products, and thus represent the low-luminosity end of the blue straggler distribution. This population has not been explored until now, as it blends photometrically with the cluster main sequence. With 11 detections, these main-sequence rapid rotators are nearly as numerous as the classical blue straggler population of the cluster. This result suggests that population studies that focus only on classical blue stragglers are missing as much as half of the mass-transfer, collision, and merger population.

These 11 detections were selected from an overall sample of $\sim$ 400 main-sequence members including 98 main-sequence binaries (Pollack et al 2018, in prep). Eight of our 11 detections are binaries, implying approximately 8% of the solar-type short-period ($P_{orb}<$ 10^4 days) binary population has been impacted by a recent stellar interaction. Of these 8, we hypothesize at least 5 are recent mass-transfer products given their secondary masses (Figure 4.7), indicating at least 5% of the FGK spectroscopic binary population has been through mass transfer within the last Gyr. Three systems are observed to be single stars, indicating $\sim$ 1% of the single main sequence stars are spun-up merger or collision products.

If mergers and collisions spin down in much the same way as we have demonstrated for mass-transfer products, these stars may also have formed within the last Gyr.

This result is illustrative of the ways binary evolution can impact a stellar population. If 11 stellar systems in M67 have been through a stellar collision or mass transfer event in the last Gyr, it is quite likely that other stars on the main sequence have also experienced stellar interactions in the more distant past. Indeed, 4 of the 11 stars in our sample are near the zero-age main-sequence (Figure 4.3), suggesting many of these interaction products can live for several Gyr before evolving off the main-sequence.

Older post-interaction systems would likely show up with intermediate rotation periods (i.e. 8-15 days). These slower rotators would be less magnetically active with smaller and shorter-lived spots, making them harder to identify through rotational modulation. Similarly, their slower rotation rates would make them undetectable using $v\sin i$ measurements in all but very-high-resolution spectroscopic studies. These slower rotation periods are also closer to typical cluster rotation rates, making such stars more difficult to distinguish from the distribution of normal M67 stars. Such stars may nevertheless contribute to the spread of rotation rates observed in the cluster, skewing measurements towards shorter rotation periods and complicating efforts to calibrate precise gyrochronology relationships in clusters.

As a simple upper bound, if we suppose formation rates of FGK-type interaction products remained constant over the 4 Gyr history of the cluster, this implies up to $\sim 30\%$ of solar-type binaries and $\sim 4\%$ of the single main-sequence stars have been through an interaction during their life times. Though a very simple estimate, these numbers are in rough agreement with other studies. Andronov et al. (2006) predict 3-4% of main-sequence stars in M67 may be merger products. Murphy et al. (2018) find $\sim$20% of the field A/F- type binaries within a similar period range are post-mass-transfer binaries. The post-interaction

fraction among older binary populations is sizable.

M67 was re-observed in K2 Campaign 16, and is slated for more observations in Campaign 18. These additional months of data will allow us to confirm these detections, refine rotation-period measurements for the cluster at large, and perhaps detect more anomalously rapid rotators. In addition, several other clusters have the K2 and Kepler light curves needed to detect these populations on the main sequence including NGC 6791, NGC 6819, and Ruprecht 147. These additional studies, combined with detailed binary-population modeling, will be required to quantify more precisely what the impact of binary interactions may be on the rotational properties of cluster stellar populations.

Kepler and K2 have opened the door to detecting lower-luminosity mass-transfer, merger, and collision products on the main sequence using rotation rates. With similar future missions like TESS and PLATO planned for the near and longer term future, rotational studies of stars in clusters and in the field will continue to be important areas of study. TESS will yield rotation periods for nearby stars in younger clusters (< 1 Gyr) and the field. Looking for rapidly rotating field stars with abundances or kinematics indicative of old age may be a viable detection method for field post-mass-transfer binaries. Due to the large scatter in rotation rates among young stars, this technique may not be well suited to identifying interaction products in TESS clusters. PLATO, planned for launch in 2026, should target more older clusters where rotational identification of post-interaction stars would be possible. As the known population continues to grow, these populations can provide new tests for binary evolution physics and cluster population models.

References

Aigrain, S., Hodgkin, S. T., Irwin, M. J., Lewis, J. R., & Roberts, S. J. 2015, MNRAS, 447, 2880

Almenara, J. M., Alonso, R., Rabus, M., et al. 2012, MNRAS, 420, 3017

Andronov, N., Pinsonneault, M. H., & Terndrup, D. M. 2006, ApJ, 646, 1160

Angus, R., Aigrain, S., Foreman-Mackey, D., & McQuillan, A. 2015, MNRAS, 450, 1787

Aoki, W., Beers, T. C., Sivarani, T., et al. 2008, ApJ, 678, 1351

Balona, L. A., & Abedigamba, O. P. 2016, MNRAS, 461, 497

Barnes, S. A. 2003, ApJ, 586, 464

Barnes, S. A., Weingrill, J., Fritzewski, D., Strassmeier, K. G., & Platais, I. 2016, ApJ, 823, 16

Breton, R. P., Rappaport, S. A., van Kerkwijk, M. H., & Carter, J. A. 2012, ApJ, 748, 115

Carney, B. W., Latham, D. W., Laird, J. B., Grant, C. E., & Morse, J. A. 2001, AJ, 122, 3419

Carney, B. W., Lee, J.-W., & Dodson, B. 2005, AJ, 129, 656

Castelli, F., & Kurucz, R. L. 2004, ArXiv Astrophysics e-prints, astro-ph/0405087

Chen, X., & Han, Z. 2008, MNRAS, 387, 1416

Corsaro, E., Stello, D., Huber, D., et al. 2012, ApJ, 757, 190

de Mink, S. E., Langer, N., Izzard, R. G., Sana, H., & de Koter, A. 2013, ApJ, 764, 166

Epstein, C. R., & Pinsonneault, M. H. 2014, ApJ, 780, 159

Fan, X., Burstein, D., Chen, J.-S., et al. 1996, AJ, 112, 628

Fornasini, F. M., Tomsick, J. A., Bodaghee, A., et al. 2014, ApJ, 796, 105

Fregeau, J. M., Cheung, P., Portegies Zwart, S. F., & Rasio, F. A. 2004, MNRAS, 352, 1

Gallet, F., & Bouvier, J. 2013, A&A, 556, A36

Geller, A. M., Hurley, J. R., & Mathieu, R. D. 2013, AJ, 145, 8

Geller, A. M., Latham, D. W., & Mathieu, R. D. 2015, AJ, 150, 97

Geller, A. M., Mathieu, R. D., Harris, H. C., & McClure, R. D. 2008, AJ, 135, 2264

—. 2009, AJ, 137, 3743

Girard, T. M., Grundy, W. M., Lopez, C. E., & van Altena, W. F. 1989, AJ, 98, 227

Gonzalez, G. 2016, MNRAS, 463, 3513

Gosnell, N. M., Mathieu, R. D., Geller, A. M., et al. 2015, ApJ, 814, 163

—. 2014, ApJ, 783, L8

Handberg, R., Brogaard, K., Miglio, A., et al. 2017, MNRAS, 472, 979

Hansen, T. T., Andersen, J., Nordström, B., et al. 2016, A&A, 588, A3

Hartman, J. D., Gaudi, B. S., Holman, M. J., et al. 2008, ApJ, 675, 1254

Holberg, J. B., Casewell, S. L., Bond, H. E., Burleigh, M. R., & Barstow, M. A. 2014, MNRAS, 444, 2022

Ivanova, N., Heinke, C. O., Rasio, F. A., Belczynski, K., & Fregeau, J. M. 2008, MNRAS, 386, 553

Jeffries, R. D., Burleigh, M. R., & Robb, R. M. 1996, A&A, 305, L45

Jeffries, R. D., & Stevens, I. R. 1996, MNRAS, 279, 180

Jorissen, A., Van Eck, S., Mayor, M., & Udry, S. 1998, A&A, 332, 877

Jorissen, A., Van Eck, S., Van Winckel, H., et al. 2016, A&A, 586, A158

Kalirai, J. S., Hansen, B. M. S., Kelson, D. D., et al. 2008, ApJ, 676, 594

Kawahara, H., Masuda, K., MacLeod, M., et al. 2018, ArXiv e-prints, arXiv:1801.07874

Kellett, B. J., Bromage, G. E., Brown, A., et al. 1995, ApJ, 438, 364

Kruse, E., & Agol, E. 2014, Science, 344, 275

Landsman, W., Aparicio, J., Bergeron, P., Di Stefano, R., & Stecher, T. P. 1997, ApJ, 481, L93

Leiner, E., Mathieu, R. D., Stello, D., Vanderburg, A., & Sandquist, E. 2016, ApJ, 832, L13

Leonard, P. J. T. 1989, AJ, 98, 217

Li, L., Zhang, F., Han, Q., Kong, X., & Gong, X. 2014, MNRAS, 445, 1331

Lovisi, L., Mucciarelli, A., Ferraro, F. R., et al. 2010, ApJ, 719, L121

Lurie, J. C., Vyhmeister, K., Hawley, S. L., et al. 2017, AJ, 154, 250

Martin, D. C., Fanson, J., Schiminovich, D., et al. 2005, ApJ, 619, L1

Mathieu, R. D. 2000, in ASP Conf. Ser., Vol. 198, Stellar Clusters and Associations: Convection, Rotation, and Dynamos, ed. R. Pallavicini, G. Micela, & S. Sciortino, 517

Mathieu, R. D., & Geller, A. M. 2009, Nature, 462, 1032

Mathieu, R. D., van den Berg, M., Torres, G., et al. 2003, AJ, 125, 246

Matt, S., & Pudritz, R. E. 2005, MNRAS, 356, 167

McCrea, W. H. 1964, MNRAS, 128, 147

Meibom, S., Barnes, S. A., Platais, I., et al. 2015, Nature, 517, 589

Meibom, S., Grundahl, F., Clausen, J. V., et al. 2009, AJ, 137, 5086

Meibom, S., & Mathieu, R. D. 2005, ApJ, 620, 970

Meibom, S., Mathieu, R. D., & Stassun, K. G. 2006, ApJ, 653, 621

Milliman, K. E., Leiner, E. L., Mathieu, R. D., & Tofflemire, B. M. 2016, AJ, arXiv:1408.0239

Milliman, K. E., Mathieu, R. D., Geller, A. M., et al. 2014, AJ, 148, 38

Montgomery, K. A., Marschall, L. A., & Janes, K. A. 1993, AJ, 106, 181

Mucciarelli, A., Lovisi, L., Ferraro, F. R., et al. 2014, ApJ, 797, 43

Murphy, S. J., Moe, M., Kurtz, D. W., et al. 2018, MNRAS, 474, 4322

Naoz, S., & Fabrycky, D. C. 2014, ApJ, 793, 137

Nemec, J. M., Balona, L. A., Murphy, S. J., Kinemuchi, K., & Jeon, Y.-B. 2017, MNRAS, 466, 1290

Packet, W. 1981, A&A, 102, 17

Parsons, S. G., Rebassa-Mansergas, A., Schreiber, M. R., et al. 2016, MNRAS, 463, 2125

Parsons, S. G., Agurto-Gangas, C., Gänsicke, B. T., et al. 2015, MNRAS, 449, 2194

Perets, H. B., & Fabrycky, D. C. 2009, ApJ, 697, 1048

Raghavan, D., McAlister, H. A., Henry, T. J., et al. 2010, ApJS, 190, 1

Rappaport, S., Podsiadlowski, P., Joss, P. C., Di Stefano, R., & Han, Z. 1995, MNRAS, 273, 731

Rebassa-Mansergas, A., Gänsicke, B. T., Schreiber, M. R., Koester, D., & Rodríguez-Gil, P. 2010, MNRAS, 402, 620

Rebassa-Mansergas, A., Ren, J. J., Irawati, P., et al. 2017, MNRAS, 472, 4193

Reinhold, T., & Gizon, L. 2015, A&A, 583, A65

Sanders, W. L. 1977, A&AS, 27, 89

Sarajedini, A., von Hippel, T., Kozhurina-Platais, V., & Demarque, P. 1999, AJ, 118, 2894

Shetrone, M. D., & Sandquist, E. L. 2000, AJ, 120, 1913

Sills, A., Adams, T., & Davies, M. B. 2005, MNRAS, 358, 716

Sills, A., Adams, T., Davies, M. B., & Bate, M. R. 2002, MNRAS, 332, 49

Sills, A., Faber, J. A., Lombardi, Jr., J. C., Rasio, F. A., & Warren, A. R. 2001, ApJ, 548, 323

Skrutskie, M. F., Cutri, R. M., & Marsh, K. A. 2007, in Bulletin of the American Astronomical Society, Vol. 39, American Astronomical Society Meeting Abstracts, 836

Smith, J. C., Stumpe, M. C., Van Cleve, J. E., et al. 2012, PASP, 124, 1000

Smith, M. A., Bianchi, L., & Shiao, B. 2014, AJ, 147, 159

Strope, R. J., Schaefer, B. E., & Henden, A. A. 2010, AJ, 140, 34

Stumpe, M. C., Smith, J. C., Catanzarite, J. H., et al. 2014, PASP, 126, 100

Szkody, P., Anderson, S. F., Brooks, K., et al. 2011, AJ, 142, 181

Taylor, B. J. 2007, AJ, 133, 370

Tremblay, P.-E., Bergeron, P., & Gianninas, A. 2011, ApJ, 730, 128

van den Berg, M., Tagliaferri, G., Belloni, T., & Verbunt, F. 2004, A&A, 418, 509

van Roestel, J., Kupfer, T., Ruiz-Carmona, R., et al. 2018, MNRAS, 475, 2560

Vanderburg, A., & Johnson, J. A. 2014, PASP, 126, 948

Vanderburg, A., Latham, D. W., Buchhave, L. A., et al. 2016, ApJS, 222, 14

Chapter 5

Conclusions

It is clear that a large number of stars are not evolving according to standard single-star stellar evolution theory. In the 4 Gyr open cluster M67, many 3D kinematic cluster members do not fall on the isochrone. This includes 12 blue stragglers, 4 yellow stragglers, and 2 sub-subgiants. 80% of these stars are found in binary systems, demonstrating the link between binarity and evolving along alternative stellar evolution pathways. Even more stars exist on the main-sequence and giant branch of the cluster that have been impacted by binary evolution processes, but elude detection in CMDs because they photometrically blend with standard populations. It is the primary goal of this thesis to push beyond the blue stragglers to understand the origin and evolution of these additional types of binary evolution products.

5.1 The M67 Yellow Straggler WOCS 1015

In Chapter 2, I perform an asteroseismic analysis to demonstrate that one of the 4 yellow stragglers in M67 is a helium-burning giant with a mass at least twice the typical cluster giant. The large mass points to an merger or collisional origin rather than a formation scenario involving mass transfer. Notably, this yellow straggler is in a binary with a companion that is either a main-sequence star near the turnoff, or a blue straggler star. Along with S1040–a yellow straggler in M67 with a hot helium white dwarf companion demonstrating it is an evolved blue straggler formed from mass transfer (Landsman et al. 1997)– this analysis shows definitively that some yellow stragglers are the evolved counter parts to blue straggler stars.

M67 is not the only cluster known to have evolved blue straggler stars. A subsequent detailed asteroseismic study of NGC 6819 (2.5 Gyr open cluster) found that 15% of the cluster's red giants were more massive than standard, and thus were evolved blue straggler stars (Handberg et al. 2017). It is likely that these stars exist in all clusters, possibly in

significant numbers, and asteroseismic analysis may be the key to finding them. Searching for these stars in a larger sample of clusters will be vital to understanding their population characteristics (Section 5.4.1). In conjunction with theoretical modeling efforts (Section 5.4.3), analysis of these evolved blue straggler populations can yield new insights into binary evolution physics.

5.2 On the Origin of Sub-subgiants

In Chapter 3, I use the stellar evolution code MESA (Paxton et al. 2015) and the population synthesis code BSE (Hurley et al. 2002) to develop models of sub-subgiant formation. I explore three different scenarios for sub-subgiant formation:

- Mass transfer in binaries with a subgiant primary.
- Rapid mass loss from a subgiant or giant star, e.g. during a grazing dynamical encounter
- Inhibition of convection in a subgiant or giant due to strong magnetic fields

We conclude that mass loss from a subgiant or early giant can create stars in the SSG CMD region. However, observed SSGs in M67 and NGC 6791 are in orbits that are wider than expected if the stars are undergoing Roche lobe overflow, and the types of dynamical interactions that could rapidly strip mass from a subgiant/giant star are expected to be extremely rare in open clusters and do not necessarily result in short-period binaries such as the SSGs. Therefore, neither of these mass loss scenarios can match the stellar and orbital characteristics of observed SSGs and produce them in sufficient quantities. On the other hand, the magnetic inhibition of convection could produce approximately the number of observed SSGs in M67 and NGC 6791. However, the physics of magnetic stellar evolution is poorly understood, and our models are therefore not physically robust. We suggest using

additional approaches to modeling magnetic fields in stellar evolution codes to model the sub-subgiants and comparing the results.

Understanding the impact of magnetic fields on stellar evolution is an active area of ongoing research, particularly among those studying low-mass main-sequence stars. Much ongoing work is devoted to understanding small discrepancies in M-dwarf and brown dwarf temperatures and radii, with magnetic fields being one potential source of the deviations. New modeling approaches and observations in this field are progressing rapidly, and the conclusions from these efforts will illuminate whether strong magnetic fields can indeed cause significantly inhibited convection. As models for low-mass main sequence stars develop, sub-subgiants can be an important second point of comparison between models and observations.

The dynamical formation scenario for sub-subgiants has drawn additional interest because of the possibility these may be created in interactions with black holes (Ivanova et al. 2017; Shishkovsky et al. 2018) and other compact objects. Certainly dynamical encounters should be more common in denser globular clusters. If the dynamical formation scenario is more viable in globular clusters as is expected, sub-subgiants could be interesting tracers of the cluster's dynamical evolution and probes of black hole populations (Ivanova et al. 2017).

Finally, as the *Gaia* mission begins to yield accurate distances and proper motions, many more clusters will have the accurate membership determinations needed to detect their sub-subgiant populations. Similarly, accurate distances to magnetically active field giants will enable much more accurate luminosity measurements, allowing us to identify possible sub-subgiants in the field. For example, the Huber et al. (2014) sample of "No Mans Land" stars that are fainter/redder than a 13 Gyr isochrone could contain examples of sub-subgiants in the field, but more accurate luminosities are needed to confirm this

assessment.

5.3 Post-interaction Stars on the M67 Main-Sequence

In Chapter 4, I demonstrate that mass-transfer blue stragglers are rapidly rotating soon after formation, reaching rotation periods of < 1 day. They then spin down as they age, roughly following the predictions for standard main-sequence stars. I then use light curves from Kepler K2 Campaign 5 to search for unusually rapidly rotating stars in M67. Given the 4 Gyr age of M67, its main-sequence stars have typical rotation periods of 20-30 days. I find 11 stars with rotation periods of < 8 days, and hypothesis that these stars have been through recent mass-transfer, mergers, or collisions that have spun them up to large rotation rates, effectively restarting their gyro-age clock. Other observations support this picture: a binary fraction three times larger than for typical main sequence stars and comparable to the binary fraction among blue straggler populations; long periods and low eccentricities consistent with post-mass transfer binaries, low-mass secondaries consistent with white dwarf companions, and in at least one case a definitive UV excess suggestive of a young (~ 300 Myr) white dwarf companion.

These detections show that the blue straggler population extends into the main sequence domain, and many stars that appear to be "normal" main sequence stars have in fact experienced a recent stellar interaction. With 11 detections, the number of such stars is comparable to the number of blue stragglers in the cluster, and thus this population is important to identify and include in any studies of cluster binary interaction products. Furthermore, the number of detections indicates $8 - 30\%$ of the cluster binary population and 1-4% of the single FGK main-sequence stars have been through a recent stellar interaction. The post-interaction main-sequence population is therefore significant, and needs to be properly accounted for (e.g. when using rotation to age-date stellar populations

or when contextualizing galactic abundance studies).

5.4 Future Work

The study of M67 presented here illustrates the plethora of non-standard stars that populate the cluster. While many of the stars are clearly not evolving normally because they do not fall on the cluster isochrone, many more stars that have been through mass-transfer, mergers, or collisions are "hiding" because they photometrically blend with the standard cluster population. Fully characterizing the extent of the post-interaction population of the cluster thus requires using novel combinations of observational techniques. M67 is the first cluster that has had the post-interaction population examined in such detail. What we have learned in this cluster should be expanded to study clusters of different ages and metallicities, used to identify similar populations among field stars, and leveraged as constraints for new population modeling and binary evolution modeling efforts.

5.4.1 Expanding to More Clusters with *Gaia* and PLATO

M67 is an unusually well-studied cluster, with excellent kinematic membership information, photometry, and more than 30 years of radial velocities yielding binary orbits out to 10^4 days. The upcoming Gaia mission will be a game changer for cluster science, yielding high quality membership information for many more clusters.

Gaia-ESO expect to obtain spectra for $\sim$ 80 galactic open clusters covering a wide range in age (1 Myr- 8 Gyr). When combined with *Gaia* astrometry, this will considerably expand the sample of clusters with available astrometry and spectra to determine kinematic cluster memberships, basic stellar parameters, and binary status. This rich data set will allow me to identify many more non-standard stars based on their CMD positions (e.g. blue stragglers, yellow stragglers, sub-subgiants), building on the work done in M67 to expand

our knowledge of these populations to more clusters across a wider range in ages.

Currently, NGC 6819, NGC 6791, M67, and Ruprecht 147 are the only old open clusters (2.5-8 Gyr) with the high-precision time-series photometry from Kepler/K2 needed to detect evolved blue stragglers using asteroseismology, or to search for rapid rotators on cluster main sequences with low amplitude spot modulation like we find among the post-interaction stars in M67 (Chapter 4). Of these four clusters, only NGC 6819 has had a thorough asteroseismic analysis of the red giant branch using detailed frequency analysis. M67 will require an asteroseismic re-analysis when results from Campaign 16 and Campaign 18 are available. I currently have an improved asteroseismic analysis of NGC 6791 underway using updated cluster membership information from the WIYN Open Cluster Study and the full 4 year time-series of the Kepler mission that has so far yielded at least 4 new detections of evolved blue stragglers in the cluster. Ruprecht 147 has not yet had an asteroseismic analysis of its giant branch, though the data is now available. Similarly, Kepler and K2 measurements are available for the main-sequences of these clusters, allowing the identification of main-sequence rapid rotators in these clusters as well.

NASA's successor to *Kepler*– the just-launched Transiting Exoplanet Survey Satellite (TESS)–will observe several nearby young clusters (< 1 Gyr), enabling continued studies of angular momentum in young stars and binaries. Due to TESS's limiting magnitude, shorter time baseline, and large pixel size, it will not be as well-suited to producing high-precision light curves of more distant, old star clusters or for asteroseismic studies, though *Gaia* memberships will leave us with no shortage of excellent cluster targets. Additional rotation studies to discover more candidate post-interaction main sequence stars in these older clusters will therefore require ground-based photometric studies or spectroscopic $v\sin i$ surveys. The WIYN Open Cluster Study provides an excellent spectral catalog to derive such $v\sin i$s for a selection of other open clusters (NGC 188, NGC 7789, NGC 2506). No

doubt *Gaia* spectroscopic follow-up missions (e.g. Gaia-ESO, 4MOST, GALAH) will enable similar studies of an even larger sample, and WIYN's Hydra Multi-Object Spectrograph would be ideally suited to join in the effort to follow up select *Gaia* clusters with more long-term radial-velocity monitoring.

Finally, the European PLAnetary Transits and Oscillations of stars (PLATO mission) is in the planning stages, with a target launch date in 2026. This mission does aim to target star clusters for asteroseismic characterization (Rauer et al. 2014) and will yield rotation periods for many new cluster and field stars. The astronomy community's investment in variability studies in both the U.S. and Europe promise to make asteroseismology, stellar rotation, and binary stars vibrant fields of study for many years to come.

5.4.2 Connection to Galactic Field Populations

A notable recent development in the study of binary evolution has been the recognition of similarities across a wide range of objects not evidently associated at first glance - blue stragglers, barium stars, carbon stars, carbon enhanced metal poor stars (CEMP-s), and post-AGB stars. Very likely, all of these classes of stars originate with mass transfer on to main-sequence stars. Large-scale abundance surveys, both in the field and in clusters, will likely be a key to decoding the relationships between all these types of stars, and identifying the full extent of their populations in the field. Again, such studies will be possible in the years to come thanks to the many ongoing and upcoming spectral surveys.

This detailed study of the post-interaction population of M67 illuminates the diversity of objects that can be created through binary evolution processes. A natural next step is to begin to understand how we may recognize these objects in the field, and how common they may be. For example, large asteroseismic surveys like Kepler (and soon TESS and PLATO) can determine masses for large populations of red giant stars in the field. What

fraction of these would we expect to be evolved blue straggler stars based on the populations we find in clusters? Can we build our sample of sub-subgiants by turning to the field, for example finding under-luminous giants by determining luminosities from *Gaia* parallaxes? What fraction of cluster blue stragglers would be identifiable in the field using abundance surveys, and what does this tell us about stellar nucleosynthesis? TESS will also deliver rotation periods for field mass-transfer products like barium stars, allowing us to further probe their rotational evolution as we have for blue stragglers. Perhaps rotation rates, combined with chemical or kinematic tracers of age, could allow for the identification of other post-mass-transfer stars in the field, much as we have done for M67 in Chapter 4. The Large Synoptic Survey Telescope (LSST) is planned for first light in 2021 and will continuously scan the sky, opening the door to finally detect significant samples of rare transient events like binary mergers. Between *Gaia*, large-scale abundance studies, and these upcoming time-series missions, the possibilities are numerous.

With the recent popularity of galactic archeology, understanding the impact of binaries on stellar abundances and age distributions in our galaxy is essential for accurately interpreting observations. What we can learn about the influence of binaries in cluster environments through detailed studies like this exploration of M67 can directly help answer these questions as we continue to bridge our understanding between observations of cluster and field populations.

5.4.3 Theoretical Modeling

The detection and understanding of the binary evolution products discussed in this thesis enable the first integrated studies of the early-stage binary evolution population of a cluster that looks beyond the blue stragglers. These populations are essentially unstudied, and thus offer a totally new set of questions and constraints for binary evolution and stellar

population modeling.

First results from observations have already yielded intriguing questions. For example, several overmassive giants in NGC 6791 are nearly twice the turnoff mass, yet the CMD locations of the blue stragglers indicate there are none with such large masses. Why do these massive blue stragglers evolve quickly to the giant branch instead of evolving through a long blue straggler stage? Most overmassive giants in NGC 6791 are single stars, while the majority in NGC 6819 are binaries. What physical differences between the two clusters can explain this result? Among M67's rapidly-rotating main sequence stars, there are several binaries with orbital periods of a few hundred days. Such orbital periods are rare among the blue straggler population, and such binaries are predicted to be unstable to Roche lobe overflow. Are these examples of post-common-envelope binaries, or did they somehow form from stable mass transfer?

Answering these and other questions will require a combination of population modeling (e.g. with N-body or Monte Carlo models), timescale analysis, and detailed stellar evolution models (e.g. with MESA; Paxton et al. 2015). While these techniques have been applied to blue straggler populations (e.g. Geller et al. 2013; Hurley et al. 2005; Chen & Han 2008), the unique power of this new study comes from integrating samples of blue stragglers with their evolved counterparts on the giant branch and their lower-mass counterparts on the main sequence, all with well-characterized stellar and orbital parameters. For example, the shorter giant evolutionary timescale provides much tighter constraints on formation frequency of evolved blue stragglers than is available for classical blue straggler populations. Though gyrochronology cannot provide precise ages so soon after formation, the presence of rapid rotation in post-interaction stars provides an upper bound on time since formation from spin-down models (e.g. Gallet & Bouvier 2013). Asteroseismology of evolved blue stragglers will provide the first precise blue straggler mass distributions,

directly constraining possible formation channels (e.g. Leiner et al. 2016). This integrated approach should yield a wealth of new physical insights into the binary evolution channels that form these objects.

5.5 Closing Thoughts

Binary evolution processes create some of the most astrophysically interesting objects in the universe – binary black holes, double degenerates, Type 1a supernovae – but our understanding of binary evolution processes is still limited. Detailed observational studies of binary populations and theoretical modeling efforts as I have presented here for the open cluster M67 are essential to understanding the impact of binarity on stellar populations.

The rich archival data on open cluster M67 has allowed us to complete a detailed examination of its early-stage binary population. Combining a long term radial-velocity study (WOCS) with new methods including asteroseismology and gyrochronology has allowed us to detect new types of post-interaction systems and assemble the most complete picture of the early-stage binary evolution population of a cluster to date. In the era of *Gaia* and large time-domain surveys, similar studies across many clusters and the field will be possible. This rich new era will provide many new constraints for theoretical binary evolution modeling, and help inform our statistical understanding of the influence of binaries on stellar populations as well as our physical understanding of the processes at work during binary stellar evolution.

References

Chen, X., & Han, Z. 2008, MNRAS, 387, 1416

Corsaro, E., Stello, D., Huber, D., et al. 2012, ApJ, 757, 190

Gallet, F., & Bouvier, J. 2013, A&A, 556, A36

Geller, A. M., Hurley, J. R., & Mathieu, R. D. 2013, AJ, 145, 8

Handberg, R., Brogaard, K., Miglio, A., et al. 2017, MNRAS, 472, 979

Huber, D., Silva Aguirre, V., Matthews, J. M., et al. 2014, ApJS, 211, 2

Hurley, J. R., Pols, O. R., Aarseth, S. J., & Tout, C. A. 2005, MNRAS, 363, 293

Hurley, J. R., Tout, C. A., & Pols, O. R. 2002, MNRAS, 329, 897

Ivanova, N., da Rocha, C. A., Van, K. X., & Nandez, J. L. A. 2017, ApJ, 843, L30

Landsman, W., Aparicio, J., Bergeron, P., Di Stefano, R., & Stecher, T. P. 1997, ApJ, 481, L93

Leiner, E., Mathieu, R. D., Stello, D., Vanderburg, A., & Sandquist, E. 2016, ApJ, 832, L13

Paxton, B., Marchant, P., Schwab, J., et al. 2015, ApJS, 220, 15

Rauer, H., Catala, C., Aerts, C., et al. 2014, Experimental Astronomy, 38, 249

Shishkovsky, L., Strader, J., Chomiuk, L., et al. 2018, ApJ, 855, 55